

University of Windsor

Scholarship at UWindor

Electronic Theses and Dissertations

Theses, Dissertations, and Major Papers

2011

Second Law Analysis of a Multiport Serpentine Microchannel Heat Exchanger

Serena Al-Obaidi
University of Windsor

Follow this and additional works at: <https://scholar.uwindsor.ca/etd>

Recommended Citation

Al-Obaidi, Serena, "Second Law Analysis of a Multiport Serpentine Microchannel Heat Exchanger" (2011). *Electronic Theses and Dissertations*. 170.
<https://scholar.uwindsor.ca/etd/170>

This online database contains the full-text of PhD dissertations and Masters' theses of University of Windsor students from 1954 forward. These documents are made available for personal study and research purposes only, in accordance with the Canadian Copyright Act and the Creative Commons license—CC BY-NC-ND (Attribution, Non-Commercial, No Derivative Works). Under this license, works must always be attributed to the copyright holder (original author), cannot be used for any commercial purposes, and may not be altered. Any other use would require the permission of the copyright holder. Students may inquire about withdrawing their dissertation and/or thesis from this database. For additional inquiries, please contact the repository administrator via email (scholarship@uwindsor.ca) or by telephone at 519-253-3000ext. 3208.

Second Law Analysis of a Multiport Serpentine Microchannel Heat Exchanger

by

Serena Al-Obaidi

A Thesis

Submitted to the Faculty of Graduate Studies
through Mechanical, Automotive, and Materials Engineering
in Partial Fulfillment of the Requirements for
the Degree of Master of Applied Science at the
University of Windsor

Windsor, Ontario, Canada

2011

© 2011 Serena Al-Obaidi

Second Law Analysis of a Multiport Serpentine Microchannel Heat Exchanger

by

Serena Al-Obaidi

APPROVED BY:

Dr. Henry Hu
Department of Mechanical, Automotive and Materials Engineering

Dr. David Ting
Department of Mechanical, Automotive and Materials Engineering

Dr. Amir Fartaj, Advisor
Department of Mechanical, Automotive and Materials Engineering

Dr. Gary Rankin, Chair of Defense
Department of Mechanical, Automotive and Materials Engineering

May 19, 2011

DECLARATION OF ORIGINALITY

I hereby certify that I am the sole author of this thesis and that no part of this thesis has been published or submitted for publication.

I certify that, to the best of my knowledge, my thesis does not infringe upon anyone's copyright nor violate any proprietary rights and that any ideas, techniques, quotations, or any other material from the work of other people included in my thesis, published or otherwise, are fully acknowledged in accordance with the standard referencing practices. Furthermore, to the extent that I have included copyrighted material that surpasses the bounds of fair dealing within the meaning of the Canada Copyright Act, I certify that I have obtained a written permission from the copyright owner(s) to include such material(s) in my thesis and have included copies of such copyright clearances to my appendix.

I declare that this is a true copy of my thesis, including any final revisions, as approved by my thesis committee and the Graduate Studies office, and that this thesis has not been submitted for a higher degree to any other University or Institution.

ABSTRACT

In the present work, second law analysis has been used for a steady-state cross flow microchannel heat exchanger (MCHX). This type of heat exchangers has been known for its higher heat transfer coefficient and higher area per volume ratio. Therefore, broad range studies are being carried out to optimize its performance and minimize its inefficiencies. In the current study, entropy generation and exergy loss have been employed to investigate a multiport serpentine slab MCHX with ethylene glycol-water and air as the working fluids. Conservation of energy and the increase in entropy principles were used to create a mathematical model that uses different parameters such as heat capacity rate ratio, fluids inlet temperatures, effectiveness and pressure drop for obtaining entropy generation. Results were found on the basis of the behaviour of the dimensionless entropy generation number with the key parameters. A good agreement between the predicted and the measured results was found.

Dedicated to

my family,

who offered me unconditional love and support

ACKNOWLEDGEMENTS

First of all, I would like to thank the Lord God without whom none of this would have been possible. Thank him for the wisdom and perseverance that he has been bestowed upon me during this research project.

It is my pleasure to thank the many people who made this thesis possible. I would like to express my sincere gratitude to Dr. Amir Fartaj for his supervision, support, guidance, and advice throughout the research project, as well as his pain-staking effort in proof reading the drafts, are greatly appreciated. Indeed, without his guidance, I would not be able to put the topic together. My experience with him was an interesting and rewarding one.

I would also like to thank my thesis committee Dr. David Ting and Dr. Henry Hu for accepting to be my committee members. Special thanks to my colleagues Faisal Siddiqui, Engr. Sarbadaman Dasgupta, and Abdul Quaiyum for their assistance with the experimental set up and test runs. Thanks are also extended to my colleagues Mohammed Saadi, Mohammed Ismail, and Shahram Fotowat. I would like to acknowledge the help of Mr. Patrick Seguin and Mr. Andrew Jenner for their technical support, and the University of Windsor for the financial support through the GA opportunity and scholarship.

I would like to express my sincere appreciation to my family who has been a constant source of love, concern, support and strength all these years. I like to express my heartfelt gratitude for their absolute confidence in me, especially my mother, “Elham Askar” who has always been there for me. Their patience and understanding during these years is greatly appreciated.

TABLE OF CONTENTS

DECLARATION OF ORIGINALITY	iii
ABSTRACT.....	iv
DEDICATION	v
ACKNOWLEDGEMENTS.....	vi
LIST OF TABLES.....	x
LIST OF FIGURES	xi
NOMENCLATURE	xiii
CHAPTER	
I. INTRODUCTION	
1.1 Heat Exchangers	1
1.2 The First and Second Law of Thermodynamics.....	6
1.3 Motivation.....	11
1.4 Objectives	13
II. REVIEW OF LITERATURE	
2.1 General Review	15
2.2 Heat Exchangers	15
2.3 Second Law Analysis	17
III. DESIGN AND METHODOLOGY	
3.1 Theory Background	23
3.2 Heat Exchangers with an Imbalance Flow	26
3.3 First Law Analysis:.....	27
3.4 Effectiveness.....	28
3.5 Second Law Analysis-Entropy Generation Approach:.....	30
3.5.1 Irreversibilities	30
3.5.2 The Mathematical Model	31
3.5.3 Entropy Generation Number	34
3.5.4 Entropy Generation Number Ratio	35
3.5.5 Exergy Destruction	36
3.5.6 Modified Entropy Generation Number	37

iv.	EXPERIMENTAL SET-UP	
	4.1 General Introduction	39
	4.2 Experimental Set-Up Components	41
	4.2.1 The Test Section and the MCHX	41
	4.2.2 The Closed Loop Thermal Wind Tunnel	44
	4.2.3 MCHX Liquid Supply System	45
	4.2.4 Data Acquisition System (DAQ)	46
	4.3 Experimental Methods and Operating Conditions	47
	4.4 Measurement and Data Collection Procedures	48
	4.4.1 Glycol Temperature and Pressure Measurements	49
	4.4.2 Glycol Mass Flow Rate Measurement	51
	4.4.3 Air Temperature Measurements	52
	4.4.4 Air Velocity and Pressure Measurements	54
	4.4.5 Airside Mass Flow Rate Measurement	55
	4.4.6 Reynolds Number Measurement	56
v.	ANALYSIS OF RESULTS	
	5.1 Balanced Cross Flow With Zero Pressure Drop	58
	5.2 Balanced Cross Flow With Airside Pressure Drop	59
	5.3 Imbalanced Cross Flow With Airside Pressure Drop	61
	5.4 Entropy Generation Number Ratio With Zero Pressure Drop	64
	5.5 Comparison of the Predicted Results With the Measured Data ...	68
vi.	CONCLUSIONS AND RECOMMENDATIONS	
	6.1 Conclusions	76
	6.2 Recommendations	79
	REFERENCES	81
	APPENDICES	
	Uncertainty Analysis	90
	A.2 Uncertainty in the MCHX Dimensions	92
	A.3 Uncertainty Associated With the DAQ System	101
	A.3.1 Uncertainty Associated With the DAQ Card	101
	A.3.2 Uncertainty Associated With the Signal Conditioner ...	102
	A.4 Uncertainty in the Liquid Side Temperatures	103
	A.5 Uncertainty in the Liquid Side Density	106
	A.6 Uncertainty in the Liquid Side Viscosity	106
	A.7 Uncertainty in the Liquid Side Specific Heat	106
	A.8 Uncertainty in the Airside Temperatures	106

A.9 Uncertainty in the Airside Density	110
A.10 Uncertainty in the Liquid Side Viscosity.....	110
A.11 Uncertainty in the Airside Specific Heat	110
A.12 Uncertainty in the Airside Pressures.....	111
A.13 Uncertainty Related to the Liquid Side Mass Flow Rate.....	114
A.14 Uncertainty Related to the Liquid Mass Flow Rate.....	117
A.15 Uncertainty of the Air Mass Flow Rate	117
A.16 Uncertainty in the Liquid Reynolds Number.....	118
A.17 Uncertainty in the Air Reynolds Number	119
A.18 Uncertainty in the Glycol Heat Transfer Rate	120
A.19 Uncertainty in the Air Heat Transfer Rate.....	120
A.20 Uncertainty in the Average Heat Transfer Rate.....	121
A.21 Uncertainty in Effectiveness.....	121
A.22 Uncertainty in the Heat Capacity Rate Ratio.....	122
A.23 Uncertainty in the Entropy Generation Number.....	123
Calibration Curves.....	126
VITA AUCTORIS	127

LIST OF TABLES

TABLE 1 CHANNEL CLASSIFICATION ACCORDING TO MEHENDALE:	16
TABLE 2 OPERATING CONDITIONS: AIR HEATING ($T_{A,i} < T_{G,i}$)	48
TABLE 3 SUMMARY OF THE CONCLUSIONS.....	78
TABLE 4 UNCERTAINTIES IN DESIGN PARAMETERS	124

LIST OF FIGURES

FIGURE 1 ENTROPY GENERATION MINIMIZATION FIELD COVERED BY (BEJAN, 1982)..... 25

FIGURE 2 SCHEMATIC DIAGRAM OF THE EXPERIMENTAL SET-UP..... 40

FIGURE 3 EXPERIMENTAL SET-UP 41

FIGURE 4 MCHX 43

FIGURE 5 INTEGRATED THERMAL WIND TUNNEL..... 45

FIGURE 6 CONNECTIVITY OF THE DAQ COMPONENTS 47

FIGURE 7 INLET GRID THERMOCOUPLES DISTRIBUTION 52

FIGURE 8 OUTLET GRID THERMOCOUPLES DISTRIBUTION 53

FIGURE 9 AIR VELOCITY AND PRESSURE DEVICES 54

FIGURE 10 ENTROPY GENERATION NUMBER VS. EFFECTIVENESS FOR A BALANCED CROSS
FLOW HEAT EXCHANGER 59

FIGURE 11 ENTROPY GENERATION NUMBER VS. EFFECTIVENESS FOR A BALANCED
CROSS FLOW HEAT EXCHANGER $C^*=1$ 60

FIGURE 12 THE EFFECT OF PRESSURE AND TEMPERATURE RATIOS ON ENTROPY GENERATION
NUMBER FOR ($C^*=0.5$)..... 61

FIGURE 13 THE EFFECT OF PRESSURE AND TEMPERATURE RATIOS ON ENTROPY GENERATION
NUMBER FOR ($C^*=0.2$)..... 62

FIGURE 14 EFFECTIVENESS AT Ns_{MAX} VS. HEAT CAPACITY RATE RATIO 63

FIGURE 15 ENTROPY GENERATION NUMBER RATIO S^* VS. EFFECTIVENESS..... 64

FIGURE 16 ENTROPY GENERATION NUMBER RATIO VS. EFFECTIVENESS AT $C^*=0.8$ 64

FIGURE 17 ENTROPY GENERATION NUMBER RATIO VS. EFFECTIVENESS AT $C^*=0.5$ 65

FIGURE 18 THE EFFECT OF T_R ON S^* AT ($P_o/P_i=0.9$) ($C^*=0.7$)..... 66

FIGURE 19 THE EFFECT OF T_R ON S^* AT $(P_o/P_i=0.4)$ ($C^*=0.7$).....	67
FIGURE 20 THE EFFECT OF T_R ON Ns FOR $(P_o/P_i=0.4)$ ($C^*=0.4$).....	68
FIGURE 21 ENTROPY GENERATION NUMBER VS. HEAT CAPACITY RATE RATIO	69
FIGURE 22 ENTROPY GENERATION NUMBER VS. HEAT CAPACITY RATE RATIO	70
FIGURE 23 ENTROPY GENERATION NUMBER VS. MAXIMUM HEAT CAPACITY RATE	71
FIGURE 24 EXERGY DESTROYED VS. C^*	72
FIGURE 25 Ns VS. Re_A	73
FIGURE 26 EXERGY DESTROYED VS. Re	74
FIGURE 27 Ns_{MODF} VS. HEAT CAPACITY RATE RATIO	75
FIGURE 28 CALIBRATION CURVE FOR PX277- 05D5V.....	126
FIGURE 29 CALIBRATION CURVE FOR PX277-01D5V.....	126

NOMENCLATURE

A	Area [m^2]
$A_{\text{HT, a, MCHX}}$	Heat transfer surface area of fins and slabs of the MCHX [m^2]
$A_{\text{f,s}}$	MCHX slab frontal area [m^2]
$A_{\text{fin,HT}}$	Single fin heat transfer surface area [m^2]
$A_{\text{fin,HT,MCHX}}$	Total numbers of fins heat transfer surface area [m^2]
$A_{\text{fin,f}}$	Frontal area of a single fin [m^2]
$A_{\text{fin,f,MCHX}}$	MCHX fins frontal area [m^2]
$A_{\text{f,obstructed}}$	Frontal area of the fins and slabs that obstructs the flow [m^2]
$A_{\text{f,MCHX}}$	MCHX frontal area [m^2]
$A_{\text{indv,slab}}$	Area of an individual slab between two fins [m^2]
$A_{\text{min,a}}$	Air flow minimum free flow area [m^2]
A_{MC}	Single microchannel area [m^2]
$A_{\text{,slabs,MCHX}}$	Area of the entire slabs for the MCHX [m^2]
C	Heat capacity rate [kW/ K]
c_p	Specific heat capacity [kJ/kg.K]
C^*	Minimum to maximum heat capacity rate ratio
D_h or d	Hydraulic diameter [m]
D_{MC}	Diameter of a single microchannel [m]
dh	Change in enthalpy [$\text{W}/(\text{m}^2 \text{K})$]
dV	Change in volume [m^3]
G	Mass velocity [$\text{kg}/\text{m}^2.\text{s}$]
h	Specific enthalpy [kJ/kg]

h	Convective heat transfer coefficient [W/(m ² .K)]
H_{fin}	Height of a single fin [m]
H_{MCHX}	Height of the MCHX [m]
H_s	Height of a single slab [m]
k	Thermal conductivity [W/ m. K]
L_{fin}	Length of a single fin in the air flow direction [m]
L_{MCHX}	The length of the MCHX [m]
$L_{HT,s}$	Slab length contributes to the heat transfer [m]
\dot{m}	Mass flow rate [kg/s]
n	Channels number
N	Number of the collected samples
$N_{fin,array,MCHX}$	Total number of finarrays of the MCHX
$N_{fin,MCHX}$	MCHX total number of fins
$N_{fin,s}$	Total number of fins per slab
$N_{HT,s,MCHX}$	Total number slabs contributing to the heat transfer in the MCHX
$N_{s,MCHX}$	Total number of slabs of the MCHX
N_s	Entropy generation number
NTU	Number of transfer units
Nu	Nusselt number
P	Pressure [kPa]
$P_{1,i}$	Hot fluid inlet pressure [kPa]
$P_{1,o}$	Hot fluid outlet pressure [kPa]
$P_{2,i}$	Cold fluid inlet pressure [kPa]
$P_{2,o}$	Cold fluid outlet pressure [kPa]

\dot{Q}	Heat transfer rate [kW]
\dot{Q}_{loss}	Heat loss in the MCHX [kW]
R	Gas constant [kJ/kg.K]
Re	Reynolds number
s	Specific entropy [kJ/kg.K]
S	Rate of entropy [kW]
S_{fin}	Spacing between two fins [m]
\dot{S}_{gen}	Rate of entropy generation [kW/K]
S^*	Entropy generation number ratio
t	Time [s]
t_{fin}	Thickness of a single fin [m]
T	Temperature [K]
$T_{a,b}$	Air bulk temperature. [°C]
$T_{c,i}$	Cold fluid inlet temperature. [°C]
$T_{c,o}$	Cold fluid outlet temperature. [°C]
$T_{g,b}$	Glycol bulk temperature. [°C]
$T_{h,i}$	Hot fluid inlet temperature. [°C]
$T_{h,o}$	Hot fluid outlet temperature. [°C]
T_R	$T_{c,i}/T_{h,i}$, inlet temperature ratio
V	Velocity [m/s]
W_s	Slab width [m]
x	Specific flow exergy [kJ/kg]
X	Exergy [kW]

\dot{V}_{MCHX} MCHX volume [m³]

Greek symbols

Δ Difference

ε Effectiveness

μ Dynamic viscosity [kg/m.s]

ρ Fluid density [kg/m³]

Superscripts

*

Dimensionless quantity or parameter

Subscripts

a Air

act. Actual

avg Average

dyn Dynamic

gen Generation

g [50:50%] Ethylene glycol-water mixture

max Maximum

min Minimum

modf Modified

tot Total

0 Environment

1 Hot fluid

2 Cold fluid

Abbreviations

DAQ	Data Acquisition System
DFM	Digital Flow Meter
EGM	Entropy Generation Minimization
LPM	Liters per minute
LSB	Least Significant Bit
MCHX	Microchannel Heat Exchanger
NI	National Instrument
PTD	Differential Pressure Transducer
RSS	Root Sum Square
RTD	Resistance Temperature Detector

CHAPTER I

INTRODUCTION

The major emphasis in this chapter is placed on introducing the terminology and concepts associated with a broad spectrum of heat exchangers and the first and second laws of thermodynamics being applied to these heat exchangers. Another objective is to present an evaluation technique based on the second law of thermodynamics being applied to a single phase cross flow microchannel heat exchanger. The focus will be on presenting first and second law analysis of heat exchangers followed by a comprehensive literature review.

1.1 Heat Exchangers

Heat Exchangers are devices used to transfer the thermal energy between two or more fluids being at different temperatures. This is usually done without any external effect of heat and work. In some heat exchangers, the heat is transferred from one fluid to the other without being in direct contact with each other. In some heat exchangers, the fluids are in direct contact with each other. However, many heat exchangers have the two fluids separated by a wall, and the heat transfer occurs through the wall. The transition of thermal energy from a hotter object to a cooler object is called Heat transfer. Heat exchangers are used in a wide variety of applications such as automotive, electronics, chemical, food industries, space application, manufacturing industry, air conditioning, refrigeration, waste heat recovery, etc. Heat exchangers achieve a straight forward purpose: controlling a system temperature by adding or removing thermal energy. Some

of the examples regarding heat exchangers are; condensers, evaporators, car radiators, cooling towers, and preheaters. A car radiator is an example of heat exchangers, where the cold air that is forced to blow into the radiator removes the heat from the liquid passing through the radiator tubes for a more efficient use of the engine. Small heat exchangers are also used in many industrial applications to maintain a required temperature. An example for large size heat exchangers is the cooling tower. It is used to reject the waste heat to the atmosphere by transferring heat from the water stream to the air stream, which is discharged to the atmosphere.

Heat exchangers can be classified according to the following main criteria: geometry of construction: (tubes- plates- extended surfaces), heat transfer mechanisms: (single-phase or two-phase), transfer processes: (direct contact and indirect contact), fluid flow arrangements: (parallel, counter, and cross flow), size (small, medium, and large), etc. Another way of classifying heat exchangers is by surface area to volume ratio, which can be categorized into compact and non compact. Heat exchangers come in a wide variety of types and sizes. Some of the known types are; shell-and-tube heat exchangers, coil heat exchangers, plate heat exchangers, and the heat exchanger used in the current study; microchannel heat exchanger. Based on the flow arrangements, heat exchangers can be known as parallel where the one fluid flows in the same direction to the other fluid stream. The second arrangement is the counter flow, where the two fluid streams flow in an opposite direction. The last arrangement is the cross flow, where the two fluid streams flow perpendicular to each other.

Shell and tube heat exchanger:

Although all heat exchangers function in the same way which is transferring heat from one fluid to another, they have different ways to perform that. The shell and tube heat

exchangers are mainly used because of their basic configuration. One fluid flows through a bundle of metal tubes while the other flows over the tubes inside the shell that surrounds the tubes.

Advantages:

- Can be used in systems that involve higher operating pressures and temperatures
- Tubes leak can be detected easily
- Pressure drop across the tubes is lower
- Less expensive compared to plate heat exchangers

Disadvantages:

- Lower heat transfer efficiency
- Difficulty in cleaning and maintaining
- Cannot increase the capacity of the tubes
- Large size which requires more space

Plate heat exchanger:

This type uses several layers of aluminum plates provided with fins. The heat is transferred from the fin to the plate and to another fin then to the second fluid. The fins are used to help the exchanger to withstand high pressures and to enhance the heat transfer of the heat exchanger. This type has an advantage over the other heat exchangers, since the fluid is exposed to a large surface area that will result in enhanced heat transfer efficiency. Many fins configurations can be used with this heat exchanger such as straight fins, offset fins, and wavy fins.

Advantages:

- Compact size

- Heat transfer efficiency is higher than the shell and tube exchanger
- Easy to clean and maintain
- Capacity can be increased by adding more plates
- Easy to remove the leaking plates

Disadvantages:

- Preliminary cost is high since the titanium plates are expensive
- Hard to detect leakage
- Limitation of the operating temperatures
- High pressure drop

The miniaturization trend of components and the development in micro scale technology led to the utilization of micro scale devices in many applications. The effective use of these devices depends mainly on their ability to transfer heat efficiently. The industry nowadays presents many challenges to the design of heat exchangers based on the developing technology. Compact size, high heat transfer, and low costs are the main requirements when it comes to heat exchangers. Another challenge that faces the industry is providing higher heat transfer and great equipment durability. This challenge is even harder to meet when the aim is to constantly maintain equipment size and limit costs. It was very important to find an alternative to the conventional heat exchangers with a smaller size but an increase in the surface area. For example, the automotive industry requires smaller efficient components that will not add weight and size to the vehicle. Microchannel heat exchangers have been presented as the solution to the problem due to their higher heat transfer area per volume ratio and small sizes. Some of the advantages of using *microchannel heat exchangers* over the other heat exchangers are:

- Increased component life
- Improved heat transfer coefficient with a large number of smaller channels
- volume and weight reduction
- Lower costs due to less material being used in fabrication
- Smaller size allows for an increase in mobility and uses
- improved durability due to better corrosion resistance

Usually fins are placed in between the microchannels to increase the heat transfer. Since the development of this technology, microchannels have been used in many applications such as automotive industry, air conditioning, oil cooler coils, and condensers. They have proven to have a superior performance over the conventional heat exchangers. When high heat transfer rate, high mass flow rates, and low pressure drop are required, MCHXs can be the best suggestion to use in thermal systems. They mainly rely on the smaller fluid hydraulic diameter of the channels ($\leq 1\text{mm}$). Kandlikar (2006) explained the relationship between the channel hydraulic diameter and heat transfer coefficient. He stated that the value of Nu for fully developed laminar flow under constant heat flux is 3.61. Additionally, the variation of Nu with the channel diameter for air and water was presented. They have concluded that with the reduction of the channel diameter, the heat transfer coefficient increases. This can be shown in the following equation.

$$h = Nu \left(\frac{k}{D_h} \right) \quad (1)$$

Where, h represents the heat transfer coefficient, Nu is Nusselt number, k is the thermal conductivity of the fluid, and D_h is the channel hydraulic diameter.

Heating or cooling of one fluid with very high temperature differences and mass flow rates demands high heat transfer rates from the system. The compromise between the high heat transfer rate and the increase in pressure drop (energy loss) is a crucial problem in the design of micro scale exchangers, since the high pressure drop demands high mechanic power to run the system. Another issue is the fouling in the small channels. Therefore, it is highly recommended that only clean fluids would be used in the MCHX along with the use of filters, since it is very expensive to perform cleaning and maintenance. These are some of the real challenges faced by engineers and researchers. However, MCHXs have been proven to have very high convective heat transfer coefficients higher than that of the conventional heat exchangers. Some of the methods used to manufacture MCHXs are; micromachining, stereolithography, chemical etching, and LIGA (lithography, molding, and electroplating) Ashman and Kandlikar (2006). The utilization of cross flow arrangement in this type of exchangers allows for higher heat transfer per unit volume or unit mass. The increase in the surface area density decreases the heat exchanger volume required for the same thermal power, the compactness feature. This results in a significant reduction in the cost as well as the space that is needed when manufacturing or installing the heat exchanger. The fluid held up in the microchannels is very small, therefore this is an essential advantage when explosive or toxic fluids are to be used.

1.2 The First and Second Law of Thermodynamics

Humans use energy resources to provide their basic needs and to have a better life quality. Energy exists in many forms such as thermal, mechanical, potential, kinetic, etc. The constant increase of energy costs and the limitation of energy resources are very

important issues that need to be considered. In recent years, researchers were trying to find ways to reduce energy consumption, and this problem raised awareness for more efficient use of energy. The reduced size and weight of the MCHX result in a lighter system, adding to that the lower pressure drop on the airside may reduce the required fan size, resulting in reducing the component cost. Also, the use of aluminum in the construction of the MCHX allows for higher corrosion resistance. These all contribute to lower energy consumption.

Evaluating a system performance using the first law of thermodynamics is common, but it will not provide information regarding the quality of the heat transfer process. Therefore, second law is considered a very important tool used to analyze the heat exchanger performance and predict how close this performance is to the second law perfectness. Usually, the second law is used along with the first law to detect the irreversibilities and show the location of the inefficiencies within systems. The second law analysis is a well known tool to describe the work potential of energy. The first law of thermodynamics deals with the quantity of energy and states that energy can neither be created nor destroyed only altered in form. The conservation of energy principle simply means that the energy entering and exiting the system should be equal. For real processes, this definition can be to some extent different due to heat loss, and exergy consumption, energy in and out do not balance. The first law ensures an energy balance but it is the second law that plays an important role in evaluating systems performance by detecting the locations of exergy destruction within a system and therefore, optimize its efficiency and performance. The performance optimization of heat exchangers is of great importance for an efficient utilization of energy.

The conventional heat balance method reveals the overall thermodynamic performance of the system, but it cannot identify the sources of irreversibilities in each component of the system. On the other hand, second law analysis for energy related systems has many advantages over the conventional heat balance method for their design and performance evaluation. It provides a more accurate measurement of the actual inefficiencies in the system and the true location of these inefficiencies. And also it provides a true measure of the efficiency of the system for complex systems.

The loss of exergy (available energy) in a thermodynamic process is mainly due to the associated irreversibilities that lead to the generation of entropy. Heat exchangers are characterized with two types of losses; due to frictional pressure drop and heat transfer due to finite temperature difference. These losses are called thermodynamic irreversibilities and an investigation of a process based on these irreversibilities is called second law analysis. Second law analysis includes thermodynamics and fundamental heat transfer principles; it is used to optimize and model devices such as heat exchangers by taking into account any types of irreversibilities. One of the second law analysis methods is the entropy generation minimization (EGM), which tells us what happens to the energy within the system as it changes from one state to the other, and where energy is being lost.

The amount of energy transferred across a heat exchanger depends upon the temperature difference of the fluids and the flow rates. When it comes to heat exchangers, efficiency is one of the major concerns that face designers. Heat exchangers with a very large size were utilized to maximize the heat transfer surface in order to solve this problem. Another problem that becomes visible is sustainability; it is about reducing the amount of material used through manufacturing, and use material that has the capacity to endure

many years. With the development of the micro scale technology, cost and size problems of heat exchangers were solved due to less material being used in manufacturing and the reduction in the size and weight solving the mobility problem.

The total energy in a system consists of available energy and unavailable energy. This system total energy is simply called *energy* and the available energy is called *exergy*. Unlike energy, exergy is consumed or destroyed, in any real processes due to irreversibilities. The exergy consumed in a process is proportional to the entropy generated. The conservation of energy law measures only the quantity of energy and a heat exchanger evaluation cannot be made based on the quantity alone; therefore the second law of thermodynamics is introduced to evaluate the quality of energy. The second law (increased entropy) illustrates that when using energy, the quality of energy deteriorates during any irreversible process. The second law analysis reveals whether an efficient thermal heat exchanger can be designed by minimizing any sources of irreversibilities or inefficiencies. Irreversibility plays a vital role in the design of any heat exchanger. Since real processes are irreversible processes, losses such as irreversibilities have to be minimized in order to gain good heat transfer quality and performance from such devices. Consideration must also be given to entropy generation when designing heat exchangers because of the associated irreversibility which can be caused by; flow imbalance, mixing, throttling, heat transfer due to finite temperature difference, and pressure drop. From thermodynamics point of view, the performance of a heat exchanger is higher at smaller (≈ 0) entropy generation.

If an ideal heat exchanger exists, it means that for given inlet conditions, it can transfer the maximum possible of heat. This heat exchanger should transfer heat from a hot fluid to a cold fluid and it has to follow the second law of thermodynamics, no entropy

generation. In real life there is no such an ideal heat exchanger because of the irreversibility and the exergy destruction. A complete thermodynamic performance evaluation of heat exchangers requires both the use of energy (first law) and second law analyses.

1.3 Motivation

The necessity in developing thermal system components that occupy the smallest space available and provide very high performance is a number one requirement for the industry nowadays. The developing technology of micro scale devices results in highly efficient heat exchangers with many advantages. Energy conservation, the efficient utilization of energy, and reduced exergy destruction are important issues that face the industry. The application of second law analysis allows the further investigation of the irreversibilities within the heat exchanger. Second law analysis reveals the degradation of energy, entropy generation, and the exergy destruction for a specific process.

The following motivations were obtained for heat exchangers working with single phase laminar flow:

- For a given volume, a microchannel heat exchanger occupies smaller space than a conventional heat exchanger, resulting in space saving and easy mobility. This is more important for systems where space availability is restricted.
- The small hydraulic diameter that results in a high heat transfer coefficient.
- Microchannel heat exchangers provide high surface area per volume ratio, therefore high heat transfer per volume.
- Minimum construction cost, reduced noise, and longer life since for laminar flow the erosion is reduced.
- The improved corrosion resistance and its one piece structure results in an improved durability and reliability.
- The use of [50-50%] ethylene glycol-water mixture as the working fluid has its advantages over using only water. Since ethylene glycol has the antifreeze damage protection.

Second law motivations:

- Provides an accurate measurement of the irreversibilities in heat exchangers.
- The increase in the thermodynamic performance of microchannel heat exchangers due to irreversibility minimization, since, irreversibilities cannot be avoided but can be reduced.

The low weight, the compact structure, and other advantages mentioned above make the microchannel heat exchangers a better alternative to the conventional heat exchangers. The reduced internal volume of the MCHX results in reducing the refrigerant charge. Also the lower airside pressure drop results in decreasing the fan speed (i.e. in condensers) which results in lower fan noise. Adding to that MCHXs are environmentally friendly since its aluminum construction is recyclable.

1.4 Objectives

Although many studies have been conducted on second law analysis of conventional heat exchangers, the author did not find any study regarding second law analysis of a microchannel heat exchanger (MCHX). The previous work on heat exchangers involved different channel shapes and sizes, but few studies were found using serpentine microchannel arrangement with circular cross section channels. Most of the work reviewed included the use of an ideal gas, water, and other incompressible fluids as the working fluids, but the use of ethylene glycol in MCHXs is scarce. According to the above statements, a necessity to study the utilization of a multiport serpentine MCHX with ethylene glycol-water mixture and air as the working fluids is found. The objectives of the current study are to investigate the second law losses for a single laminar flow MCHX and to study the effect of different parameters on its thermodynamic performance. This study considers the effect of entropy generation, exergy loss, pressure drop losses, heat transfer losses, and the effectiveness on this heat exchanger. The proposed study includes the following objectives,

- Identify the main irreversibilities that can occur in a heat exchanger.
- Introduce design parameters that may affect the thermal performance of a heat exchanger.
- Introduce second law analysis in heat exchangers and apply it to investigate and optimize their thermal performance.
- The use of the entropy generation minimization method to create a mathematical model to predict the entropy generation in heat exchangers working with one fluid as an incompressible and the other one as an ideal gas.

- Investigate the second law losses on the change in heat capacity rate ratio, maximum heat capacity rate, effectiveness, Reynolds number, and pressure drop.

In order to achieve the objectives of the current work, experiments will be conducted. For these experiments, a multiport serpentine microchannel heat exchanger with [50-50% ethylene glycol and air as the working fluids will be utilized in a single laminar phase. A mathematical model will be generated to predict the behaviour of this heat exchanger based on different parameters. The results obtained from the model will be compared with the measured data, and a comparison between the predicted results and the measured data will be presented.

CHAPTER II

REVIEW OF LITERATURE

2.1 General Review

This chapter will spot the light on some of the work that has been done on heat exchangers, and the use of second law analysis in heat exchangers. Due to the importance of heat exchangers in many engineering applications, a wide range of extensive studies have been carried out to optimize the performance of such devices. Several studies indicated that second law losses such as irreversibilities due to finite temperature difference, and pressure drop have a significant influence on the performance of heat exchangers. Although many works can be found on second law analysis of conventional heat exchangers, studies on second law analysis of microchannel heat exchangers with ethylene glycol-water mixture and air as the working fluids couldn't be found. Many researchers used different types of heat exchangers and channel configuration or arrangement. To acquaint the reader with such type of information, followed are some of the scopes of the major findings.

2.2 Heat Exchangers

A Heat exchanger is a very important component of many systems such as mechanical, electrical, and chemical. Usually, heat exchangers applications involve heating or cooling of a fluid. Other applications may include recovering the heat or rejecting it, applications can be extended further to include concentrate, crystallize, and control a fluid. The introduction of micro scale technology was first presented by

Tuckerman and Pease (1981) for cooling of electronic circuits. Their work was considered to be the first study on the use of microchannels in cooling systems, and it motivated many researchers to examine further the use of microchannels in heat transfer systems. Nowadays microchannel heat exchangers have been known as having high performance due to the very small channel diameter and enhanced surface area. Mehendale et al. (2000) reported the classification of heat exchangers with different channel diameters:

Table 1 Channel classification according to Mehendale:

Micro- heat exchangers	$D_h = 1 - 100 \mu\text{m}$
Meso- heat exchangers	$D_h = 100 \mu\text{m} - 1 \text{ mm}$
Compact heat exchangers	$D_h = 1 - 6 \text{ mm}$
Conventional heat exchangers	$D_h > 6 \text{ mm}$.

The introduction of microscale devices in thermal systems was first presented by Tuckerman and Pease (1981). Kang and Tseng (2007) developed a theoretical model that predicts the thermal and fluidic characteristics of a micro cross flow heat exchanger. The effect of pressure drop and effectiveness in the micro heat exchanger was presented using this model. They have concluded that the heat transfer rate and the pressure drop were affected by the average temperature of the hot and cold streams at the same effectiveness. They have also found that the relationship between the pressure drop and the heat transfer rate is also affected by the dimensions effect. Chad Harris et al. (2000) used a micro heat exchanger to maximize heat transfer for a given frontal area and specified pressure drop while using water-glycol and an ideal gas as the working fluids. They compared different

construction materials of micro heat exchangers with a conventional car radiator, and their results showed that the cross flow micro heat exchanger predicted performance is better than the radiator performance. Also, the micro heat exchanger was found to transfer more heat per volume or mass than the conventional heat exchanger. Li and Peterson (2007) developed a 3D heat transfer model for silicon based microchannel heat sinks. The thermal resistance was calculated for different pumping powers. A comparison of the numerical results with the Tuckerman and Pease experimental results was made. It was found that the overall cooling capacity can be enhanced by more than 20% by the means of using the optimized spacing and channel dimensions. Heat exchangers as a system component was also studied and analyzed by Yang et al. (2008).

Khan and Fartaj (2010) investigated the heat and fluid flow for various working fluids of different microchannel air-to-liquid cross flow test specimens. Their study reviewed the many potential applications of the microchannel heat exchangers, since they provide high heat transfer, reduced weight, energy, and space over traditional heat exchangers. The investigation of heat transfer was also extended to include different heat exchanger geometries [Kavakakpinar and Bicer (2005), San and Pai (2009)]

2.3 Second Law Analysis

Second law analysis has been recognized as an effective technique to evaluate the thermodynamic performance of heat exchangers. Combined with the first law of thermodynamics, it can detect and measure the ineffectiveness of systems and the main causes for the loss of exergy within these systems. Second law analysis has been applied to heat exchangers by many researchers. McClintock (1951) was the first to introduce the irreversibility concept to the design of heat exchangers. This concept was used to

estimate and minimize the waste energy in heat exchangers. Since that, the entropy generation concept in a heat exchanger was studied extensively by Bejan (1977, 1978, 1979, and 1982). Bejan introduced balanced and imbalanced counter flow heat exchangers, for a fixed irreversibility and minimum heat transfer surface. The investigation of the minimization of the size of heat exchangers was performed using the irreversibility concept. The dimensionless entropy generation number, N_s , was presented, and it was defined as the total entropy generation divided by the minimum heat capacity rate of the fluids.

Xu (1996) introduced a modified entropy generation number which is the entropy generation per unit amount of heat which was compared with Bejan's entropy generation number. This new number is presented to evaluate the irreversibility of the heat exchanger. They have investigated the entropy generation due to friction and found that a minimum entropy generation number exists as the NTU and the heat capacity rate ratio are varied.

Ogulata and Doba (1997) performed an entropy generation minimization on a cross flow plate type heat exchanger. They took into consideration the temperatures and velocity of the air, as well as the pressure losses within the system. They have found that the minimum entropy generation number depends on the optimum flow path length, mass velocity, and heat transfer area. The variation of entropy generation number with these parameters was analysed and presented.

Many factors that have an influence on the heat exchanger performance were discussed by Shah and Sekulic (2003). They reviewed different heat exchanger design methods using different flow arrangements. Thermodynamic analysis and heat exchanger optimization were also introduced. First and second law of thermodynamics modeling

was performed, then different types of irreversibilities were presented; finite temperature differences, fluid mixing, and frictional pressure drop irreversibilities.

The necessity of a systematic design of heat exchangers using second law analysis was recalled and discussed by Yilmaz (2001). For heat exchangers, a performance evaluation criteria based on the second law analysis was introduced. Their work showed that some of the second law performance criteria which include; using entropy or exergy as an evaluation parameter are related to each other, and attention should be paid on the constraints as well as the characteristics when selecting one of those criteria.

A study was conducted on the optimization of plate fin heat sinks by Culham and Muzychka (2001). They presented a procedure using the minimization of entropy generation for heat transfer and fluid friction to optimize the design parameters (geometric, heat dissipation, material properties, and flow conditions) of the heat sink in order to reduce the operating temperature.

Allouache and Chikh (2006) utilized a combination of the first and second law analysis to analyze the performance of a double pipe heat exchanger using a porous medium. Entropy generation due to heat transfer and fluid frictions was found with the considered parameters. Results show that the inlet temperature difference between the two fluids, effective thermal conductivity, and porous layer thickness and its permeability affect the minimization of the rate of entropy generation. Also, for the total entropy generation, it was found that the fully porous annular gap provided the best results.

Second law of thermodynamics was utilized by Saboya et al. (1999), on different heat exchanger flow arrangements; counter, parallel, and cross flow. A comparison between the heat exchangers was made to find out which one has the lower irreversibility rate. Their conclusion was that; although it is said that the counter flow arrangement will have

lower irreversibility. If the counter flow has the less irreversibility, then this irreversibility is less than the other heat exchangers, and when it has more reversibility it more than the other heat exchangers. A second law analysis on a parallel plate microchannel with asymmetrically heated walls was applied by Sadeghi and Saidi (2010). They have found that as the wall heat fluxes ratio increases, the greater the entropy generation will be for positive Brinkman numbers, while for negative values of Brinkman, the reversed case is true. Furthermore, the influences of rarefaction on entropy generation were shown to be negligible for low Peclet number flows.

A mathematical model based on the conservation of energy equation and the central finite difference method was presented by Naphon (2006) to obtain the entropy generation, exergy loss, and temperature distribution in a horizontal concentric tube heat exchanger. Experimental and theoretical results were presented; results show that the inlet conditions of the two working fluids in a heat exchanger have significant effect on heat transfer characteristics, entropy generation, entropy generation number, and exergy loss. Another combined thermodynamic analysis of heat transfer and fluid flow on a counter flow double pipe heat exchanger using air as the working fluid were performed by Mohamed (2006). His work explained that heat exchanger irreversibility occurs due to the flow imbalance. He found that operating the heat exchanger on effectiveness of more than 0.5 would result in lower irreversibility. Through adopting a new equation, the entropy generation numbers were expressed for imbalanced similar design heat exchangers. A comparison of his results with the data obtained using Bejan's definition for entropy generation number was made. Also, he showed that the temperature difference effect on entropy generation number is higher compared with the pressure drop effect.

A theoretical analysis of a heat exchanger with negligible fluid flow pressure drop was presented by Assad (2010). The objective of his study was to find whether to operate the heat exchanger based on a hot fluid minimum or maximum heat capacity rate. He introduced the entropy generation number ratio S^* , and found that S^* depends on the inlet temperatures ratio of the cold and hot fluids when S^* exceeds 1. A thermodynamic optimization of a cross flow heat exchanger with a ram air on the cold side was presented by Alebrahim (2010). Their study was consisted of two parts; first, they optimized the heat exchanger, by optimizing the geometric features, such as the ratio of channel spacing, and flow lengths, then the results were reported for this optimization. In their second part of study, the irreversibility due to discharging the ram air flow to the atmosphere was taken into consideration when finding the entropy generation rate. They concluded that the features that have been optimized were relatively insensitive to the effect of discharging the ram air flow, leading to more robustness in the thermodynamic optimum. More work on entropy generation and exergy analysis can be found in [Sarangi and Choowdhury (1982), Grazzini and Gori (1988), Aceves-Saborio et al. (1989), Sahiti et al. (2008)]

A new expression of effectiveness was presented by Xiong (1996), where an ideal heat exchanger model and temperature histogram methods were used. They studied the relation between entropy generation number and effectiveness. A Comprehensive Thermal Performance Coefficient (CTPE) was developed and presented to express both the quantity and the quality of the transferred heat in a heat exchanger. Second law analysis on heat exchangers was studied by Hesselgreaves (2000). New derived relationships for a balanced counter flow arrangement to find the local rate generation process. He reported that the flow Mach number controls the entropy generation

relationship for gas flows and he found it consistent with other research work. As part of the system, the heat exchanger was analyzed using second law analysis methods; energy, exergy, and entropy by Fartaj (2004). More work has been extended to include second law analysis on fins. Second law analysis on a mini cross flow heat exchanger equipped with constructal distributor/collector was implemented by Fan and Luo (2009). They investigated the heat transfer as well as the hydraulic characteristics of that heat exchanger. In their work, the addition of constructal component and its effect on the thermal performance, entropy generation, exergy loss, and the second law effectiveness of the heat exchanger were discussed. They found that the integration of the constructal component can increase the pressure drop which will lead to higher irreversibility, and they recommended working in the laminar regime. The relationship between entropy generation extrema and heat exchanger effectiveness was also discussed by Shah and Skiepko (2004). He et al. (2009) investigated the second law analysis applied to a novel heat exchanger with helical baffles using cold water and hot oil as the working fluids. Heat transfer, pressure drop, entropy generation, and exergy loss were investigated and compared with the conventional shell and tube heat exchanger results. From the second law of thermodynamics viewpoint, they found that the efficiency of the heat exchanger with helical baffles is higher than that of the conventional heat exchanger with segmental baffles. Some other related work on second law in heat exchangers can also be found in [Vargas (2001), Bejan (1988), Poulikakos (1982), and Bulck (1991), Guo et al. (2010)].

CHAPTER III

DESIGN AND METHODOLOGY

3.1 Theory Background

It is very important to study the performance optimization of heat exchangers since the efficient utilization of energy is an increasingly important issue. As has been stated earlier, energy can be conserved but cannot be destroyed, and it loses its quality. Since energy is the ability to do work, concerns should be made on conserving the available work, not energy. Energy analysis fails to recognize the lost work or the possibility of improvements or efficient use of resources. Heat exchangers are used in many fields of technology; therefore, the design of heat transfer devices as well as the heat transfer is an important issue. There are several ways used by researchers to reduce the amount of exergy destruction within a system, especially heat exchangers. Engineering thermodynamics listed several approaches to calculate the irreversibility within heat exchangers based on the second law of thermodynamics, followed are the three common techniques:

1. Exergy analysis
2. Thermoeconomics
3. Entropy generation minimization (EGM)

Exergy as defined by Bejan (1988) is the maximum work that can be obtained from a flow as it reaches the dead state. Since exergy destruction is related to the production of entropy, minimizing the entropy production will lead to decrease the exergy loss, improve the heat exchanger efficiency, and conserve energy. The smaller the heat exchanger, the higher the temperature difference and exergy destruction are. The

evaluation of heat exchangers based on exergy analysis has been used by many researchers [Das and Roetzel (1998), Prasad and Shen (1994), Can and et al. (1998), Prasad and Shen (1994), Bruges (1959), Reistad (1970), Golem and Brzustowski (1976), Mukherjee et al. (1987), and Yilbas et al. (1999)].

Another way to calculate the irreversibility is by using thermoeconomic analysis which involves the minimization of entropy generation and the thermal components cost Zubair et al. (1987). Rosen (1999) stated that “exergy is the commodity value of a system”, and he listed the objectives of using this technique as:

1. The right distribution of the economic recourses in order to improve the system design and operation.
2. The economic practicability and cost-effectiveness of a system.

Many works can be found regarding thermoeconomic analysis London and Shah (1983), Cornelissen (1997), and Tsatsaronis (1993).

For the third method Entropy Generation Minimization (EGM), in real world, there is no such an ideal heat exchanger. For this reason, processes are called irreversible, and the irreversibility in a process yields to an increase in the entropy production. Some of the losses associated with this method are; the losses due to heat transfer at finite temperature difference, and the losses due to fluid friction. Therefore, the purpose of this technique is to reduce these irreversibilities in order to keep the entropy generation at its minimum. The EGM method depends on the use of fluid mechanics, heat transfer, and thermodynamics in its application as it is illustrated in Figure (1).

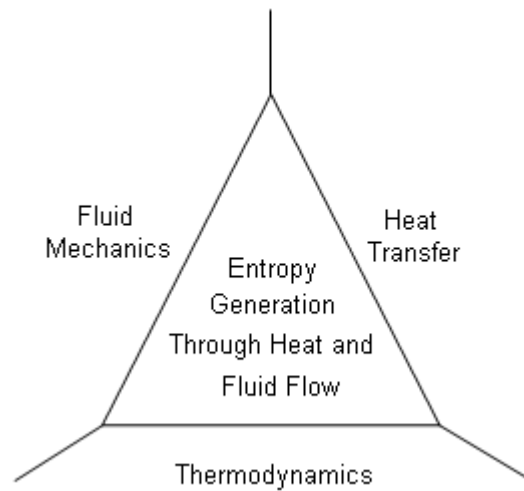


Figure 1 Entropy generation minimization field covered by (Bejan, 1982)

This method uses the non dimensional entropy generation number, N_s , which is defined as the entropy generation divided by the fluid heat capacity rate that is considered the most common way of Non-dimensionalizing entropy generation. Its value can range between $(0-\infty)$.

The difference between the exergy method and the entropy generation minimization method is that exergy uses only the first law, second law, and the properties of the environment. However, EGM characteristics are system modeling, development of \dot{S}_{gen} as a function of the model parameters and the ability to minimize the entropy generation rate.

For any thermal system, the first law is not enough to define the thermal performance of that system because of the existence of irreversibilities. The system consumes exergy due to the lack of ineffectiveness in its ability to transfer the available energy. Consider a cross flow heat exchanger, where two fluids are used, cold and hot.

Assumptions should be made to analyze and create a mathematical model that predicts the amount of entropy generation for a heat exchanger, these assumptions are;

- The heat exchanger runs at steady state.
- The effects of kinetic and potential energy are negligible.
- The specific heat of the two fluids is treated constant and their values were taken at an average temperature.
- The heat transfer by radiation from the heat exchanger or the test chamber to the surrounding is negligible.
- The axial conduction heat transfer along the heat exchanger slab is considered negligible.
- The heat transfer by conduction from the heat exchanger to the surrounding is negligible.

Many things are to be considered when evaluating the heat exchanger performance. Some of these considerations may include whether the flow is balanced or not, the presence or absence of the pressure drop, and running the system with minimum or maximum heat capacity rate on the hot fluid side.

3.2 Heat Exchangers with an Imbalance Flow

An imbalance heat exchanger means that the thermal capacity rates for both fluids are not the same $\dot{m}c_{p1} \neq \dot{m}c_{p2}$ and they are different with the ratio called $C^* = \frac{C_{min}}{C_{max}}$, where C_{min} and C_{max} are $(\dot{m}c_p)$, the minimum and maximum heat capacity rates of the two fluids, respectively.

3.3 First Law Analysis:

Energy balance, which includes the first law and the conservation of mass principle, is usually used to model heat exchangers. Efforts are made to use energy more efficiently and make good use of the available energy. In the current study, the heat exchanger is used to transfer the energy from the hot liquid flow to the cold air flow; this will lower the internal energy of the liquid and raises the internal energy of the air. The actual heat transfer rate given by the hot fluid was calculated on the liquid side as,

$$\delta Q = \dot{m}dh \quad (2)$$

Where Q is the heat transfer rate to the fluid concerned associated with the infinitesimal state change. The energy balance equation for a heat exchanger can be expressed as,

$$\dot{m}_{\text{hot}}c_{p_{\text{hot}}}(h_{\text{hot,in}} - h_{\text{hot,out}}) + \dot{m}_{\text{cold}}c_{p_{\text{cold}}}(h_{\text{cold,out}} - h_{\text{cold,in}}) = 0 \quad (3)$$

For a heat exchanger, the enthalpy balance for each of the fluids (hot and cold) is:

$$\dot{Q}_{\text{hot}} = \dot{m}_{\text{hot}}c_{p_{\text{hot}}}(h_{\text{hot,in}} - h_{\text{hot,out}}) \quad (4)$$

$$\dot{Q}_{\text{cold}} = \dot{m}_{\text{cold}}c_{p_{\text{cold}}}(h_{\text{cold,out}} - h_{\text{cold,in}}) \quad (5)$$

In terms of specific heat and temperature difference and according to the first law (conservation of energy), the actual heat transfer can be written as,

$$\dot{Q}_{hot} = \dot{m}_{hot}c_{p_{hot}} (T_{hot,in} - T_{hot,out}) \quad (6)$$

$$\dot{Q}_{cold} = \dot{m}_{cold}c_{p_{cold}} (T_{cold,out} - T_{cold,in}) \quad (7)$$

The difference of the two heat transfer rates, the heat loss, is illustrated in equation (8),

$$\dot{Q}_{loss} = \dot{Q}_{hot} - \dot{Q}_{cold} \quad (8)$$

If the heat exchanger is well insulated and there is no heat loss to the surrounding, therefore, for experimental calculations, the average heat transfer rate is considered and it is found as,

$$\dot{Q}_{avg} = \frac{\dot{Q}_{hot} + \dot{Q}_{cold}}{2} \quad (9)$$

3.4 Effectiveness

Effectiveness of a heat exchanger is defined as the ratio of the actual heat transfer rate to the maximum possible heat transfer rate. It is the measure of the heat exchanger performance, and it expects how a heat exchanger may function. Effectiveness is considered to be the best method used to compare different heat exchangers. Effectiveness is dependent on the flow arrangement, heat capacity rate ratio, heat transfer, and the temperature difference. The basic definition of heat exchanger effectiveness can be expressed as,

$$\varepsilon = \frac{Q_{act}}{Q_{max}} \quad (10)$$

Since effectiveness represents the actual heat transfer over the maximum, the actual heat transfer rate Q for a heat exchanger can be found either by using the energy transferred from the hot fluid or the energy received by the cold fluid and it can be found using equations (6) or (7). While, the maximum possible heat that can be transferred is determined by,

$$Q_{max} = C_{min}(T_{h,i} - T_{c,i}) \quad (11)$$

Where, C_{min} is the minimum heat capacity rate of the two fluids. The effectiveness based on the hot and the cold fluids respectively can be expressed as:

$$\varepsilon = \frac{C_{hot}(T_{h,i} - T_{h,o})}{C_{min}(T_{h,i} - T_{c,i})} \quad (12)$$

$$\varepsilon = \frac{C_{cold}(T_{c,o} - T_{c,i})}{C_{min}(T_{h,i} - T_{c,i})} \quad (13)$$

$$\varepsilon = \frac{C_{hot}(T_{h,i} - T_{h,o})}{C_{min}(T_{h,i} - T_{c,i})} = \frac{C_{cold}(T_{c,o} - T_{c,i})}{C_{min}(T_{h,i} - T_{c,i})} \quad (14)$$

Effectiveness values range between 0 and 1. It can also used to find the outlet temperatures of a stream.

3.5 Second Law Analysis-Entropy Generation Approach:

3.5.1 Irreversibilities

When using a heat exchanger that operates in steady state conditions and the flow of hot and cold fluids occurs from the inlets to the exits, the total loss of the available energy is defined as irreversibility. Irreversibility can be represented by the heat transfer rate and the frictional pressure drop and it measures the quality reduction of the heat exchanger. The analysis based on second law provides valuable guides during the design process since, reducing irreversibilities means reducing energy expenses. The entropy balance equation based on the second law of thermodynamics for a control volume heat exchanger running at a steady state (no entropy change with respect to time) can be written (Cengel 2006) as,

$$\dot{S}_{gen} + \int \frac{\partial Q_{loss}}{T} + \sum_{in} \dot{m}s - \sum_{out} \dot{m}s = 0 \quad (15)$$

Where, \dot{m} is the mass flow rate, s is the specific entropy of the fluid (kJ/kg.K). Q_{loss} is the heat loss, and \dot{S}_{gen} is the rate of the entropy generation.

When a well insulated heat exchanger is presented that has no heat loss to the surrounding, the entropy generation equation, using the entropy change of the two fluids, can be found as:

$$\dot{S}_{gen} = \dot{m}_{hot}(s_{hot,out} - s_{hot,in}) + \dot{m}_{cold}(s_{cold,out} - s_{cold,in}) \quad (15)$$

A process is called reversible when it can return to its initial state without the need to apply an additional power or to lose energy, and it is called irreversible when it requires power or loses energy. There are many losses or irreversibilities that can be detected within a system, due to flow imbalance, mixing, finite temperature difference, throttling, and pressure drop losses. This study will spot the light on two main types of irreversibilities in a heat exchanger; due to finite temperature difference and pressure drop. Hence, the total entropy generation equation that includes the two irreversibilities can be presented as,

$$\dot{S}_{gen} = \dot{S}_{gen,\Delta T} + \dot{S}_{gen,\Delta P} \quad (16)$$

3.5.2 The Mathematical Model

First case: the liquid side has the minimum heat capacity:

Consider two streams in a cross flow heat exchanger, hot (incompressible fluid) and cold (ideal gas). The entropy generation rate based on the two irreversibilities discussed earlier can be presented as in [Cengel (2006)]:

$$\dot{S}_{gen,\Delta T} = C_1 \ln \left(\frac{T_{1o}}{T_{1i}} \right) + C_2 \ln \left(\frac{T_{2o}}{T_{2i}} \right) \quad (17)$$

$$\dot{S}_{gen,\Delta P} = -\dot{m}_1 R_1 \ln \left(\frac{P_{1o}}{P_{1i}} \right) - \dot{m}_2 R_2 \ln \left(\frac{P_{2o}}{P_{2i}} \right) \quad (18)$$

$$\dot{S}_{gen,total} = C_1 \ln \left(\frac{T_{1o}}{T_{1i}} \right) - \dot{m}_1 R_1 \ln \left(\frac{P_{1o}}{P_{1i}} \right) + C_2 \ln \left(\frac{T_{2o}}{T_{2i}} \right) - \dot{m}_2 R_2 \ln \left(\frac{P_{2o}}{P_{2i}} \right) \quad (19)$$

Where R (kJ/kg.K) is the gas constant, T_{1i} , T_{1o} , P_{1i} , and P_{1o} are the inlet and outlet temperatures and pressures of the hot fluid, T_{2i} , T_{2o} , P_{2i} , and P_{2o} are the inlet and outlet temperatures and pressures of the cold fluid. From the experiments, the hot fluid was considered to have the minimum heat capacity rate, while, the cold fluid has the maximum heat capacity rate. For this case, the outlet temperatures of the two fluids can be derived using eq. (14):

$$T_{1o} = T_{1i} - \varepsilon(T_{1i} - T_{2i}) \quad (20)$$

$$T_{2o} = T_{2i} - \varepsilon C^*(T_{1i} - T_{2i}) \quad (21)$$

Dividing equations (20) by T_{1i} , and equation (21) by T_{2i} we get:

$$\frac{T_{1o}}{T_{1i}} = 1 - \varepsilon \left(1 - \frac{T_{2i}}{T_{1i}}\right) \quad (22)$$

$$\frac{T_{2o}}{T_{2i}} = 1 + \varepsilon C^* \left(\frac{T_{1i}}{T_{2i}} - 1\right) \quad (23)$$

The outlet pressure drop of the two fluids can be written as:

$$P_{1o} = P_{1i} - \Delta P_1 \quad (24)$$

$$P_{2o} = P_{2i} - \Delta P_2 \quad (25)$$

Since for incompressible fluids $dV \cong 0$ [Cengel (2006)], therefore, the second term in equation (19) will be neglected, and the entropy generation of the liquid is due to the temperature difference only. Equation (19) will be rewritten as follows:

$$\dot{S}_{gen,total} = C_1 \ln \left(\frac{T_{1o}}{T_{1i}} \right) + C_2 \ln \left(\frac{T_{2o}}{T_{2i}} \right) - \dot{m}_2 R_2 \ln \left(\frac{P_{2o}}{P_{2i}} \right) \quad (25)$$

The ratio of the outlet to inlet pressure of the airside can be written as,

$$\frac{P_{2o}}{P_{2i}} = 1 - \frac{\Delta P_2}{P_{2i}} \quad (26)$$

Using equations (22), (23), (25), and then substituting them into (26), the entropy generation rate can be written as:

$$\dot{S}_{gen} = C_1 \ln(1 - \varepsilon(1 - T_R)) + C_2 \ln \left(1 + \varepsilon C^* \left(\frac{1}{T_R} - 1 \right) \right) - \dot{m}_2 R_2 \ln \left(1 - \frac{\Delta P_2}{P_{2i}} \right) \quad (27)$$

Where, $T_R = \frac{T_{2i}}{T_{1i}}$ is the fluids inlet temperatures ratio.

Second case: the liquid side has the maximum heat capacity rate:

Consider a case where the hot fluid has the maximum heat capacity rate, while the cold fluid has the minimum heat capacity rate, the inlet fluids temperatures ratio will be,

$$\frac{T_{1o}}{T_{1i}} = 1 - \frac{\varepsilon}{C^*} (1 - T_R) \quad (28)$$

$$\frac{T_{2o}}{T_{2i}} = 1 + \varepsilon \left(\frac{1}{T_R} - 1 \right) \quad (29)$$

Using the definition of the pressure ratio from eq. (26), the entropy generation for this case will be:

$$\dot{S}_{gen} = C_{max} \ln(1 - \varepsilon C^*(1 - T_R)) + C_{min} \ln \left(1 + \varepsilon \left(\frac{1}{T_R} - 1 \right) \right) - \dot{m}_2 R_2 \ln \left(1 - \frac{\Delta P_2}{P_{2i}} \right) \quad (30)$$

3.5.3 Entropy Generation Number

The entropy generation number or the dimensionless entropy generation rate was first introduced by [Bejan (1977)]. It was defined as the ratio of the entropy generation to the smallest heat capacity rate of the fluids. The heat exchanger will have a better performance if the entropy generation is at its minimum (close to 0). This dimensionless number can clearly express how a heat exchanger performance is close to an ideal heat exchanger in terms of thermal losses. Applying Bejan's definition to the first case will yield,

$$N_{s1} = \frac{\dot{S}_{gen}}{\dot{m}_1 c_{p1}} \quad (31)$$

Substituting eq. (27) into eq. (31), we get,

$$N_{s1} = \ln(1 - \varepsilon(1 - T_R)) + \frac{1}{C^*} \ln \left(1 + \varepsilon C^* \left(\frac{1}{T_R} - 1 \right) \right) - \frac{\dot{m}_2 R_2}{\dot{m}_1 c_{p1}} \ln \left(1 - \frac{\Delta P_2}{P_{2i}} \right) \quad (32)$$

Equation (32) represents the entropy generation number for which the hot fluid has the minimum heat capacity rate. Using the same approach by taking eq. (30), and substituting it into eq. (31), N_{s2} is the entropy generation number, for which the hot fluid has the maximum heat capacity rate as follows,

$$N_{s2} = \frac{\dot{S}_{gen}}{\dot{m}_2 \cdot c_{p2}} \quad (33)$$

$$N_{s2} = C^* \ln(1 - \varepsilon C^* (1 - T_R)) + \ln \left(1 + \varepsilon \left(\frac{1}{T_R} - 1 \right) \right) - \frac{R_2}{C_{p2}} \ln \left(1 - \frac{\Delta P_2}{P_{2i}} \right) \quad (34)$$

The predicted entropy generation results can be obtained from equations (33), and (34).

3.5.4 Entropy Generation Number Ratio

The entropy generation number ratio was first presented by [Assad (2010)] to compare the two entropy generation numbers obtained from the two cases mentioned earlier, and to show whether to operate the heat exchanger with minimum or maximum heat capacity rate on the hot fluid side. Considering both cases having the same heat capacity rate ratio and effectiveness, S^* is defined as,

$$S^* = \frac{N_{s1}}{N_{s2}} \quad (35)$$

Where, this ratio can illustrate the effect of a flow with a minimum or maximum heat capacity rate on the entropy generation.

3.5.5 Exergy Destruction

In view of the fact that energy loses its potential when it experiences a change, thus it cannot be the measure of that potential. Exergy is the maximum work that can be received from a stream as it reaches the dead state. Exergy destruction occurs due to irreversibilities within the system. While the exergy destruction approaches its minimum ($\rightarrow 0$), a heat exchanger reaches its maximum thermal performance. In this work, exergy destroyed is the difference between the exergy supplied by the hot [50-50%] ethylene glycol-water and the exergy gained by the cold air stream. The exergy balance for a steady flow system can be presented as,

The exergy balance for an irreversible system can be shown as:

$$X_{in} - X_{out} - X_{destroyed} = \Delta X_{system} \quad (36)$$

For a steady flow process, when dX/dt is equal to zero, equation (36) will be reduced to,

$$X_{in} - X_{out} - X_{destroyed} = 0 \quad (37)$$

$$m_h(x_{hi} - x_{ho}) = m_c(x_{ci} - x_{co}) + X_{destroyed} \quad (38)$$

Where, x is the specific flow exergy, and $X_{destroyed}$ is the exergy destroyed within the system. This equation can be also written as,

$$\text{Exergy supplied by the hot fluid} = \text{Exergy gained by the cold fluid} + \text{Exergy destruction} \quad (39)$$

The change of exergy per unit mass of fluid is:

$$(x_i - x_o) = (h_i - h_o) - T_0(s_i - s_o) \quad (40)$$

Where, s represents the specific entropy of the fluid. Since, exergy destroyed is proportional to the entropy generation according to Gouy-Stodola theorem;

$$\dot{X}_{destroyed} = T_0 \dot{S}_{gen} \quad (41)$$

3.5.6 Modified Entropy Generation Number

The entropy generation found using Bejan's definition can be only applied to a power generation or a process in which the heat exchanger works with two streams having an unspecified heat load and an uncontrolled entropy generation Hesselgreaves (2000). Therefore, the heat exchanger works only to allow the system to work with certain irreversibility. This scenario will lead to the entropy generation paradox, where the decrease of the entropy generation number will lead to the decrease in the effectiveness of the heat exchanger. Witte and (1983), London and Shah (1983) used $(\frac{\dot{Q}}{T_0})$ to non-dimensionalize the entropy generation. This approach has a disadvantage since it introduced T_0 , the atmosphere temperature to the analysis. For these mentioned reasons, a modified entropy generation number was presented by Hesselgreaves in order to solve the entropy generation paradox. The new non-dimensional entropy generation is by

dividing the entropy generation by $(\frac{\dot{Q}}{T_{c,i}})$. Therefore, the modified entropy generation number can be shown as,

$$N_{s,mod} = \frac{T_{c,i}\dot{S}_{gen}}{\dot{Q}} \quad (42)$$

Where, \dot{Q} is the actual heat transfer rate that can be obtained from the effectiveness definition as,

$$\dot{Q} = \dot{m}c_p\varepsilon(T_{h,i} - T_{c,i}) \quad (43)$$

Therefore, the entropy generation number is found as,

$$N_{s,mod} = \frac{\left[C_1 \ln(1-\varepsilon(1-T_R)) + C_2 \ln\left(1 + \varepsilon C^* \left(\frac{1}{T_R} - 1\right)\right) - \dot{m}_2 R_2 \ln\left(1 - \frac{\Delta P_2}{P_{2i}}\right) \right] [T_{c,i}]}{\dot{Q}} \quad (44)$$

$$N_{s,mod} = \frac{\left[\ln(1-\varepsilon(1-T_R)) + \frac{1}{C^*} \ln\left(1 + \varepsilon C^* \left(\frac{1}{T_R} - 1\right)\right) - \frac{R_2 c_{p,2}}{C^*} \ln\left(1 - \frac{\Delta P_2}{P_{2i}}\right) \right] [T_{c,i}]}{\varepsilon(T_{h,i} - T_{c,i})} \quad (45)$$

This modified entropy generation number is for the case where the minimum heat capacity rate is on the hot glycol side.

CHAPTER IV

EXPERIMENTAL SET-UP

4.1 General Introduction

A detailed schematic diagram of the experimental set up used in this study is shown in Figure 2. The test section (Khan and Fartaj 2010) that has been used was designed and fabricated for the University of Windsor, Thermal Management research laboratory. It mainly consists of an integrated closed loop thermal wind tunnel, test section, built in heat exchanger, and a data acquisition system. Inside the test section, a serpentine slab microchannel heat exchanger designed and manufactured for the University of Windsor thermal management laboratory is mounted. This experimental set-up includes many components that are essential to help in researching and performing different analysis regarding various types of heat exchangers such as circular tubes, elliptical tubes, and microchannel as well as the study of thermal systems. The other components of the experimental set up are; water tank, water heater, water pump, closed loop pipe network for water circulation, digital flow meter, air compressor, flexible hose, impeller flow meter, temperature gages, thermocouples (type T), resistance temperature detectors (RTDs), pressure gages, pressure transducers, valves, data acquisition system with LabView software, etc. All the experiments were conducted in the B05 laboratory located at the University of Windsor, Essex Hall building.

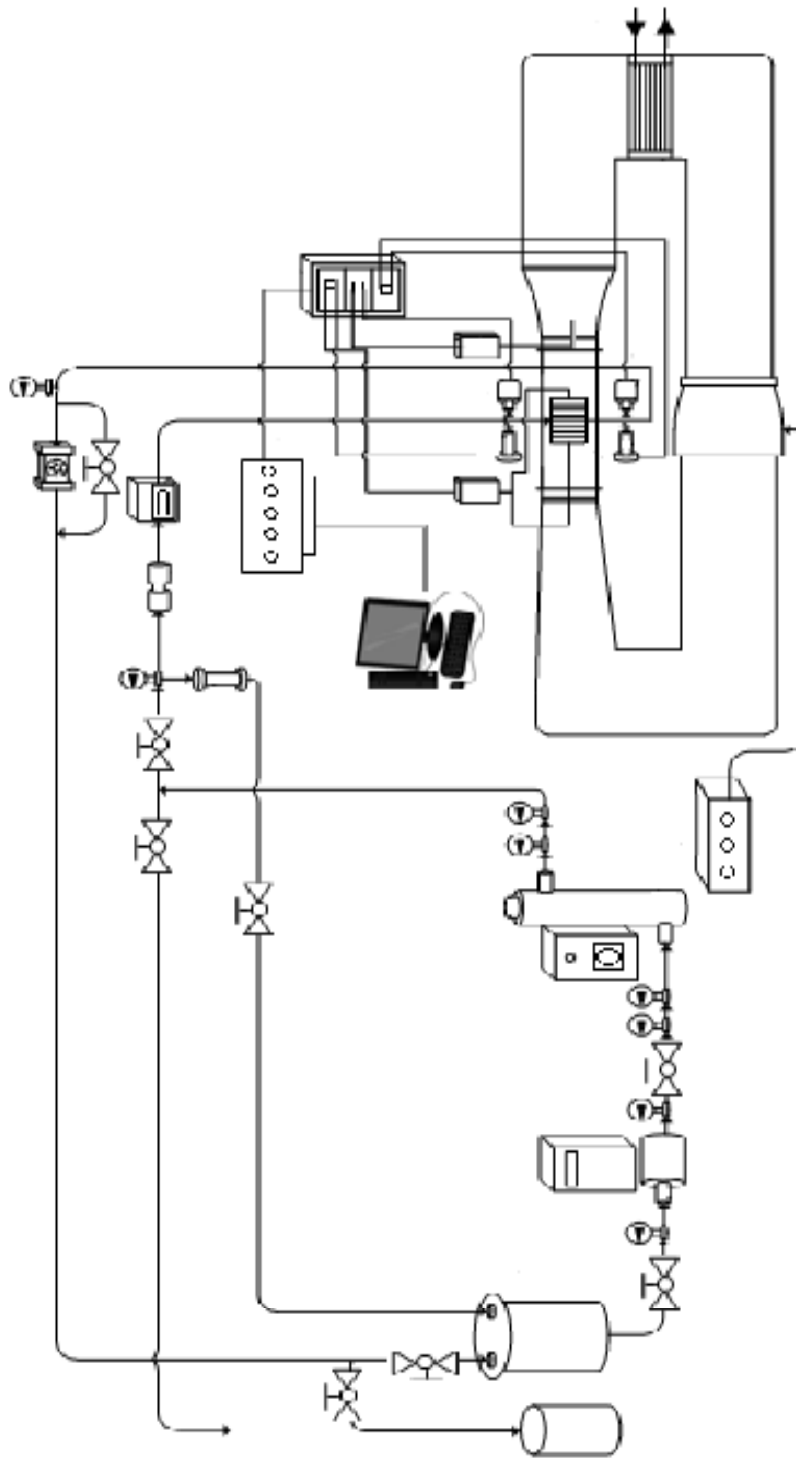


Figure 2 Schematic diagram of the experimental set-up

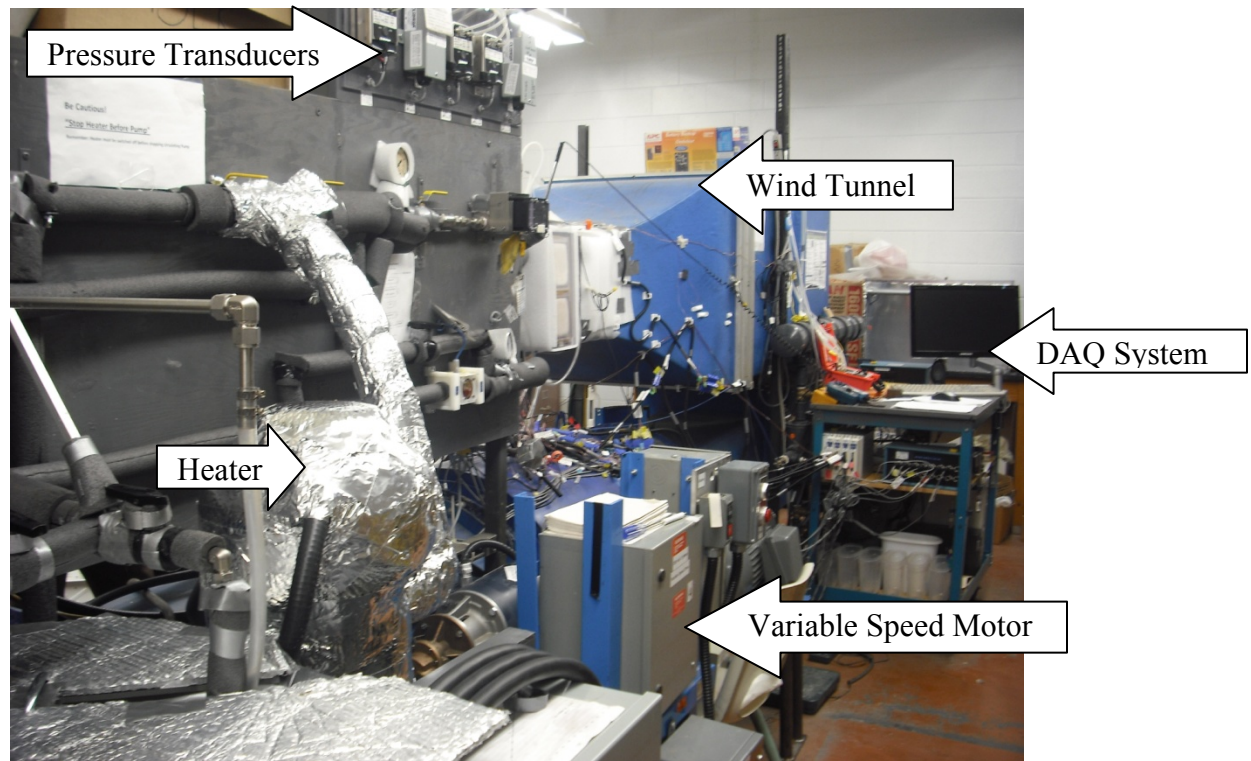


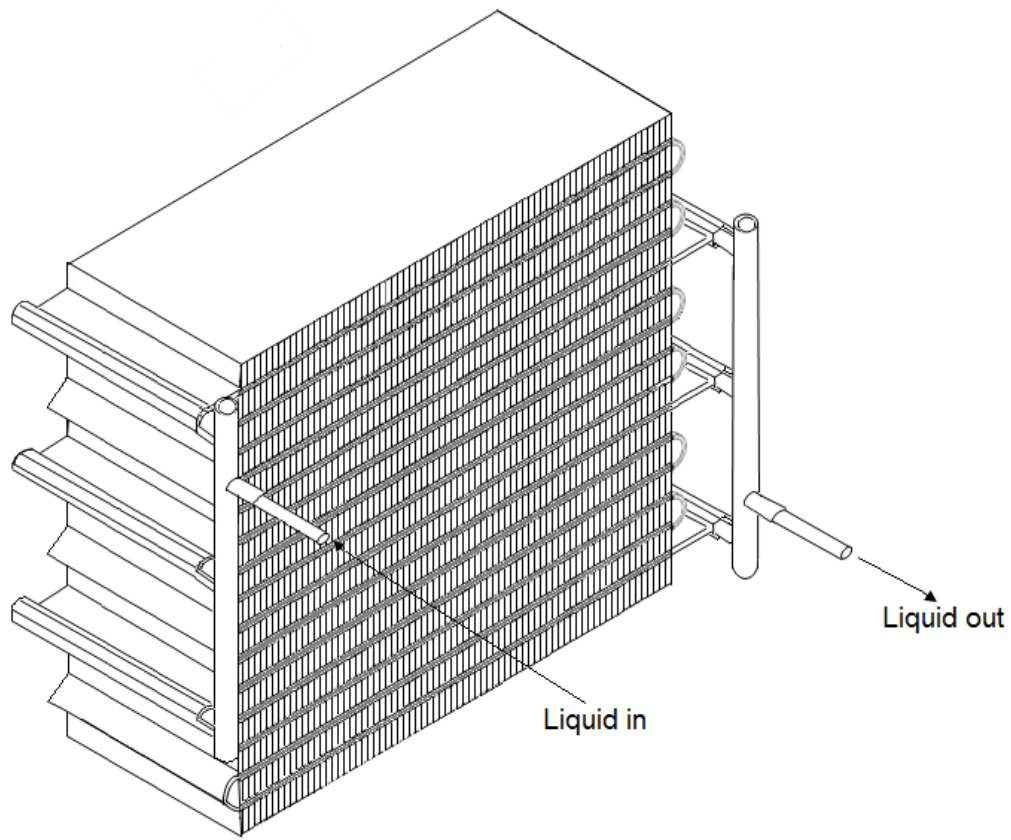
Figure 3 Experimental set-up

4.2 Experimental Set-Up Components

4.2.1 The Test Section and the MCHX

The microchannel heat exchanger (MCHX) is mounted in a well insulated test section with an inside dimensions of 305mm×305mm, and 610mm length. This test section has a square cross section and it is made of Plexiglas with a thermal conductivity of 0.19W/m.°C. This test section is well situated inside the wind tunnel in order to have a uniform flow of air through this chamber, and it also allows the installation of a Pitot static tube or a hot wire anemometer for velocity measurements. Holes are made on the side walls of the test section for pressure and velocity measurements.

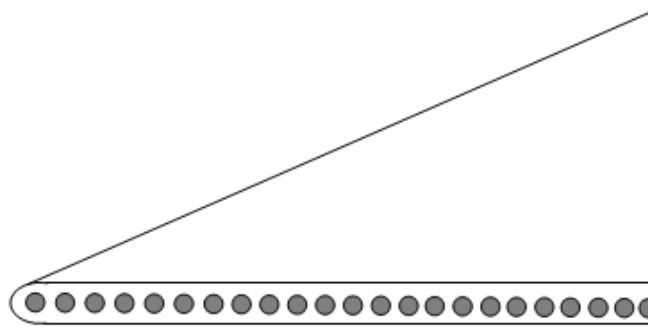
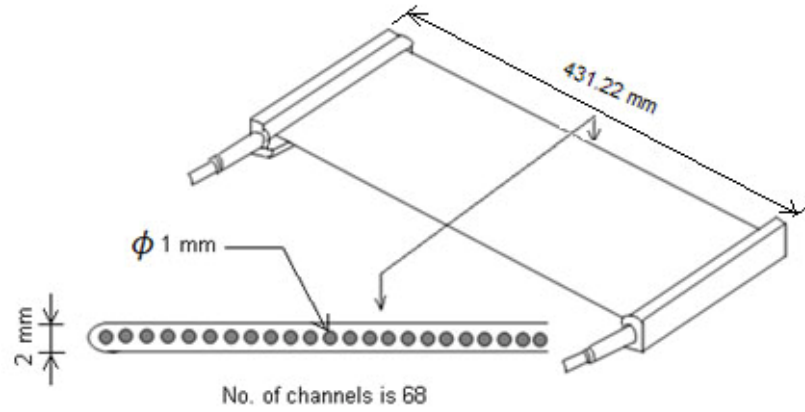
The MCHX used in this study is an aluminum heat exchanger with a cross flow arrangement as shown in Figure 4.a. It is a finned serpentine prototype MCHX of 3 circuits; each circuit has 5 serpentine slabs and each slab consists of 68 channels with a channel diameter of 1mm. Those 68 channels are distributed evenly over a 100 mm slab width as shown in Figure 4.b.



(a)

The MCHX dimensions are 305 mm wide, 285 mm high, and its depth in a parallel direction to the air flow is 100 mm. Its major components are inlet and exit pipes and headers. This MCHX is provided with wavy fins made of aluminum sheet having a fin density of 12 fins per 25.4 mm. The fin dimensions are as follows; 18 mm in height, the

distance from the centre of one of the fins to the other is 2.12 mm, and the length of the finned area is 304.79mm.



(b)

Figure 4 MCHX

(a) Serpentine microchannel heat exchanger

(b) Microchannel heat exchanger slab

This combination of fins and channels is captured at the end by the header manifolds. The test chamber was insulated in such a way that only the heat exchange between the liquid and the air flows occurs.

4.2.2 The Closed Loop Thermal Wind Tunnel

For the experiments, an integrated closed loop thermal wind tunnel was used that has a contraction ratio of 6.25 and a wall thickness of 10 mm. Its dimensions are 5440 mm long, 750 mm width, and 1640 mm height. The wind tunnel has the ability to provide velocities of up to 30 m/s without the presence of the MCHX, and of 11 m/s with the current MCHX placed inside it. In order to achieve the required velocities of air, a blower is mounted inside the wind tunnel to provide the flow of the forced air inside the tunnel, and it operates by the use of a hydraulic pump. This hydraulic pump is powered by an electrical variable speed motor. A built in heat exchanger (secondary heat exchanger) was installed inside the wind tunnel in the upstream air flow. This secondary heat exchanger is used to provide the control over the desired air temperatures. The air flow direction inside the wind tunnel is shown in Figure (5).

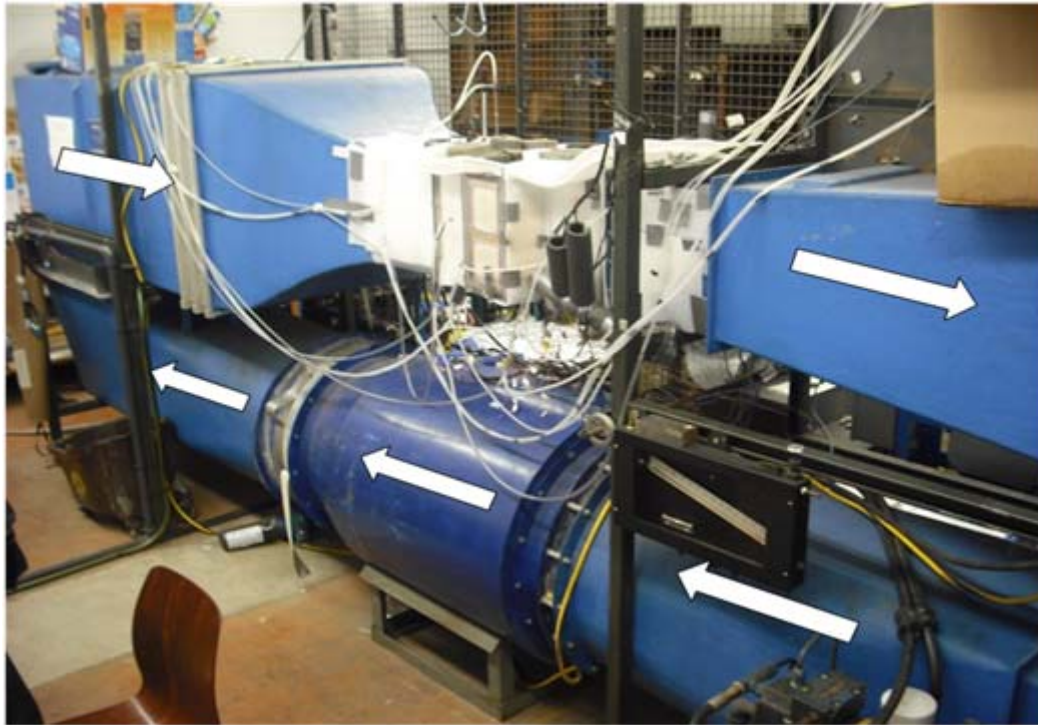


Figure 5 Integrated thermal wind tunnel

4.2.3 MCHX Liquid Supply System

The liquid supply system comprises two main cycles; the MCHX cycle and the secondary heat exchanger cycle. For the first one, 50-50% ethylene glycol-water mixture is circulated using the pump from the liquid tank to the MCHX by the means of the inlet pipes system and header. The hot liquid exchanges its heat with the cold air stream and then returns to liquid container through the exit header and the outlet pipes system. The main components of this system are; liquid container, motor pump, liquid heater, inlet and outlet pipes, flow measurement devices, (resistance temperature detectors) RTDs, (differential pressure transducers) PTDs, pressure and temperature gauges, valves, and a micro filter. A 6KW electric inline heater that can handle different incompressible fluids and also gases for a determined pressure of up to 6.8 MPa was used to heat up the liquid. ultra precise 1/10DIN RTDs of the PT 100 series as well as PX series pressure

transducers PTD were installed at the inlet and the outlet section of the MCHX to measure the temperatures and the pressures of the glycol. All the temperature and pressure measurements sensors were connected to the DAQ for conversion and final readings.

The second liquid supply cycle consists of; the main building water supply system, inlet and outlet pipes system, hoses, and temperature and pressure gauges. Hot and cold water streams are supplied to the secondary heat exchanger through the inlet pipes system. This heat exchanger is mainly used to control the air inlet temperature.

4.2.4 Data Acquisition System (DAQ)

The investigation of the second law analysis in a MCHX requires a thorough understanding of certain parameters used. These parameters include; air and liquid inlet and outlet temperatures and pressures, velocity, volume flow rate, etc. The DAQ has been designed to process the data from the measuring devices into voltage readings except for the RTD and the thermocouples, since it gives the temperature reading in degree Celsius directly. The DAQ system includes a computer that has Windows XP operating system, NI PCI 6052E DAQ card, this card is connected to the signal conditioning. The signal conditioning helps to convert the signal from different sensors and transducers to a form that can be easily read and it consists of an SCXI 1000 chassis with an SCXI 1102 module, 1300 and 1303 terminal blocks as well as a secondary terminal block.

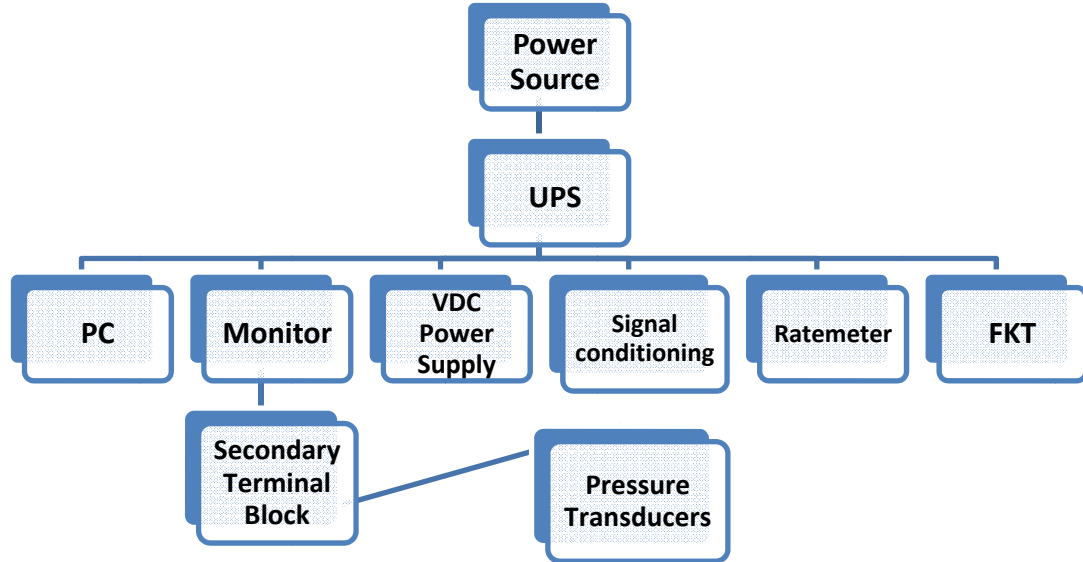


Figure 6 Connectivity of the DAQ components

This secondary terminal block works with DC power supply. This power supply is an HP with model #721A. An APC Back-UPS XS1300 power supply with a USB interface is used to protect the other equipments of the DAQ system from power surges and fluctuations. The DAQ is a 16-Bit system with 128 channels and equipped with LabView software version 8.

4.3 Experimental Methods and Operating Conditions

The investigation of the second law in a microchannel heat exchanger was the main objective of this study. Heating the air using hot liquid occurs when the air temperature is lower than that of the liquid temperature ($T_{a,i} < T_{g,i}$). The (50-50%) ethylene glycol-water mixture flowed through the circular microchannels, while the air coming from the wind tunnel was forced to flow perpendicular to the liquid flow. The heat transfer occurred

from the hot fluid to the cold fluid, and since the test section was well insulated, therefore, it is assumed that all the heat given by the hot fluid is gained by the cold fluid. A secondary heat exchanger is installed in the wind tunnel which was supplied with cold and hot water from the building main supply unit. The main purpose of the secondary heat exchanger is to take up the heat that is rejected by the hot fluid to the air and maintain the inlet air temperature to the desired value. The system was left running for about 25 minutes, this was done to make sure that the system reached the steady state and no fluctuation will occur in the flow while recording the readings. Air velocities were manually varied by controlling a valve connected to the hydraulic pump that is derived by an electric motor. With the use of an electric heater, the inlet liquid temperature was controlled and set to a fixed value. Conditions are as follows in table (2);

Table 2 Operating Conditions: Air Heating ($T_{a,i} < T_{g,i}$)

Liquid inlet temperature, $T_{g,i}$	74 ± 1 °C
Liquid mass flow rate	0.0325 ± 0.005 kg/s
Liquid side Reynolds number	200 ± 5
Airside Reynolds numbers, $V_a \approx 3-11$ m/s	850-3170
Air inlet temperature, $T_{a,i}$	(28, 33, 38, 43) °C

4.4 Measurement and Data Collection Procedures

Different experimental runs were performed at different air inlet temperatures and velocities. Five different air velocities were investigated (3, 5, 7, 9, and 11 m/s) for each inlet temperature with a range of Reynolds number between (850-3100). Four different

air inlet temperatures were investigated (28, 33, 38, and 43 °C) under constant liquid temperature and mass flow rate. The variation in air velocities allowed for obtaining more data to examine the effect of different Reynolds numbers as well as different air mass flow rates on entropy generation and exergy destroyed. The hot fluid inlet temperature was maintained to a constant value of $74\pm 1^\circ\text{C}$ and a liquid mass flow rate of $0.0253\pm 0.005\text{kg/s}$ by controlling the frequency of the gear pump. After maintaining the glycol mass flow rate to the desired value, the air velocity is set to a certain value through the control of the hydraulic pump and the water supply to the secondary heat exchanger. The heater is turned on and set to a predetermined value to maintain the glycol inlet temperature. The glycol is circulated through the inlet pipes to the MCHX and the system is left for about 25 minutes to stabilize before taking any readings. After the system was stabilized, four airside inlet temperatures were tested against five air velocities. A set of 20 data at these operating conditions were taken for final calculations.

4.4.1 Glycol Temperature and Pressure Measurements

To measure the inlet and outlet liquid side temperatures, resistance temperature detectors (RTDs) were used. These RTDs are ultra precise RTDs sensors from Omega Company. They are made of 100Ω platinum of 1/10 DIN class with a temperature range of -100 to 400°C . The RTDs are mounted at the inlet and outlet pipes of the MCHX for glycol temperatures measurement. Those RTDs are connected to the DAQ system (SCXI signal conditioning device) for final temperatures reading.

$$T_{g,i} = \left[\frac{1}{n} \sum_{j=1}^n (T_{g,i}) \right] \quad (46)$$

Where, n is the total number of samples at 1kHz for 180-200 seconds. In the same way, the glycol outlet temperature was found as,

$$T_{g,o} = \left[\frac{1}{n} \sum_{j=1}^n (T_{g,o}) \right] \quad (47)$$

The liquid side temperature difference is obtained as,

$$\Delta T_g = T_{g,i} - T_{g,o} \quad (48)$$

Omega pressure transducers of the PX series were used to measure the liquid side pressures. The inlet pressure transducer has a pressure range of (0-100 psig) and (0-5 VDC). The inlet pressure value was found by taking the measurements collected during the experiment as follows,

$$P_{g,i} = \left[\frac{1}{n} \sum_{j=1}^n (P_{g,i}) \right] \quad (49)$$

While, the outlet pressure transducer has a range of (0-10 psig) and (0-5VDC).

$$P_{g,o} = \left[\frac{1}{n} \sum_{j=1}^n (P_{g,o}) \right] \quad (50)$$

Where, n in the two equations refers to the number of samples taken over 180-200 seconds at 1kHz. The liquid side pressure drop was calculated as,

$$\Delta P_g = P_{g,i} - P_{g,o} \quad (51)$$

4.4.2 Glycol Mass Flow Rate Measurement

The mass flow rate on the liquid side was determined during the experiment by collecting the glycol through the exit pipe for a period of time. The mass of the glycol and time were recorded. It was found through dividing the mass over the time as follows.

$$\dot{m}_g = \left[\frac{1}{n} \sum_{j=1}^n \left(\frac{m_g}{t} \right) \right] \quad (52)$$

Where, n is the number the test was repeated (4 to 5 repeats). The glycol velocity was determined from the following equation.

$$V_g = \frac{\dot{m}_g}{\rho_g A_{ch}} \quad (52)$$

Where, ρ_a is the air density, V_a is the velocity of the air, and A_{ch} is the constant cross section of the test chamber.

$$V_g = \frac{\dot{m}_g}{(3*68)\rho_g A_{ch}} \quad (53)$$

$$V_g = \frac{4\dot{m}_g}{204\pi\rho_g D_{mc}^2} = \frac{\dot{m}_g}{51\pi\rho_g D_{mc}^2} \quad (54)$$

4.4.3 Air Temperature Measurements

The average temperatures of the air, inlet and outlet, were measured using type-T thermocouples which were connected to the DAQ. A grid of 9 openings and in each opening calibrated thermocouples were placed uniformly inside the inlet section prior to entering to the MCHX for inlet temperature measurements, and then their average was taken through the readings provided by the DAQ system.

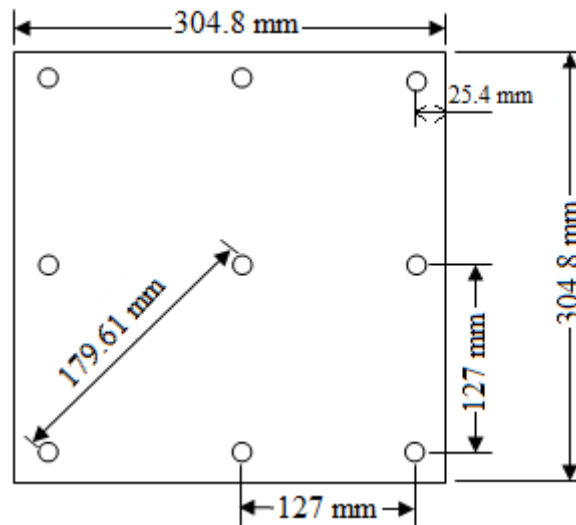


Figure 7 Inlet grid thermocouples distribution

The average of the 9 thermocouples was taken for the air inlet temperature as follows.

$$T_{a,i} = \frac{1}{N} \sum_{j=1}^N \left[\frac{1}{n} \sum_{j=1}^n (T_{a,i}) \right] \quad (55)$$

Where, N is the number of thermocouples, n is the total number of samples at 1kHz for 180-200 seconds.

A grid of 25 equally spaced thermocouples was mounted across the exit cross section after exiting from the MCHX to measure the outlet air temperatures at different locations then the average of these measurements was considered.

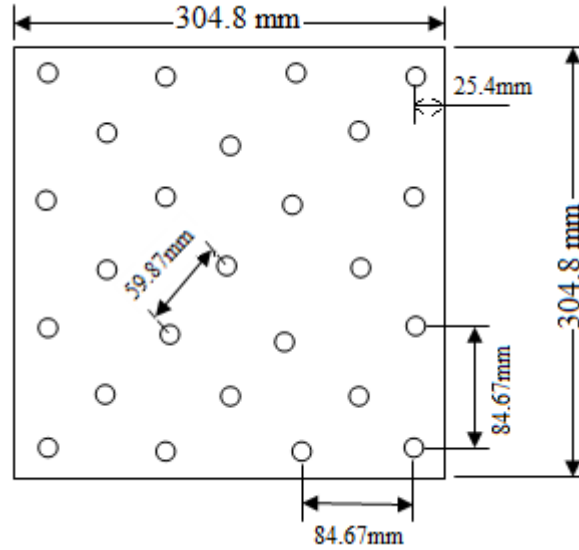


Figure 8 Outlet grid thermocouples distribution

The average of the 25 thermocouples was taken for the air inlet temperature as follows.

$$T_{a,o} = \frac{1}{N} \sum_{j=1}^N \left[\frac{1}{n} \sum_{j=1}^n (T_{a,o}) \right] \quad (56)$$

Where, N is the number of thermocouples, n is the total number of samples at 1kHz for 180-200 seconds. The airside temperature difference is therefore,

$$\Delta T_a = T_{a,i} - T_{a,o} \quad (56)$$

The data acquisition system reads the signals from the thermocouples probes and provides the output readings in terms of degree Celsius.

4.4.4 Air Velocity and Pressure Measurements

The pressure measurements of the airside were taken using a portable FlowKinetics (3DP1A) of the FKT series, a device that provides the readings for the atmospheric pressure, gas temperature, air velocity, gas relative humidity, and up to 3 independent differential pressures.

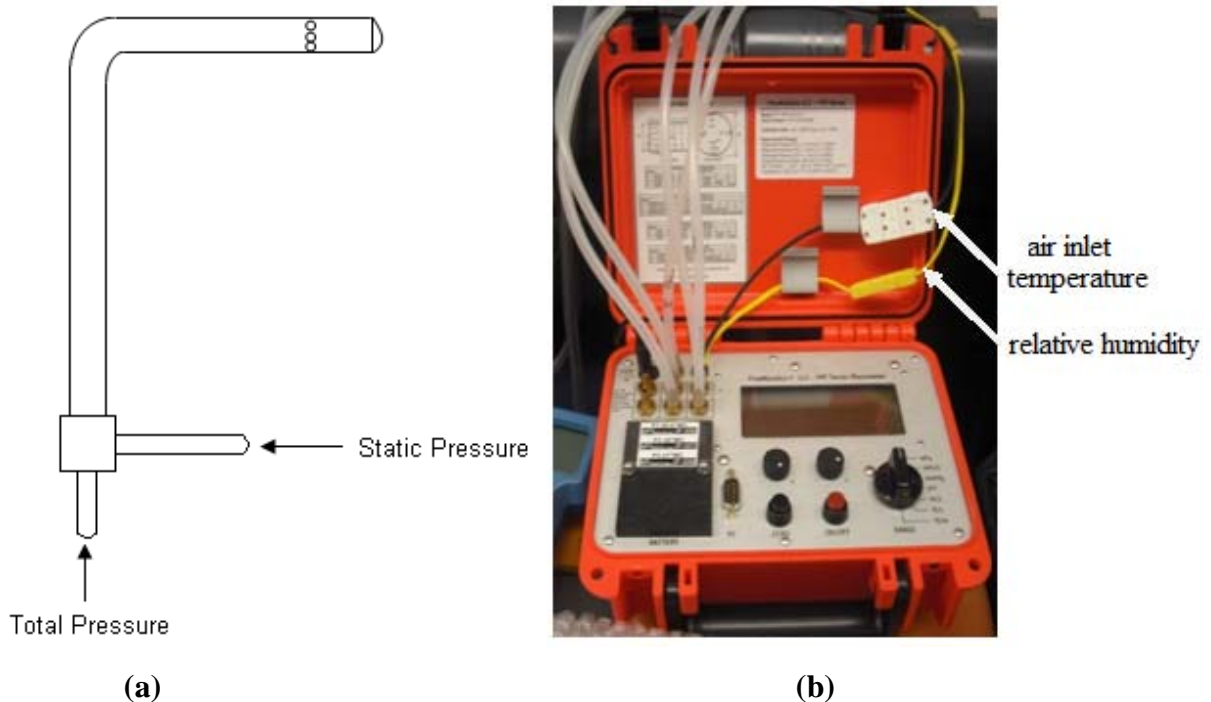


Figure 9 Air velocity and pressure devices

(a) Pitot static tube

(b) FlowKinetics device

The velocity of the air was measured using a Pitot static tube which measures the total pressure of the air P_{tot} at the tip, and the static pressure P_{static} at the side port and it is

connected to the FlowKinetics device. The dynamic pressure can be obtained from the difference of these two pressures to determine the air velocity.

$$\Delta p_{pitot} = \left[\frac{1}{n} \sum_{j=1}^n (\Delta p_{pitot}) \right] \quad (57)$$

Where, n is number of the times the test was repeated (4 to 5 repeats). After determining the dynamic pressure, the air velocity can be determined as,

$$V_a = C \sqrt{\frac{2P_{dyn}}{\rho}} \quad (58)$$

Where, V_a is the air velocity, ρ is the air density, P_{dyn} is the dynamic pressure, and C is the correction factor based on the Pitot static tube manufacturing. For this study, C was taken to be 1. Differential pressure transducers were provided to measure the pressure drop across the MCHX at different locations. The transducers used were; at the top location (PX653), middle (PX277), and bottom (PX653). These transducers were taken the power from the terminal block and were connected to the DAQ system to provide the pressure readings in terms of voltage. Each pressure transducer has its own calibration curve to convert the voltage reading to a Pa reading.

4.4.5 Airside Mass Flow Rate Measurement

The air mass flow rate depends on the air velocity, which is determined from the dynamic pressure. The mass flow rate of the air across the heat exchanger was found as follows.

$$\dot{m}_a = \rho_a A_{ch} V_a \quad (59)$$

Where, ρ_a is the air density, V_a is the velocity of the air, and A_{ch} is the constant cross section of the test chamber.

4.4.6 Reynolds Number Measurement

The dimensionless Reynolds number represents the ratio of the inertial effects in the flow to the viscous effects in the flow. The nature of the fluid flow depends on Reynolds number.

$$Re = \frac{\text{inertia force}}{\text{viscous force}} = \frac{\rho V L}{\mu} \quad (60)$$

Where, ρ is the fluid density, V is the fluid velocity, μ is the fluid dynamic viscosity, and L is the characteristic length. When small Reynolds numbers are considered, the inertia is not that significant, therefore the flow is laminar and smooth. However when high Reynolds numbers are considered, the inertia plays an important role and it is dominant therefore the flow is turbulent. Reynolds number on the liquid side is found using the following.

$$Re_g = \frac{\rho V D}{\mu} = \frac{\dot{m}_g}{51\pi\mu_g D_{mc}} \quad (61)$$

Reynolds number on the airside is determined by calculating the mass velocity in the heat exchanger first, it can be found as,

$$G_a = \frac{\dot{m}_a}{A_{a,min}} \quad (62)$$

Where, $A_{a,\min}$ is the minimum free flow area. Therefore, Reynolds number at the airside can be found as,

$$Re_g = \frac{\rho V D}{\mu} = \frac{G_a D_{h,a}}{\mu_a} \quad (63)$$

These design parameters were used to study the performance of the MCHX and possible ways of optimization.

CHAPTER V

ANALYSIS OF RESULTS

The present study explored the application of the second law analysis to a microchannel heat exchanger. As well as present some of the parameters (ϵ , T_R , airside pressure drop, and C^*) that can affect the performance and effectiveness of the heat exchanger. The air operating conditions (temperature and mass flow rate) were varied while the glycol operating conditions were kept constant at a temperature of $74 \pm 1^\circ\text{C}$ with a variation of air inlet temperature (28, 33, 38, $45 \pm 0.2^\circ\text{C}$). The mass flow rate on the liquid side entering the MCHX was kept constant at 0.0253 ± 0.005 kg/s which correspond to a glycol Reynolds number of 200 ± 5 . Air velocities were varied from (3-11 m/s) which give a Reynolds number of (810 - 3100). The following sections examine the effect of several parameters on the heat exchanger effectiveness. These parameters comprise the heat capacity rate ratio, fluids inlet temperature difference, effectiveness, and airside pressure drop.

5.1 Balanced Cross Flow with Zero Pressure Drop

The first case to be considered is the case where the heat capacity rate ratio, C^* , is equal to 1. Adding to that, there is no pressure drop effect on the fluid side; the heat exchanger may run with incompressible fluids as the working fluids. This case was discussed briefly by other researchers [Assad (2010), Hesselgreaves (2000), Fan and Luo (2009)], and it is also presented here for further examination and comparison.

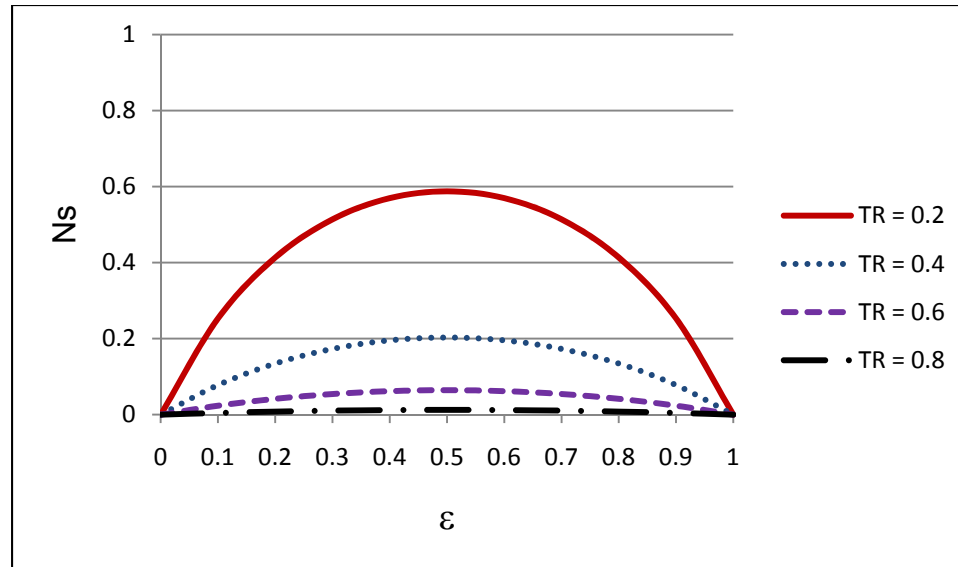


Figure 10 Entropy generation number vs. effectiveness for a balanced cross flow heat exchanger

Figure 10 shows the entropy generation number as a function of effectiveness for various fluids inlet temperatures ratios (T_R). For a given T_R , N_s increases until it reaches its maximum at $\epsilon = 0.5$ then starts decreasing as the effectiveness increases. Also, one can notice that at higher T_R values, N_s tends to be lower, and the heat exchanger effectiveness does not have a significant effect on the entropy generation number.

5.2 Balanced Cross Flow with Airside Pressure Drop

For the first case, where the hot fluid has the minimum heat capacity rate and considering an imbalanced flow using different pressure ratios, the entropy generation number and effectiveness graph can be shown as in Figure 11.

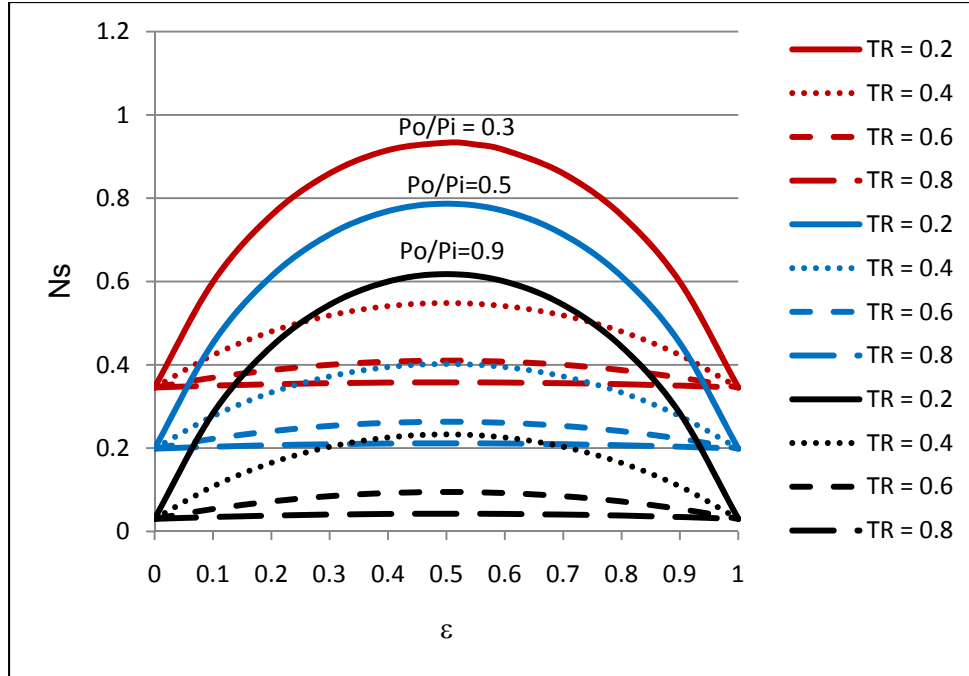


Figure 11 Entropy generation number vs. effectiveness for a balanced cross flow heat exchanger $C^*=1$

Figure 11 shows the effect of the pressure drop and the fluids inlet temperatures ratio on entropy generation number for a balanced cross flow heat exchanger. It is observed that at a higher pressure ratio, N_s will tend to be lower. Higher pressure ratio means low pressure drops across the heat exchanger which indicates lower contribution of the frictional pressure drop effect on the entropy generation. It is also noticed that at the same pressure ratio and effectiveness, and higher T_R value, N_s will be lower. It is concluded that N_s is lower at higher T_R values and pressure ratios.

5.3 Imbalanced Cross Flow with Airside Pressure Drop

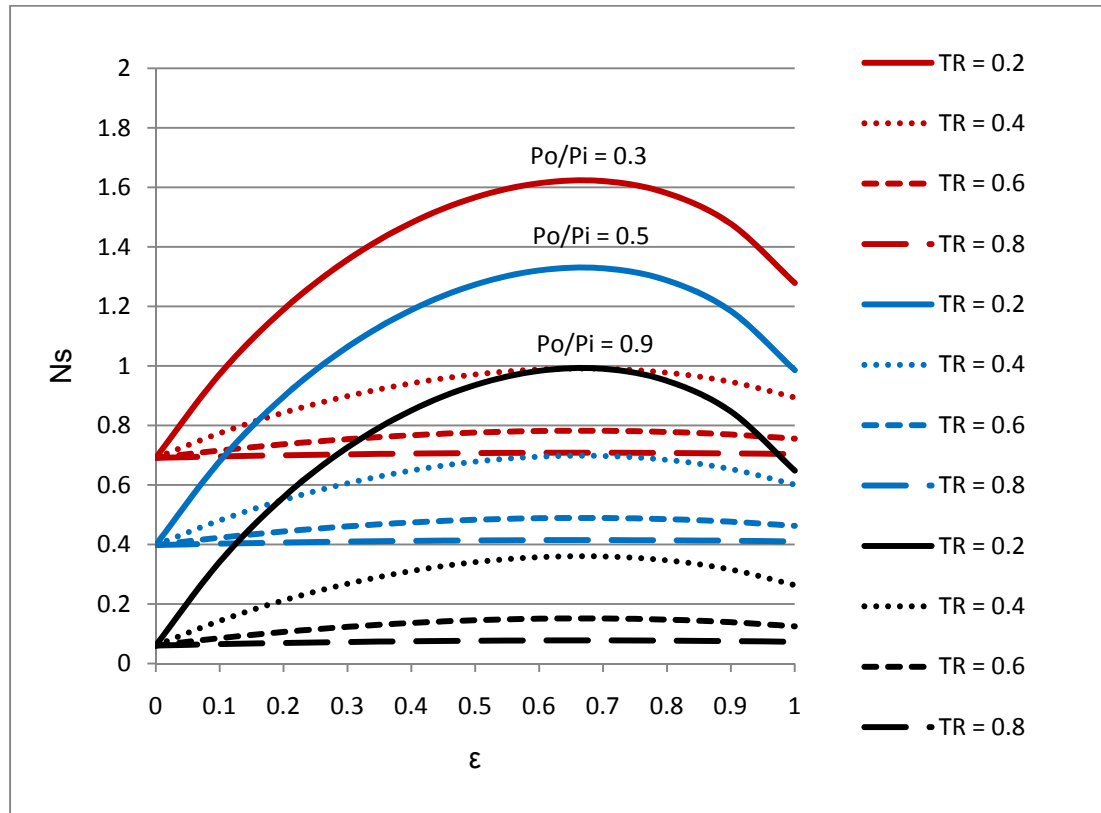


Figure 12 The effect of pressure and temperature ratios on entropy generation number for ($C^*=0.5$)

Figure 12 shows the effect of temperature and pressure ratios on N_s for an imbalanced cross flow arrangement ($C^* < 1$). Different fluids inlet fluids temperatures ratios and various pressure drops were examined. As it is shown in Figure 12, the increase in effectiveness results in an increase in N_s values up to $\epsilon = 0.7$ (at $C^*=0.5$), after which any increase in effectiveness causes a drop in N_s values.

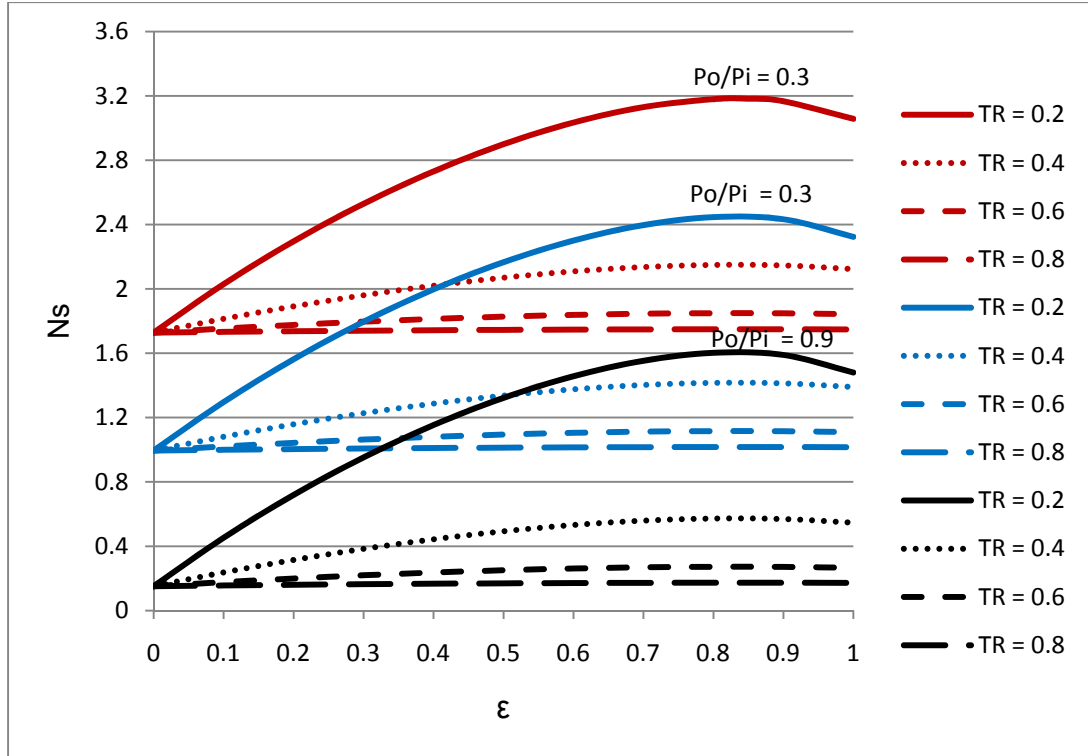


Figure 13 The effect of pressure and temperature ratios on entropy generation number for ($C^*=0.2$)

Figure 13 shows the effect of temperature and pressure ratios on N_s for an imbalanced cross flow arrangement ($C^* = 0.2$). The same conclusion can be taken as in Figure 12. The increase in effectiveness results in an increase in N_s values up to $\epsilon = 0.85$, after which any increase in effectiveness causes a slight drop in N_s values. Adding to that, as the inlet fluids temperatures ratio changes from lower to higher values, considering the same pressure drop, a very large entropy generation number decrease is seen. Lower inlet fluids temperatures ratio means maximum inlet temperature difference of the two fluids.

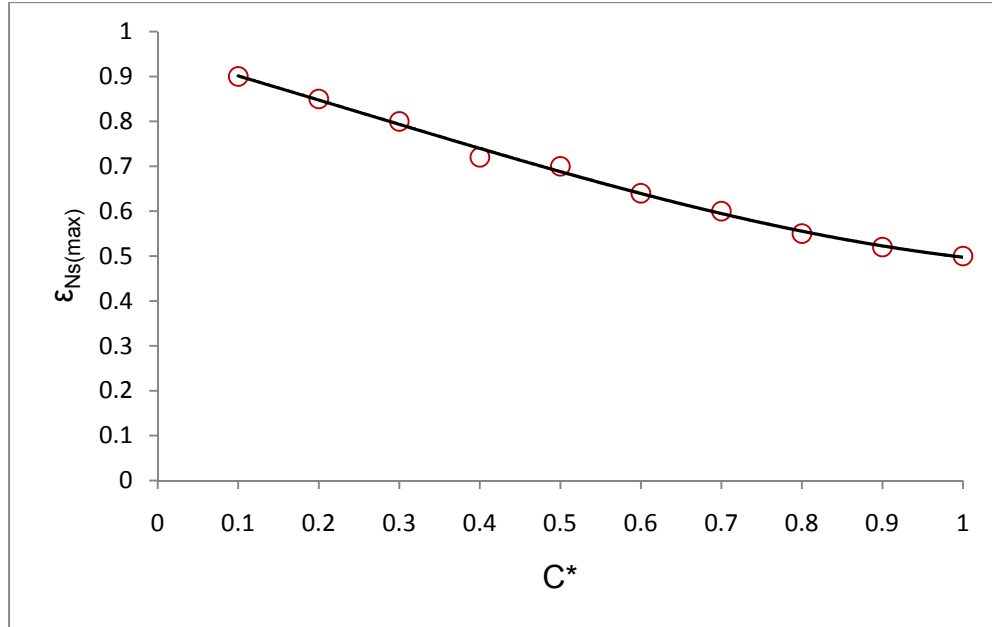


Figure 14 Effectiveness at $N_{s_{\max}}$ vs. heat capacity rate ratio

Figure 14 shows the relationship between the effectiveness at a maximum entropy generation number with the heat capacity rate ratio. Effectiveness values decrease when C^* increases therefore, the lowest entropy generation number can be found at the highest C^* values. This graph determines the undesired values of effectiveness while running the heat exchanger at certain C^* value. This can be seen for any heat exchanger working with $T_R \leq 0.7$, where the entropy generation number will have a maximum value. For $T_R \geq 0.7$, the entropy generation number will have the same values at any effectiveness given.

5.4 Entropy Generation Number Ratio with Zero Pressure Drop

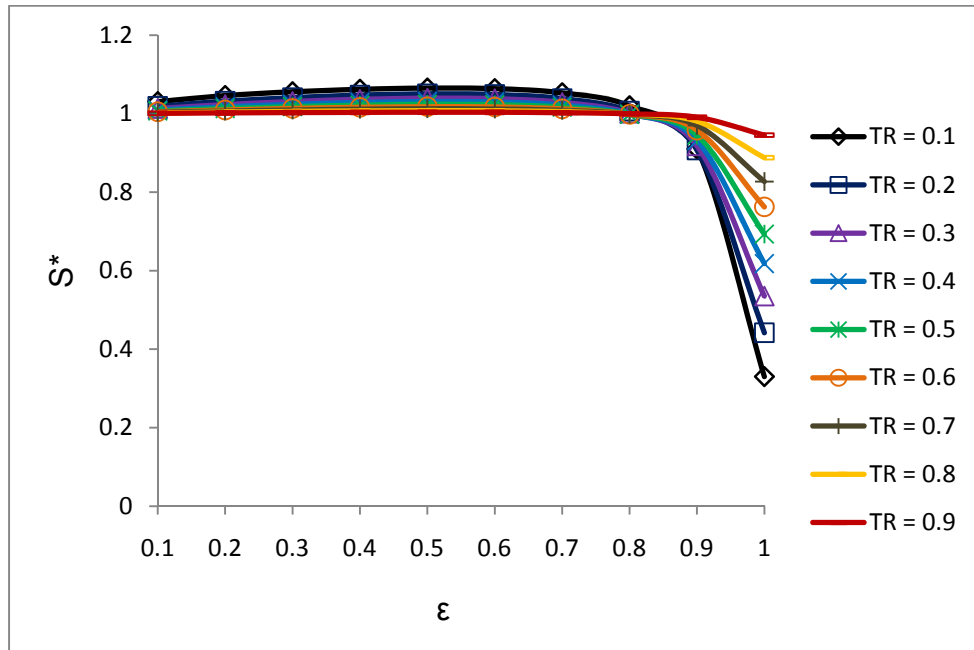


Figure 15 Entropy generation number ratio S^* vs. effectiveness at $C^*=0.9$ [Assad 2010]

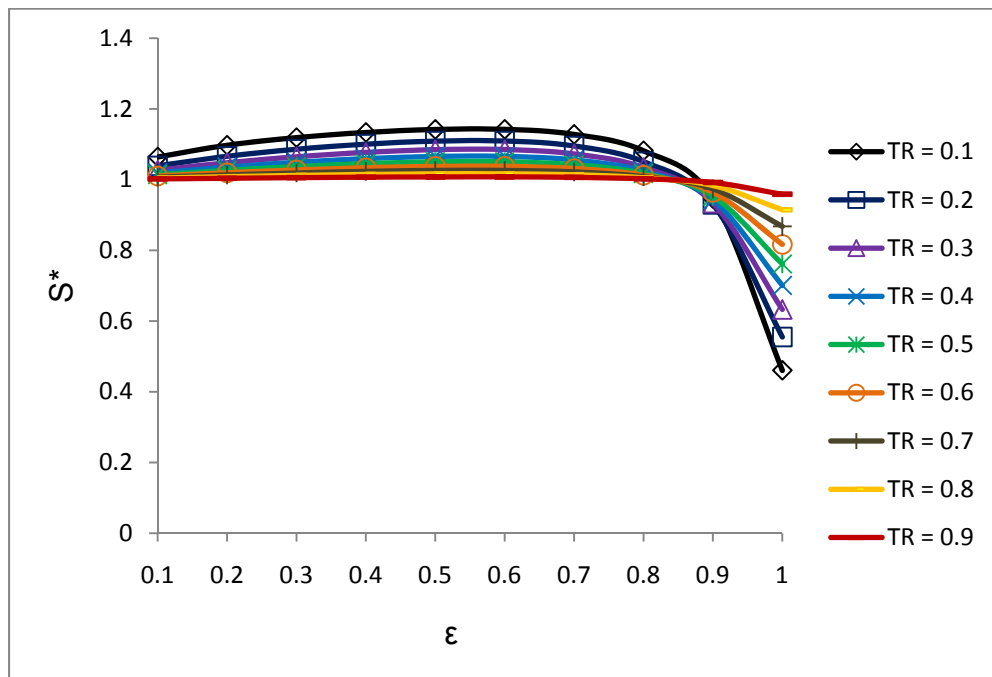


Figure 16 Entropy generation number ratio vs. effectiveness at $C^*=0.8$

Figures 15 and 16 show the effect of fluids inlet temperatures ratios on the entropy generation number ratio, S^* , with respect to effectiveness for a given C^* value. For incompressible fluids, the pressure drop effect is very small which can be neglected (Cengel 2006). It was concluded by (Assad 2010) that when $C^*=0.9$, and $\varepsilon = 0.8$, S^* will have the same value for any fluids inlet temperatures ratio. When ($\varepsilon < 0.8$), S^* was found to be higher at lower T_R values. While when ($\varepsilon > 0.8$), S^* was found to be lower at lower T_R values. However, any decrease in C^* will lead to an increase in the value of the critical point until $C^*=0.5$ is reached where the S^* will have the same value with different T_R values at $\varepsilon=1$ (Figure 17).

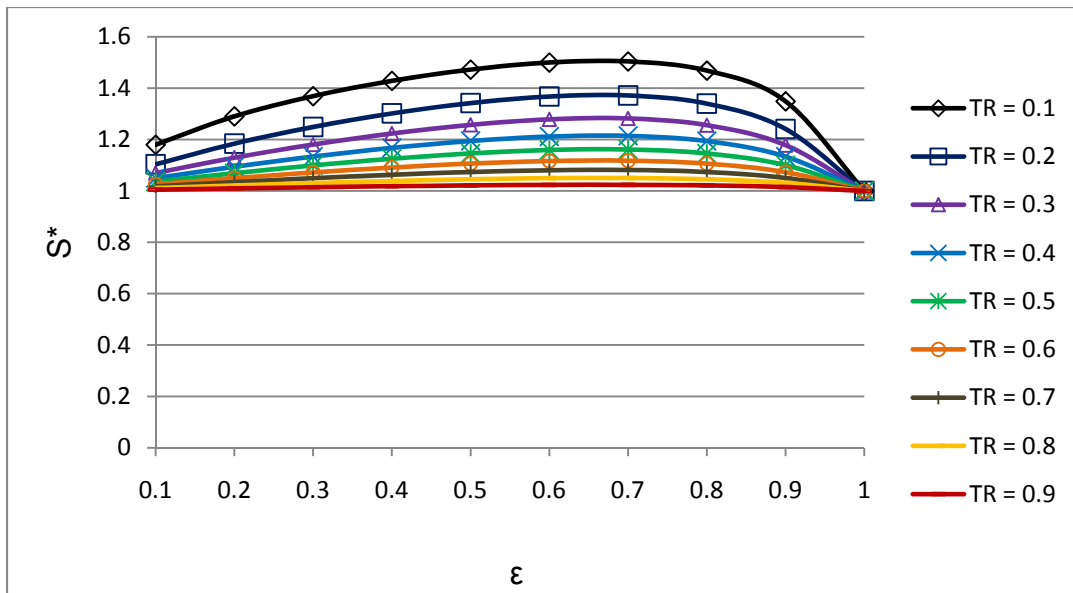


Figure 17 Entropy generation number ratio vs. effectiveness at $C^*=0.5$

Decreasing C^* values below 0.5 will no more yield the same conclusion, no critical point was found. The current study takes into consideration the pressure drop effect on S^* for different values of C^* and T_R .

In this work, two pressure ratios were chosen to be discussed, 0.4 and 0.9 at a fixed value of $C^*=0.7$ (Figures 18 and 19). It has been done using different T_R , and ε values with fixed C^* value. The S^* values were found and a comparison between the two figures was presented. A wide range of T_R was presented from (0.1 – 1), and pressure drop effect was studied and discussed.

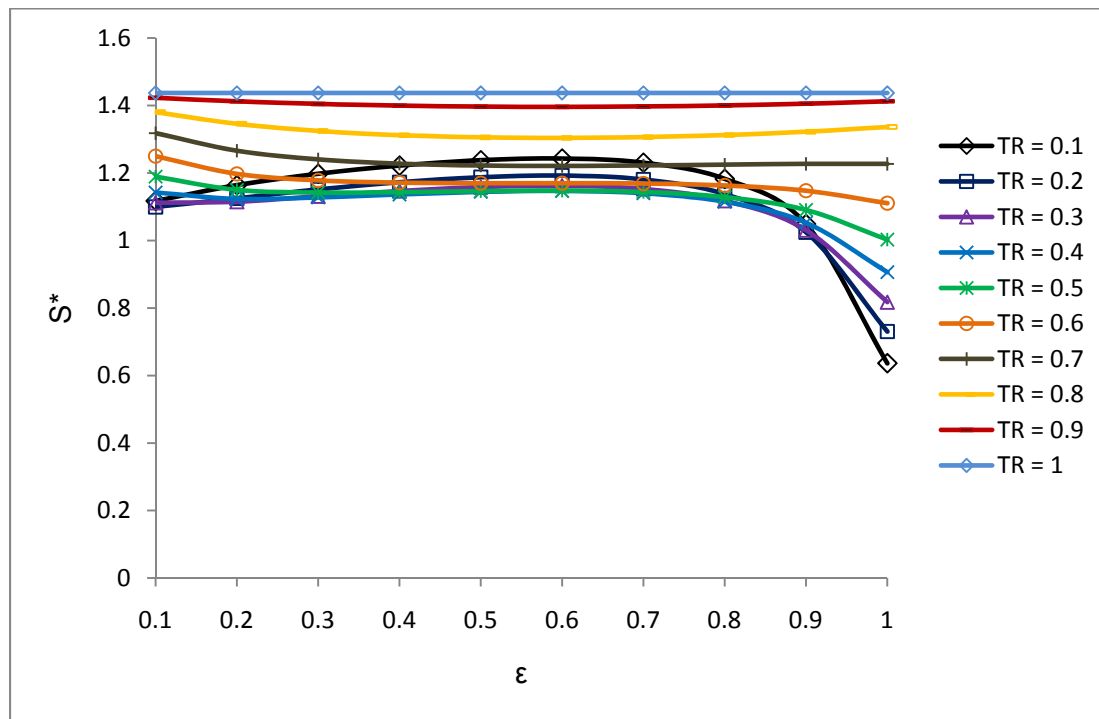


Figure 18 Effect of T_R on S^* at ($P_o/P_i=0.9$) ($C^*=0.7$)

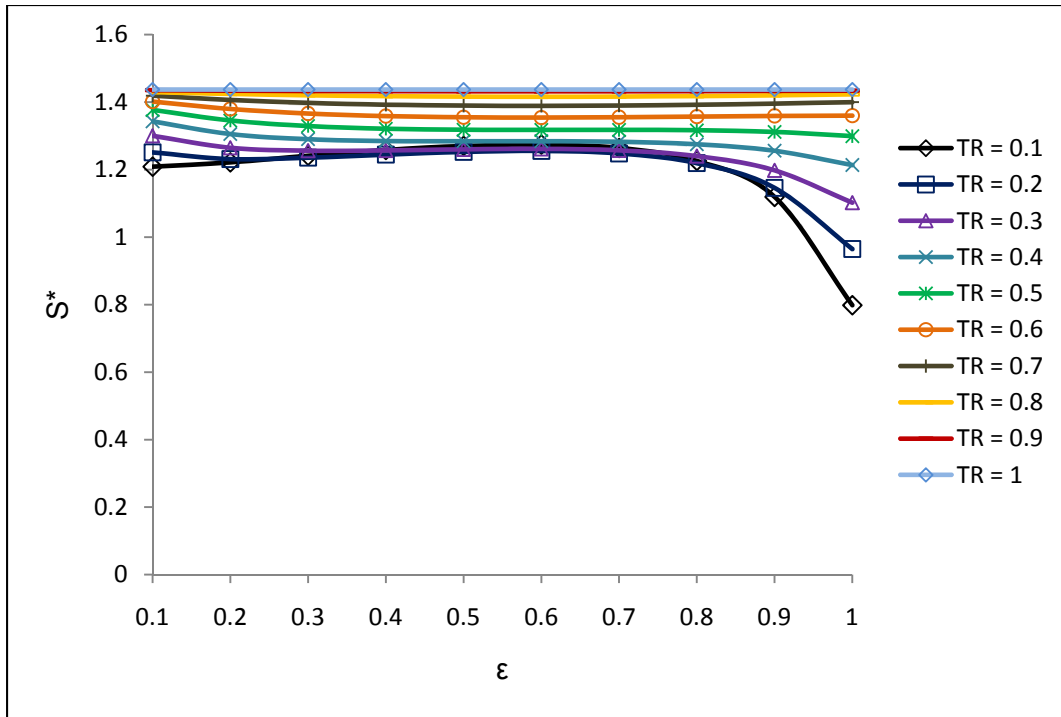


Figure 19 Effect of T_R on S^* at ($P_o/P_i=0.4$) ($C^*=0.7$)

As it is shown in figures 18 and 19, for a given value of C^* and T_R , when the pressure ratio decreases, S^* was found to increase. It is noticed that any increase in T_R will lead to a decrease in the effect of effectiveness on S^* . This decrease continues until a point where there is no significant change with the increase of T_R values. This effect can clearly be observed at lower T_R values. The conclusion that has been reached is valid with any imbalanced flow at constant C^* value.

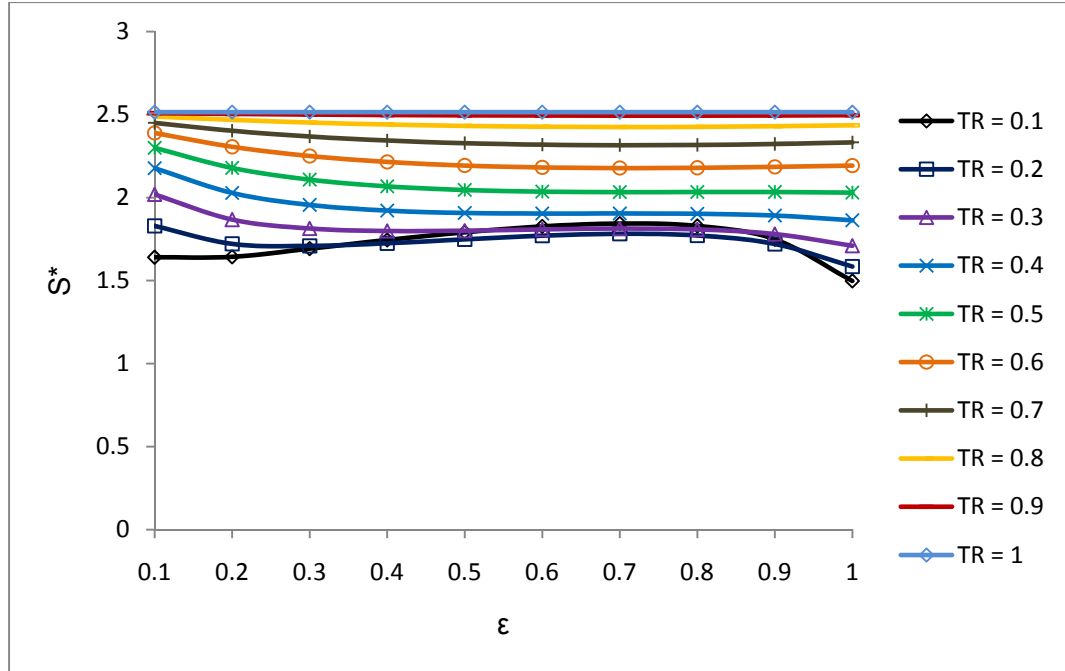


Figure 20 Effect of T_R on S^* for $(P_o/P_i=0.4)$ ($C^*=0.4$)

The effect of C^* on S^* at the same pressure ratio is illustrated by comparing Figures 19 and 20. It is clearly shown that S^* is increasing when C^* is decreasing. This increase is more at higher values of T_R . By comparing Figures 18, 19, and 20, the effect of C^* on S^* was found to be greater than the effect of pressure ratio on S^* .

5.5 Comparison of the Predicted Results With the Measured Data

The heat transfer and pressure drop irreversibilities for a microchannel heat exchanger were investigated theoretically and experimentally. The data obtained from the experiments were used to validate the mathematical model and find the predicted values for entropy generation. Some parameters are included in the optimization of the heat exchanger performance, these parameters are; heat capacity rate ratio, pressure ratio, effectiveness, and fluids inlet temperatures ratio. During the experiments, the hot liquid

was kept as having the minimum heat capacity rate, while the airside was considered to have the maximum heat capacity rate and its velocity was varied.

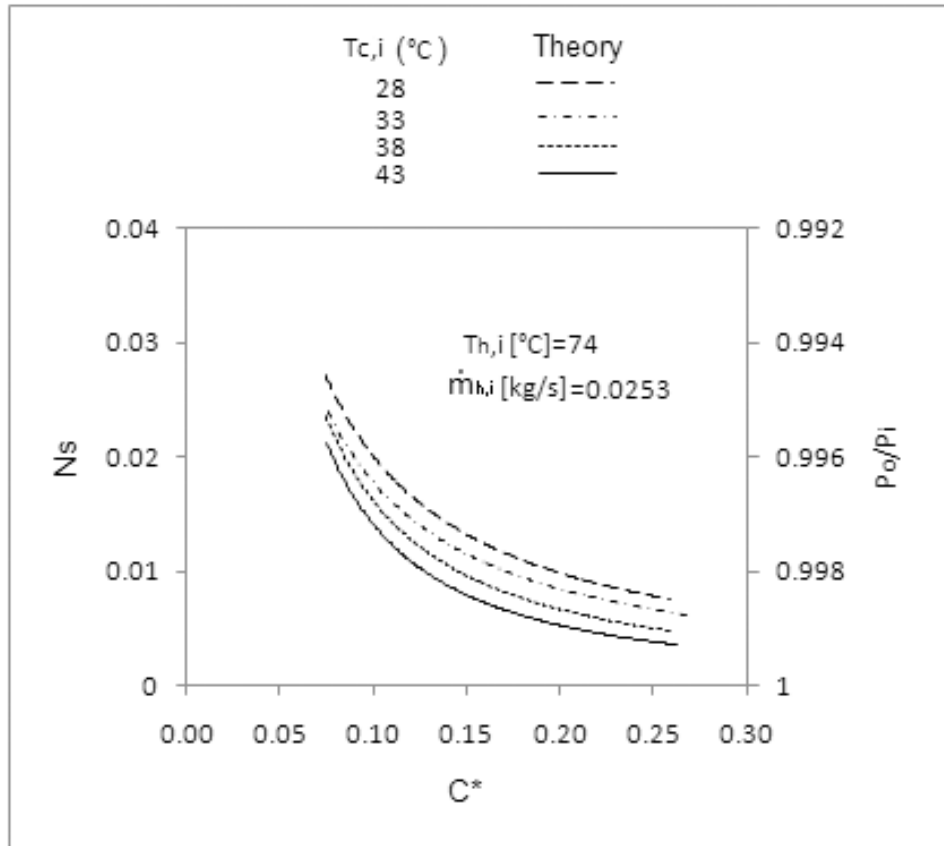


Figure 21 Entropy generation number vs. heat capacity rate ratio

The relationship between N_s and C^* is presented in Figure 21. This figure illustrates the effect of different fluids inlet temperatures and pressure ratios on N_s at various heat capacity rate ratios. For a fixed value of C^* , and higher T_R and pressure ratios, N_s was found to be lower. This can be explained since higher fluids inlet temperatures ratio indicates minimum inlet temperature difference of the two fluids, higher effectiveness, and better heat transfer quality. Similarly, higher pressure ratio demonstrates reduced airside pressure drop, which signifies lower frictional pressure losses. Higher fluids inlet

temperatures ratio and airside pressure ratio result in lower entropy generation for the heat exchanger.

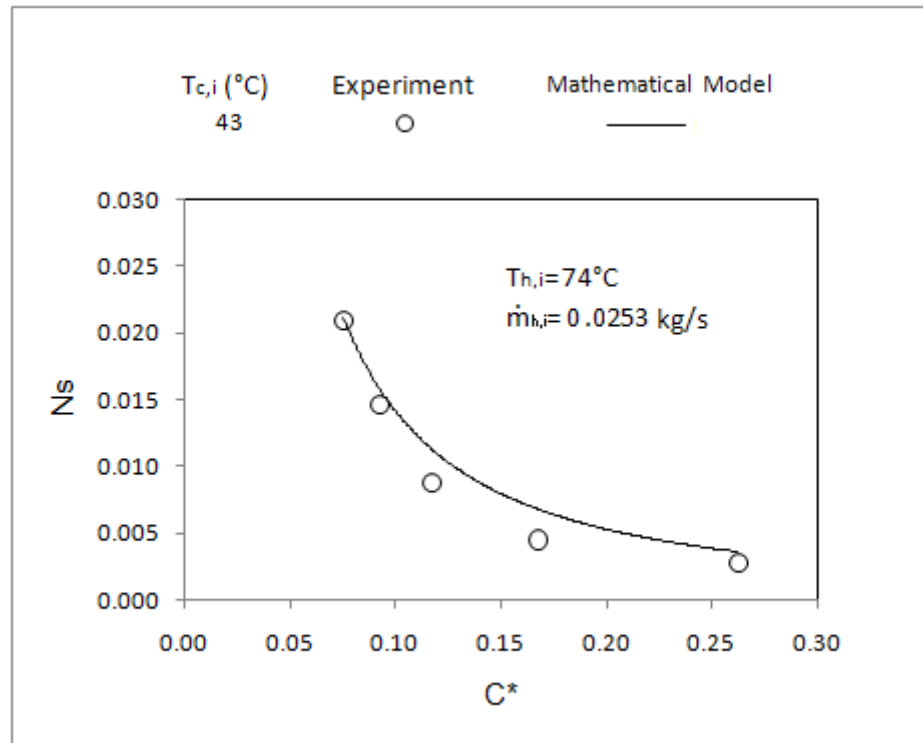


Figure 22 Entropy generation number vs. heat capacity rate ratio

Figure 22 shows a comparison between the experimental and the predicted data for the same fluids inlet temperatures ratio. The figure demonstrates that when C^* increases, N_s will tend to decrease. Since C^* in this work depends mainly on the airside mass flow rate, C_{\min} was replaced by the hot liquid heat capacity rate which was constant during the entire experiments. Increasing C^* means decreasing air mass flow rate thus decreasing the air velocity. From this figure, it is shown that the mathematical model provided a good prediction of the experimental results. The deviation from the mathematical model can be explained due to the uncertainties associated with the experiments.

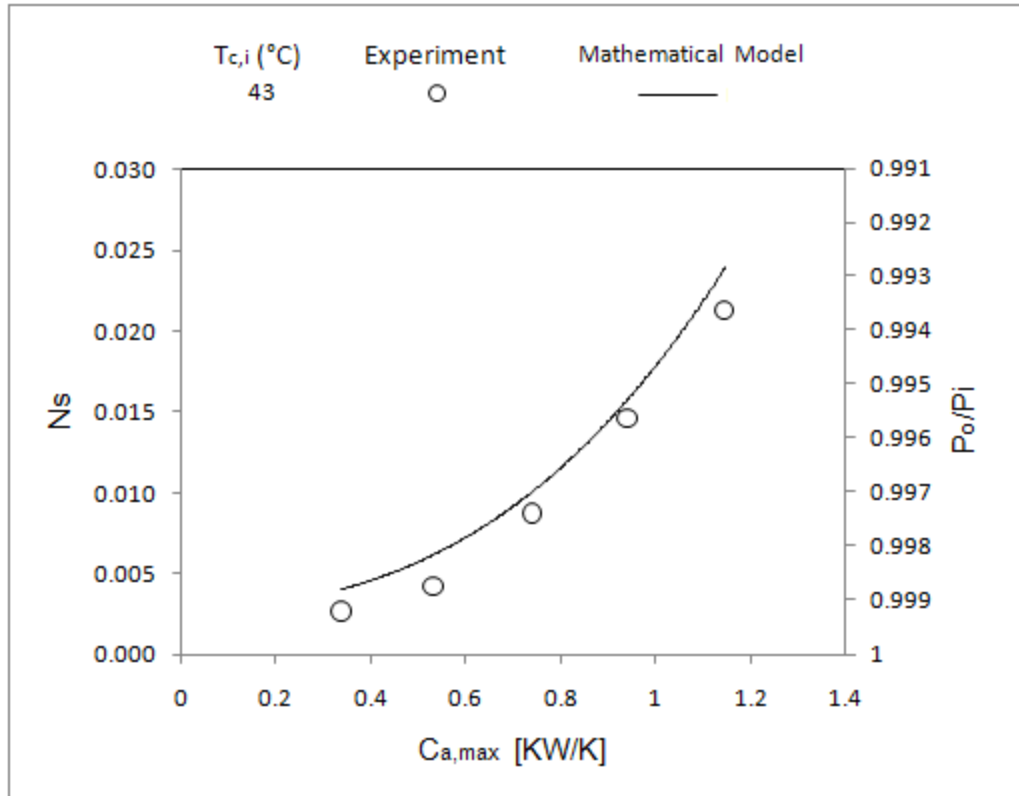


Figure 23 Entropy generation number vs. maximum heat capacity rate

Figure 23 shows a comparison between the experimental and the predicted results at the same fluids inlet temperatures ratio. This figure shows that when C_{max} increases, N_s will tend to increase. Where, C_{max} in this work represents the airside heat capacity rate. Increasing C_{max} will increase the N_s since, the air velocity and pressure drop are high. This figure also shows that the air mass flow rate has a significant effect on the N_s

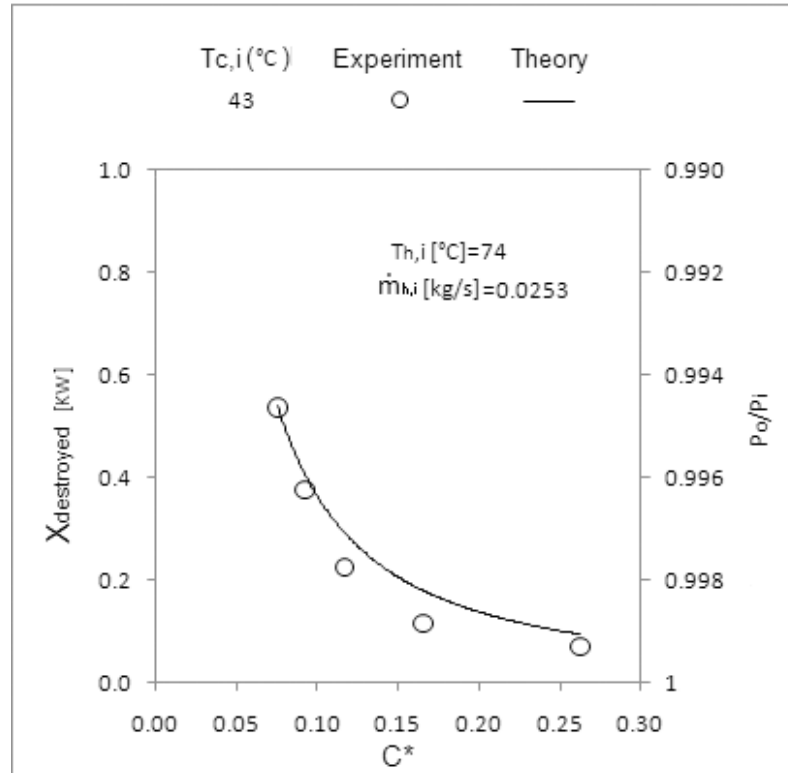


Figure 24 Exergy destroyed vs. C^*

Figure 24 represents the relationship between the exergy destruction in the heat exchanger and the heat capacity rate ratio for the same fluids inlet temperatures ratio. It is illustrated that at higher C^* values, and higher pressure ratio, exergy destroyed is lower. It can be seen that exergy destroyed followed the same trend as the entropy generation, they both tend to decrease with the increase in C^* . This consistency is due to that exergy destroyed is proportional to the entropy generation as was mentioned earlier.

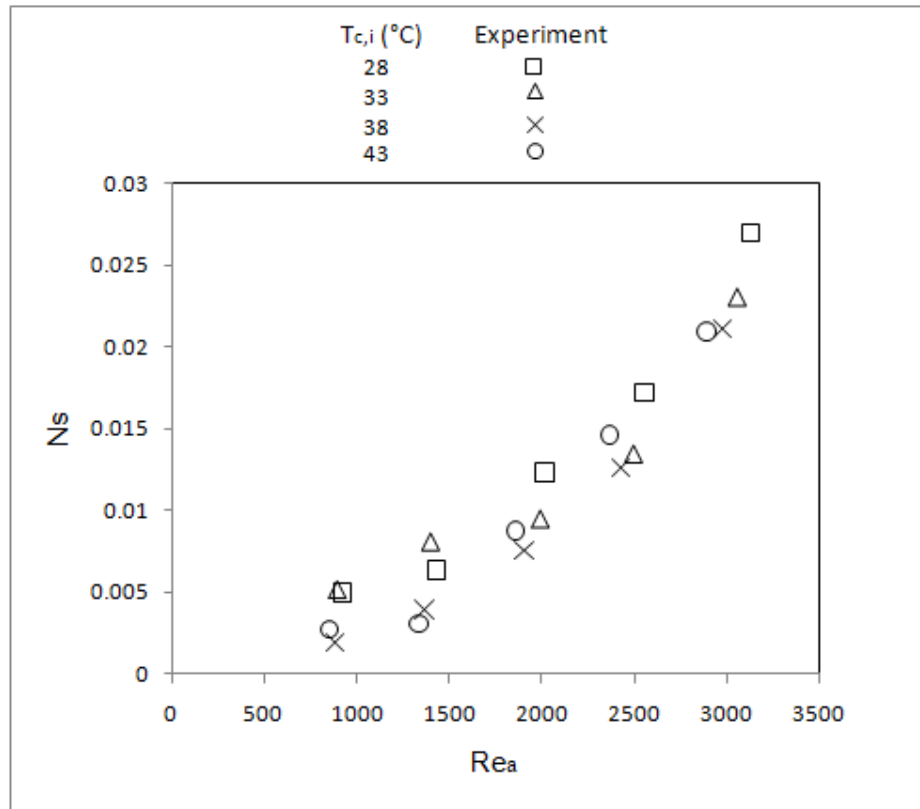


Figure 25 N_s vs. Re_a

Figure 25 illustrates the effect of different airside Reynolds numbers on entropy generation number at different fluids inlet temperatures ratios. Increasing Reynolds numbers will increase N_s values. The increase in Reynolds numbers is due to the increase in airside velocity. This increase in Re will increase the airside pressure drop as well, and as a result increase the entropy generation of the MCHX, while, for the same Reynolds number and higher fluids inlet temperatures ratio and pressure ratio, N_s is lower.

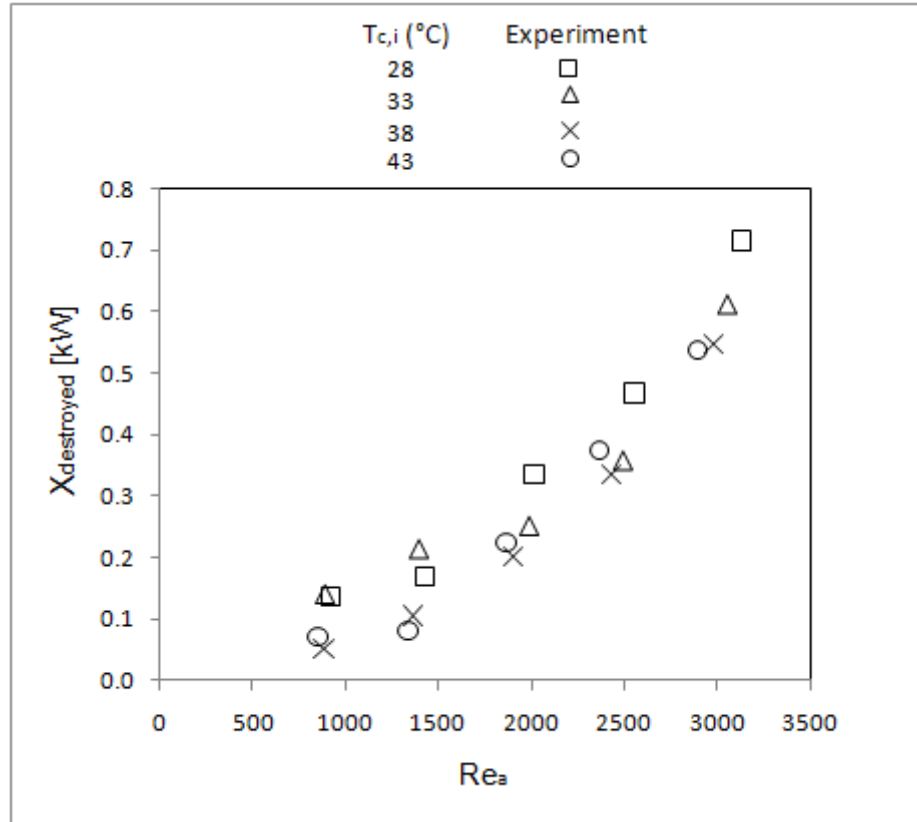


Figure 26 Exergy destroyed vs. Re

Figure 26 represents the exergy destruction changes with different Reynolds numbers. Since exergy destroyed is proportional to entropy generation, then it follows the same trend (Figure 25) and yields the same conclusion as entropy generation number behaves when changing Reynolds numbers. It increases at a constant T_R when Re numbers are high due to the high pressure drop on the airside which increases the frictional pressure drop losses.

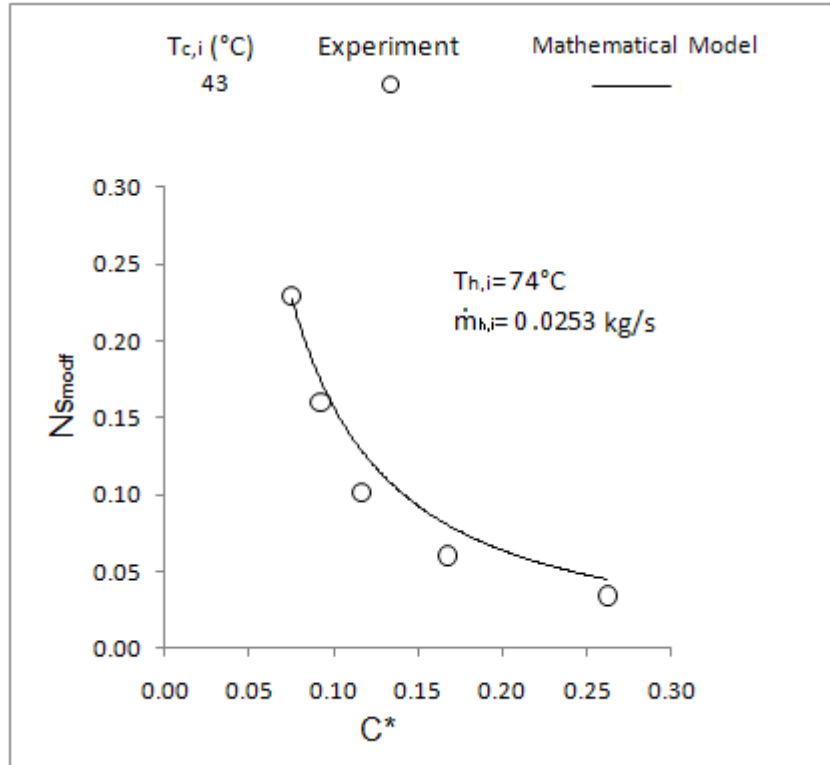


Figure 27 $N_{S_{modif}}$ vs. heat capacity rate ratio

Figure 27 represents the modified entropy generation number behaviour with the heat capacity rate ratio, C^* . As C^* increases, the entropy generation increases and $N_{S_{modif}}$ increases as well. This $N_{S_{modif}}$ includes the effect of heat transfer through the MCHX, since, $N_{S_{modif}} = \frac{\dot{S}_{gen} T_{c,i}}{Q}$, the increase in C^* will increase the actual heat transfer and as a result this will lead to the decrease in $N_{S_{modif}}$.

CHAPTER VI

CONCLUSIONS AND RECOMMENDATIONS

6.1 Conclusions

Microchannel heat exchangers (MCHX) are a rapidly growing technology; they are used both because of their compact size, as well as their small hydraulic diameter, which results in higher heat transfer. The thermodynamic performance of a MCHX was analyzed and evaluated by a second law analysis. A mathematical model was created to predict the behaviour of the entropy generation number as a function of heat capacity rate ratio, fluids inlet temperatures, effectiveness, and airside pressure drop. Entropy generation and exergy destruction values were determined for the MCHX. Predicted and experimental results exhibited good agreement.

The main conclusions that have been reached are listed below.

- Considering the case when $C^*=1$ and there is no pressure drop in the heat exchanger. The entropy generation number is zero (at $\varepsilon = 0$ or 1). However, in the case when $C^* < 1$ and/or $P_o/P_i < 1$, the value of N_s will increase.
- The effectiveness at a maximum entropy generation number was found for different C^* values. This will help in determining the values of ε and C^* which yield the lowest irreversibilities obtained from a heat exchanger. Effectiveness effect at maximum N_s was only found when $T_R \leq 0.7$.
- For a given value of C^* , when $0.5 \leq C^* \leq 1$ and $P_o/P_i = 1$, the S^* values were found to be the same regardless of the fluids inlet temperatures ratio. When $P_o/P_i < 1$, S^* values vary with different fluids inlet temperatures ratio.

- For a given value of T_R , N_s was found to decrease when C^* and the pressure ratio are increased. As C^* value is lowered, the value of N_s decreases at a higher rate.
- N_s values were found to increase with the increase in the airside heat capacity rate, C_{\max} at the same air inlet temperature but different pressure drop.
- The results from the predicted data for N_s and $X_{\text{destroyed}}$ with C^* were found to be in a good agreement with the measured data.
- The entropy generation number, and $X_{\text{destroyed}}$ show an increasing trend, when Reynolds number increases. They increase rapidly with higher Re numbers because higher pressure drops are produced (Figures 25, 26).
- The $N_{s\text{modf}}$ relation with C^* yield the same conclusion obtained from Bejan's entropy generation.

The current study examined the effect of C^* , ε , T_R , and P_o/P_i on entropy generation number, entropy generation number ratio, and the exergy destruction. It presents the important relations between the entropy generation number and the mentioned parameters. The results allow for the thermal optimization of the MCHX by choosing the best combination of parameters to reduce the irreversibility. In this study, an optimal set of conditions was found to be $C^*=1$, $T_R \approx 1$, and $P_o/P_i \approx 1$, which resulted in reducing losses due to heat transfer and pressure drop. Since energy and cost are the main concerns in the industry nowadays, the presented relationships would help in designing a heat exchanger with minimum losses.

Table 3 Summary of the conclusions

PARAMETERS EFFECT							
C^*	T_R	$P_{a,o}/P_{a,i}$	Ns	ε	S^*	$X_{destroyed}$	Re
=1	↑	-	↓	= C	-	-	-
= C	= C	-	↑	↑ 0 - 0.5	-	-	-
= C	= C	-	↓	↑ 0.5 - 1	-	-	-
= C	↑	↑	↓	= C	-	-	-
↓	= C	= C	↑	= C	-	-	-
↓	= C	↓	↑	↑	-	↑	-
= C	↑	-	-	= C ^a	↑	-	-
= C	↑	-	-	= C ^b	↓	-	-
= C	↑	= C	-	= C	↑	-	-
= C	= C	↓	-	= C	↑	-	-
↓	= C	= C	-	= C	↑	-	-
= C	↑	↑	↓	= C	-	-	-
↓	= C	↓	↑	↑	-	↑	-
= C	↑	= C	↓	= C	-	↓	= C

C (constant)

- (not studied or no effect)

↑ (increase) , ↓ (decrease)

a (after the critical point, Figures 15, 16)

b (before the critical point, Figures 15, 16)

6.2 Recommendations

Large number of studies has been performed on heat exchangers using heat balance and second law analysis. Many relationships have been presented to improve the design of heat exchangers. The presented conclusions in this study will also help improve the thermodynamic performance of the MCHX. A further investigation of more operating conditions can be used to verify the presented results and enhance the MCHX performance. Also the use of different fin types, slabs, channel configurations and dimensions would also result in the MCHX improvement.

The present study can be extended to include the following changes,

- Since this study focused on air heating, air cooling can be investigated for the same heat exchanger.
- Investigate the fluid flow and heat transfer enhancement through a wide range of air velocities and Reynolds numbers.
- Comparison of the present study with conventional heat exchangers such as shell and tube, plate heat exchangers, etc.

Some limitations with the current study include the following observations,

- The use of a chiller instead of the cold water supply system to ensure a more stabilized cold water temperatures.
- The use of an electric motor for the wind tunnel fan instead of the hydraulic pump to guarantee a steady flow of air and provide wider range of air velocity.
- The investigation of different fluids such as water or other incompressible fluids (i.e. transmission fluid for automotive application).

- Examine a wide range of air Reynolds number and investigating the case of a MCHX with turbulent flow.

REFERENCES

- Aceves-Saborio, S., Ranasinghe J., G. M. Reistad (1989). An Extension to the Irreversibility Minimization Analysis Applied to Heat Exchangers. ASME J. Heat Transfer **111**(1):29–36.
- Alebrahim, A. (2010). Entropy generation minimization in a ram-air cross-flow heat exchanger. International journal of applied thermodynamics **2**(4): 145.
- Allouache, N. and S. Chikh (2006). Second Law Analysis in a Partly Porous Double Pipe Heat Exchanger. Journal of Applied Mechanics **73**(1): 60-65.
- Ashman, S. and G. S. Kandlikar (2006). A review of manufacturing processes for microchannel heat exchanger fabrication. Proc. 4th Int. Conf. Nanochannels, Microchannels, Minichannels (ICMM2004), p.855.
- Assad, M. E. H. (2010). Effect of maximum and minimum heat capacity rate on entropy generation in a heat exchanger. International Journal of Energy Research **34**(14): 1302-1308.
- Bejan, A. (1977). The Concept of Irreversibility in Heat Exchanger Design: Counterflow Heat Exchangers for Gas-to-Gas Applications. Journal of Heat Transfer **99**(3): 374-380.

- Bejan, A. (1978). General criterion for rating heat-exchanger performance. International Journal of Heat and Mass Transfer **21**(5): 655-658.
- Bejan, A. (1979). A Study of Entropy Generation in Fundamental Convective Heat Transfer. Journal of Heat Transfer **101**(4): 718-725.
- Bejan, (1982). Entropy Generation through Heat and Fluid Flow. John Wiley & Sons, New York, 1982.
- Bejan, A. (1988). Advanced Engineering Thermodynamics. New York etc., John Wiley & Sons. 758 pp. ISBN 0-471-83043-7
- Bruges, E.A. (1959). Available Energy and the Second Law Analysis. Butterworths, London,.
- Bulck, V. D. E. (1991). Optimal Design of Crossflow Heat Exchangers. Journal of Heat Transfer **113**(2): 341-347.
- Can, A., Eryener D., E. Buyruk (1998). Experimental studies on influence of process variables to the exergy losses at the double tube heat exchanger. in: Kakaç S., Bergles A.E., Mayinger F., Yüncü H. (Eds.), Heat Transfer Enhancement of Heat Exchangers, NATO ASI Series, Series E: Applied Sciences **355**:641–648.

- Cengel, Yunus A. and Michael A. Boles (2006). Thermodynamics: An Engineering Approach. 5th ed., New York, McGraw-Hill: ISBN-10 / ASIN: 0073107689.
- Cornelissen, R.L. (1997). Thermodynamics and sustainable development. Ph.D. thesis. Twente Centre for Studies in Technology and Sustainable Development (CSTM).
- Culham, R. J. and Y. S. Muzychka (2001). Optimization of plate-fin heat sinks using entropy generation minimization. IEEE Transactions on Components and Packaging Technologies **24**: 159–165.
- Das, S.K. and W. Roetzel (1998). Second law analysis of a plate exchanger with an axial dispersive wave. Cryogenics **38**:791–798.
- Fan, Y. and L. Luo (2009). Second law analysis of a crossflow heat exchanger equipped with constructal distributor/collector. International Journal of Exergy **6**(6): 778-792.
- Fartaj, S. A. (2004). Comparison of energy, exergy, and entropy balance methods for analysing double-stage absorption heat transformer cycles. International Journal of Energy Research **28**(14): 1219-1230.

- Golem, P.J. and T.A. Brzustowski (1976). Second law analysis of energy processes. Part II. The performance of simple heat exchangers. Trans. Can. Soc. Mech. Engrg. **4**:219– 226.
- Grazzini, G. and F. Gori (1988). Entropy parameters for heat exchangers design. Internat. J. Heat Mass Transfer **31**:2547–2554.
- Guo, J., Cheng L., M. Xu (2010). Multi-Objective Optimization of Heat Exchanger Design by Entropy Generation Minimization. ASME J. Heat Transfer **132**:081801.
- Harris, C., Despa M., and K. Kelly (2000). Design and fabrication of a cross flow micro heat exchanger. Microelectromechanical Systems, Journal of **9**(4): 502-508.
- He, Y. L., Lei Y. G., Tao W. Q., Zhang J. F., Chu P., R. Li. (2009). Second-Law Based Thermodynamic Analysis of a Novel Heat Exchanger. Chemical Engineering & Technology **32**(1): 86-92.
- Hesselgreaves, J. E. (2000). Rationalisation of second law analysis of heat exchangers. International Journal of Heat and Mass Transfer **43**(22): 4189-4204.
- Kang, S.W. and S.C. Tseng (2007). Analysis of effectiveness and pressure drop in micro cross-flow heat exchanger. Applied Thermal Engineering **27** (5–6), pp. 877–885.

- Kandlikar, S. G. (2006). Heat Transfer and Fluid Flow in Minichannels and Microchannels. Burlington, Elsevier Science Ltd.
- Kavakakpinar, E. and Y. Bicer. (2005). Investigation of heat transfer and exergy loss in a concentric double pipe exchanger equipped with swirl generators. International Journal of Thermal Sciences **44**(6): 598-607.
- Khan, M. G. and A. Fartaj. (2010). A review on microchannel heat exchangers and potential applications. International Journal of Energy Research.
- Li, J. and G. P. Peterson (2007). 3-Dimensional numerical optimization of silicon-based high performance parallel microchannel heat sink with liquid flow. International Journal of Heat and Mass Transfer **47**(19-20): 4215-4231.
- London, A.L. and R.K. Shah (1983). Costs of irreversibilities in heat exchanger design, Heat Transfer Engrg. **4**:59–73.
- McClintock, F. A. (1951). The design of heat exchangers for minimum irreversibility. ASME Paper No. 51-A-108.
- Mehendale, S. S., Jacobi, A. M. Shah, R. K. (2000). Fluid Flow and Heat Transfer at Micro- and Meso-Scales With Application to Heat Exchanger Design. Applied Mechanics Reviews **53**(7): 175-193.

- Mohamed, H. A. (2006). Entropy Generation in Counter Flow Gas to Gas Heat Exchangers. Journal of Heat Transfer **128**(1): 87.
- Mukherjee, P., Biswas G., P.K. Nag (1987). Second law analysis of heat transfer in swirling through a cylindrical duct. J. Heat Transfer **308**–313.
- Naphon, P. (2006). Second law analysis on the heat transfer of the horizontal concentric tube heat exchanger. International Communications in Heat and Mass Transfer **33**(8): 1029-1041.
- Ogulata, R.T. and F. Doba (1997). Experiments and entropy generation minimization analysis of a cross-flow heat exchanger. International Journal of Heat and Mass Transfer **41**: 373–381.
- Poulikakos, D. (1982). Fin geometry for minimum entropy generation in forced convection. Journal of Heat Transfer **104**(Journal Article): 616.
- Prasad, R.C. and J. Shen (1993). Performance evaluation of convective heat transfer enhancement devices using exergy analysis. Internat. J. Heat Mass Transfer **36**:4193– 4197.

- Prasad, R.C. and J. Shen (1994). Performance evaluation using exergy analysis-application to wire-coil inserts in forced convection heat transfer. Internat. J. Heat Mass Transfer **37**: 2297–2303.
- Reistad, G.M. (1970). Availability: concepts and applications. Ph.D. thesis, University of Wisconsin, Madison.
- Rosen, M.A. (1999). Second law analysis: Approaches and implications. Internat. J. Energy Res. **23**:415–429.
- Saboya, F. E. M. and C. E. S. M. da Costa (1999). Minimum irreversibility criteria for heat exchanger configurations. Journal of energy resources technology **121**(4): 241.
- Sadeghi, A. and M. H. Saidi. (2010). Second Law Analysis of Slip Flow Forced Convection Through a Parallel Plate Microchannel. Nanoscale and Microscale Thermophysical Engineering **14**(4): 209-228.
- Sahiti, N., Krasniq F. i, Feizullahu X., Bunjaku J., A. Muriqi. (2008). Entropy generation minimization of a double-pipe pin fin heat exchanger. Applied Thermal Engineering **28**(17-18): 2337-2344.
- San, J.-Y. and K.-L. Pai (2009). Performance of a serpentine heat exchanger: Part II – Second-law efficiency. Applied Thermal Engineering **29**(14-15): 3088-3093.

- Sarangi, S. and K. Choowdhury (1982). On the generation of entropy in a counterflow heat exchanger. Cryogenics **22**:63–65.
- Shah, R. K. and D. P. Sekulic. (2003). Fundamentals of Heat Exchanger Design. John Wiley & Sons.
- Shah, R. K. and T. Skiepko (2004). Entropy Generation Extrema and Their Relationship With Heat Exchanger Effectiveness—Number of Transfer Unit Behavior for Complex Flow Arrangements. ASME J. Heat Transfer **126**(6):994–1002.
- Tsatsaronis, G. (1993). Thermoeconomic analysis and optimization of energy systems. Prog Energy Combust Sci **19**:227–57.
- Tuckerman, D. B. and R. F. W. Pease (1981). High-performance heat sinking for VLSI. Electron Device Letters, IEEE **2**(5): 126-129.
- Vargas, J. and A. Bejan (2001). Thermodynamic optimization of finned crossflow heat exchangers for aircraft environmental control systems. International Journal of Heat Fluid Flow **22**:657–665.
- Xiong, D. (1996). On effectiveness and entropy generation in heat exchanger. Journal of thermal science **5**(4): 248.

- Xu, Z. M. (1996). A modified entropy generation number for heat exchangers. Journal of thermal science **5**(4): 257.
- Yang, W. W., Fartaj A., D. S-K. Ting (2008). Exergy analysis of advanced transcritical CO2 air conditioning cycles. International Journal of Exergy **5**(2): 150-163.
- Yilbas, B.S., Shuja S.Z., M.O. Budair (1999). Second law analysis of a swirling flow in a circular duct with restriction. Internat. J. Heat Mass Transfer **42**:4027–4041.
- Yilmaz, M. (2001). Performance evaluation criteria for heat exchangers based on second law analysis. Exergy **1**(4): 278.
- Zubair, S.M., Kadaba P.V., R.B. Evans (1987). Second-law based thermoeconomic optimization of two-phase heat exchangers. J. Heat Transfer **109**:287–294.

APPENDICES

APPENDIX A

Uncertainty Analysis

A.1 Uncertainty Analysis of the DAQ System:

The data acquisition system (DAQ) includes several components such as; DAQ card, signal conditioning, terminal blocks, and uninterruptable power supply. Other devices connected to the DAQ system are; resistance temperature difference (RTD), pressure transducers (PTD), thermocouples, and a flow meter. A lot of information regarding each component specifications can be found using the manufacturer's data sheet. Some of the equipments specifications provided by the manufacturers include linearity, hysteresis, thermal drifts, and repeatability. These specifications combined are called *bias* errors except the repeatability which is a *precision* error. Precision errors can also be found from the experimental data by taking the standard deviation. In the current study, independent and dependent parameters were identified for the uncertainty calculation. The independent parameter is the parameter measured directly using an instrument such as temperatures, pressures, the MCHX length, etc. While the dependent parameters are considered to be a function of the independent parameter such as mass flow rate, average fluid temperature, Reynolds number, heat transfer rate, and entropy generation.

The precision error can be found using the Root Sum Square (RSS) method as follows.

$$B = \pm \sqrt{B_1^2 + B_2^2 + \dots + B_n^2} \quad (\text{A.1})$$

While the precision error using RSS can be found as,

$$P = \pm \sqrt{P_1^2 + P_2^2 + \dots + P_n^2} \quad (\text{A.2})$$

The total uncertainty based on the bias and precision errors as well as using the RSS method is,

$$U = \pm \sqrt{B^2 + P^2} \quad (\text{A.3})$$

At a sampling rate of 1 kHz, experimental data were recorded for a period of 3 to 4 minutes for each one of the operating conditions. Fluid properties such as specific heat, density, and viscosity were found at an average temperature of the fluid. The maximum and minimum average temperatures were found and the uncertainty of the fluid properties was calculated based on these temperatures as,

$$U_{fluid\ property} = \frac{1}{2} |[fluid_{property} @T_{b,max}] - [fluid_{property} @T_{b,min}]| \quad (\text{A.4})$$

In order to find the uncertainty of the dependent parameters, the Root Sum Square (RSS) method was applied. Assuming that the dependent parameter is Y, and it is a function of different independent parameters $X_1, X_2, X_3, \dots, X_n$.

$$Y = f(X_1, X_2, X_3, \dots, X_n) \quad (\text{A.5})$$

Therefore, the absolute uncertainty can be obtained as,

$$U_Y = \sqrt{\left(\frac{\partial Y}{\partial X_1} U_{X_1}\right)^2 + \left(\frac{\partial Y}{\partial X_2} U_{X_2}\right)^2 + \left(\frac{\partial Y}{\partial X_3} U_{X_3}\right)^2 + \left(\frac{\partial Y}{\partial X_n} U_{X_n}\right)^2} \quad (\text{A.6})$$

Using equation (A.3) to find the derivative $\left(\frac{\partial Y}{\partial X_1}, \frac{\partial Y}{\partial X_2}, \frac{\partial Y}{\partial X_3}, \frac{\partial Y}{\partial X_n}\right)$ and equation (A.5) to find $(U_{X_1}, U_{X_2}, U_{X_3}, U_{X_n})$, the uncertainty of any parameter can be represented in the absolute value as $Y \pm U_Y$.

$$Y \pm U_Y = Y \pm \sqrt{\left(\frac{\partial Y}{\partial X_1} U_{X_1}\right)^2 + \left(\frac{\partial Y}{\partial X_2} U_{X_2}\right)^2 + \left(\frac{\partial Y}{\partial X_3} U_{X_3}\right)^2 + \left(\frac{\partial Y}{\partial X_n} U_{X_n}\right)^2} \quad (\text{A.7})$$

A.2 Uncertainty in the MCHX Dimensions

The measurements taken by the digital caliper involves both bias and precision errors. The bias error is due to the digital caliper while, the precision error is due to the repeated measurements of the same parameter at different location of the MCHX. The parameters measured include the number of fins per slab ($N_{fin,s}$), fin height (H_{fin}), slab width (W_s), microchannel diameter (D_{MC}), and fin length (L_{fin}). The standard deviation involving the precision error for each of the parameters at $T_{N,95\%} = 2$ is obtained according to the following equations.

The uncertainty in the number of fins per slab is calculated as follows.

$$P_{N_{fin,s}} = \pm t_{N,95\%} S_{N_{fin,s}} \approx \pm 2 \frac{S_{N_{fin,s}}}{\sqrt{N}} \quad (\text{A.8})$$

$$U_{N_{fin,s}} = \pm \sqrt{(B_{digital\ caliper})^2 + (P_{N_{fin,s}})^2} \quad (\text{A.9})$$

The uncertainty in the fin height can be obtained from the following.

$$P_{H_{fin}} = \pm t_{N,95\%} S_{H_{fin}} \approx \pm 2 \frac{S_{H_{fin}}}{\sqrt{N}} \quad (\text{A.10})$$

$$U_{H_{fin}} = \pm \sqrt{(B_{digital\ caliper})^2 + (P_{H_{fin}})^2} \quad (\text{A.11})$$

The uncertainty in the slab width is calculated as follows.

$$P_{W_s} = \pm t_{N,95\%} S_{W_s} \approx \pm 2 \frac{S_{W_s}}{\sqrt{N}} \quad (\text{A.12})$$

$$U_{W_s} = \pm \sqrt{(B_{digital\ caliper})^2 + (P_{W_s})^2} \quad (\text{A.13})$$

The uncertainty in the microchannel diameter is found as follows.

$$P_{D_{MC}} = \pm t_{N,95\%} S_{D_{MC}} \approx \pm 2 \frac{S_{D_{MC}}}{\sqrt{N}} \quad (\text{A.14})$$

$$U_{D_{MC}} = \pm \sqrt{(B_{digital\ caliper})^2 + (P_{D_{MC}})^2} \quad (\text{A.15})$$

The uncertainty in the fin length is calculated as in the following.

$$P_{L_{fin}} = \pm t_{N,95\%} S_{L_{fin}} \approx \pm 2 \frac{S_{L_{fin}}}{\sqrt{N}} \quad (\text{A.16})$$

$$U_{L_{fin}} = \pm \sqrt{(B_{digital\ caliper})^2 + (P_{L_{fin}})^2} \quad (\text{A.17})$$

Where, $N = 60$ measurements.

After the calculation of the basic MCHX dimensions, the frontal area of the MCHX slab is found from the length and the height of the slab as.

$$A_{f,s} = L_{HT,s} H_s \quad (\text{A.18})$$

$$\frac{\partial A_{f,s}}{\partial L_{HT,s}} = H_s \quad (\text{A.19})$$

$$\frac{\partial A_{f,s}}{\partial H_s} = L_{HT,s} \quad (\text{A.20})$$

The uncertainty associated with the frontal area of the MCHX single slab is.

$$U_{A_{f,s}} = \pm \sqrt{\left(\frac{\partial A_{f,s}}{\partial L_{HT,s}} U_{L_{HT,s}}\right)^2 + \left(\frac{\partial A_{f,s}}{\partial H_s} U_{H_s}\right)^2} \quad (\text{A.21})$$

The total number of fins can be found as.

$$N_{fin_{MCHX}} = N_{fin_{array,MCHX}} N_{fin,s} \quad (\text{A.22})$$

$$\frac{\partial N_{fin_{MCHX}}}{\partial N_{fin_{array,MCHX}}} = N_{fin,s} \quad (\text{A.23})$$

$$\frac{\partial N_{fin_{MCHX}}}{\partial N_{fin,s}} = N_{fin_{array,MCHX}} \quad (\text{A.24})$$

The uncertainty is found as.

$$U_{N_{finMCHX}} = \pm \sqrt{\left(\frac{\partial N_{finMCHX}}{\partial N_{finarray,MCHX}} U_{N_{finarray,MCHX}}\right)^2 + \left(\frac{\partial N_{finMCHX}}{\partial N_{fin,s}} U_{N_{fin,s}}\right)^2} \quad (A.25)$$

A single fin frontal area can be represented by,

$$A_{fin,f} = H_{fin} t_{fin} \quad (A.26)$$

$$\frac{\partial A_{fin,f}}{\partial H_{fin}} = t_{fin} \quad (A.27)$$

$$\frac{\partial A_{fin,f}}{\partial t_{fin}} = H_{fin} \quad (A.28)$$

Its uncertainty can be calculated as.

$$U_{A_{fin,f}} = \pm \sqrt{\left(\frac{\partial A_{fin,f}}{\partial H_{fin}} U_{H_{fin}}\right)^2 + \left(\frac{\partial A_{fin,f}}{\partial t_{fin}} U_{t_{fin}}\right)^2} \quad (A.29)$$

The fins frontal area of the MCHX can be written as.

$$A_{fin,fMCHX} = N_{finMCHX} A_{fin,f} \quad (A.30)$$

$$\frac{\partial A_{fin,fMCHX}}{\partial N_{finMCHX}} = A_{fin,f} \quad (A.31)$$

$$\frac{\partial A_{fin,fMCHX}}{\partial A_{fin,f}} = N_{finMCHX} \quad (A.32)$$

Its uncertainty can be found as follows.

$$U_{A_{fin,fMCHX}} = \pm \sqrt{\left(\frac{\partial A_{fin,fMCHX}}{\partial N_{finMCHX}} U_{H_{fin}}\right)^2 + \left(\frac{\partial A_{fin,fMCHX}}{\partial A_{fin,f}} U_{A_{fin,f}}\right)^2} \quad (A.33)$$

The total frontal area of the MCHX slabs and fins which obstructs the flow of the air is,

$$A_{f,Obstructed} = A_{fin,fMCHX} + A_{f,s} \quad (A.34)$$

$$\frac{\partial A_{f,Obstructed}}{\partial A_{fin,fMCHX}} = 1 \quad (A.35)$$

$$\frac{\partial A_{f,Obstructed}}{\partial A_{f,s}} = 1 \quad (A.36)$$

The uncertainty is calculated as,

$$U_{A_{f,Obstructed}} = \pm \sqrt{\left(\frac{\partial A_{f,Obstructed}}{\partial A_{fin,fMCHX}} U_{A_{fin,fMCHX}}\right)^2 + \left(\frac{\partial A_{f,Obstructed}}{\partial A_{f,s}} U_{A_{f,s}}\right)^2} \quad (A.37)$$

The MCHX frontal area consists of the length and the height of the MCHX within the test chamber is calculated as,

$$A_{fMCHX} = L_{MCHX} H_{MCHX} \quad (A.38)$$

$$\frac{\partial A_{fMCHX}}{\partial L_{MCHX}} = H_{MCHX} \quad (A.39)$$

$$\frac{\partial A_{fMCHX}}{\partial H_{MCHX}} = L_{MCHX} \quad (A.40)$$

The uncertainty is found as in the following.

$$U_{A_{f_{MCHX}}} = \pm \sqrt{\left(\frac{\partial A_{f_{MCHX}}}{\partial L_{MCHX}} U_{L_{MCHX}}\right)^2 + \left(\frac{\partial A_{f_{MCHX}}}{\partial H_{MCHX}} U_{H_{MCHX}}\right)^2} \quad (A.41)$$

The minimum free flow area of the air flow is,

$$A_{min,a} = A_{f_{MCHX}} - A_{f,obstructed} \quad (A.42)$$

$$\frac{\partial A_{min,a}}{\partial A_{f_{MCHX}}} = 1 \quad (A.43)$$

$$\frac{\partial A_{min,a}}{\partial A_{f,obstructed}} = -1 \quad (A.44)$$

The uncertainty associated with the minimum free flow area is,

$$U_{A_{min,a}} = \pm \sqrt{\left(\frac{\partial A_{min,a}}{\partial A_{f_{MCHX}}} U_{A_{f_{MCHX}}}\right)^2 + \left(\frac{\partial A_{min,a}}{\partial A_{f,obstructed}} U_{A_{f,obstructed}}\right)^2} \quad (A.45)$$

The single slab total area that does not have fins is given in the following equation.

$$A_{indv,slab} = 2W_s(L_{HT,s} - N_{s,fin}t_{fin}) \quad (A.46)$$

$$\frac{\partial A_{indv,slab}}{\partial W_s} = 2(L_{HT,s} - N_{s,fin}t_{fin}) \quad (A.47)$$

$$\frac{\partial A_{indv,slab}}{\partial L_{HT,s}} = 2W_s \quad (A.48)$$

$$\frac{\partial A_{indv,slab}}{\partial N_{s,fin}} = -2W_s t_{fin} \quad (A.49)$$

$$\frac{\partial A_{indv,slab}}{\partial t_{fin}} = -2W_s N_{s,fin} \quad (A.50)$$

The uncertainty in this area can be calculated as,

$$U_{A_{indv,slab}} = \pm \sqrt{\left(\frac{\partial A_{indv,slab}}{\partial W_s} U_{W_s}\right)^2 + \left(\frac{\partial A_{indv,slab}}{\partial L_{HT,s}} U_{L_{HT,s}}\right)^2 + \left(\frac{\partial A_{indv,slab}}{\partial N_{s,fin}} U_{N_{s,fin}}\right)^2 + \left(\frac{\partial A_{indv,slab}}{\partial t_{fin}} U_{t_{fin}}\right)^2} \quad (A.51)$$

The area of the slabs for the whole MCHX which does not have fins included can be found as,

$$A_{slabs,MCHX} = N_{HT,slab,MCHX} \times A_{indv,slab} \quad (A.52)$$

$$\frac{\partial A_{slabs,MCHX}}{\partial N_{HT,slab,MCHX}} = A_{indv,slab} \quad (A.53)$$

$$\frac{\partial A_{slabs,MCHX}}{\partial A_{indv,slab}} = N_{HT,slab,MCHX} \quad (A.54)$$

The uncertainty in all slabs of the MCHX can be calculated as follows.

$$U_{A_{slabs,MCHX}} = \pm \sqrt{\left(\frac{\partial A_{slabs,MCHX}}{\partial N_{HT,slab,MCHX}} U_{N_{HT,slab,MCHX}}\right)^2 + \left(\frac{\partial A_{slabs,MCHX}}{\partial A_{indv,slab}} U_{A_{indv,slab}}\right)^2} \quad (A.55)$$

The heat transfer area of fins and slabs combined can be found using the following equation.

$$A_{HT,a,MCHX} = A_{fin,HT,MCHX} + A_{slabs,MCHX} \quad (A.56)$$

$$\frac{\partial A_{HT,a,MCHX}}{\partial A_{fin,HT,MCHX}} = 1 \quad (A.57)$$

$$\frac{\partial A_{HT,a,MCHX}}{\partial A_{slabs,MCHX}} = 1 \quad (A.58)$$

The total uncertainty associated with heat transfer surface area of the MCHX is,

$$U_{A_{HT,a,MCHX}} = \pm \sqrt{\left(\frac{\partial A_{HT,a,MCHX}}{\partial A_{fin,HT,MCHX}} U_{A_{fin,HT,MCHX}}\right)^2 + \left(\frac{\partial A_{HT,a,MCHX}}{\partial A_{slabs,MCHX}} U_{A_{slabs,MCHX}}\right)^2} \quad (A.59)$$

The hydraulic diameter of the air side MCHX can be found as.

$$D_{h,a,MCHX} = 4W_s \left(\frac{A_{min,a}}{A_{HT,a,MCHX}}\right) \quad (A.60)$$

Where,

$$\frac{\partial D_{h,a,MCHX}}{\partial W_s} = 4 \left(\frac{A_{min,a}}{A_{HT,a,MCHX}}\right) \quad (A.61)$$

$$\frac{\partial D_{h,a,MCHX}}{\partial A_{min,a}} = 4 \left(\frac{W_s}{A_{HT,a,MCHX}}\right) \quad (A.62)$$

$$\frac{\partial D_{h,a,MCHX}}{\partial A_{HT,a,MCHX}} = -4W_s \left(\frac{A_{min,a}}{A_{HT,a,MCHX}^2}\right) \quad (A.63)$$

The uncertainty is calculated as follows.

$$U_{D_{h,a,MCHX}} = \pm \sqrt{\left(\frac{\partial D_{h,a,MCHX}}{\partial W_s} U_{W_s}\right)^2 + \left(\frac{\partial D_{h,a,MCHX}}{\partial A_{min,a}} U_{A_{min,a}}\right)^2 + \left(\frac{\partial D_{h,a,MCHX}}{\partial A_{HT,a,MCHX}} U_{A_{HT,a,MCHX}}\right)^2} \quad (A.64)$$

The cross sectional area of a single microchannel can be found as.

$$A_{MC} = \left(\frac{\pi}{4}\right) D_{MC}^2 \quad (A.65)$$

$$\frac{\partial A_{MC}}{\partial D_{MC}} = \frac{\pi}{2} D_{MC} \quad (A.66)$$

Its uncertainty is found as.

$$U_{A_{MC}} = \pm \sqrt{\left(\frac{\partial A_{MC}}{\partial D_{MC}} U_{D_{MC}}\right)^2} \quad (A.67)$$

The inner surface area of a single microchannel is,

$$A_{MC,i} = \pi L_s D_{MC} \quad (A.68)$$

Where,

$$\frac{\partial A_{MC,i}}{\partial L_s} = \pi D_{MC} \quad (A.69)$$

$$\frac{\partial A_{MC,i}}{\partial D_{MC}} = \pi L_s \quad (A.70)$$

The uncertainty is found as,

$$U_{A_{MC,i}} = \pm \sqrt{\left(\frac{\partial A_{MC,i}}{\partial L_s} U_{L_s}\right)^2 + \left(\frac{\partial A_{MC,i}}{\partial D_{MC}} U_{D_{MC}}\right)^2} \quad (\text{A.71})$$

A.3 Uncertainty Associated With the DAQ System

A.3.1 Uncertainty Associated With the DAQ Card

This section shows all the errors, bias and precision, that can be involved in the DAQ system components. The DAQ card gives bias errors to the measured data. These errors are in the form of Least Significant Bit (LSB), differential non linearity, offset error, and relative accuracy. The sources of these bias errors along with the uncertainty related to the DAQ card can be represented by the RSS method as follow,

$$B_1 = LSB = \frac{\text{Peak to Peak Voltage}}{2^{\text{no. of bits}}} \quad (\text{A.72})$$

$$= \frac{50 - (-50) \times 10^{-3} V}{2^{16}} = 1.523 \times 10^{-6} V \quad (\text{A.73})$$

$$B_2 = \text{Relative Accuracy} = \pm 1.5 LSB \quad (\text{A.74})$$

$$= 2.289 \times 10^{-6} V \quad (\text{A.75})$$

$$B_3 = \text{Differential Non Linearity} = \pm 0.5 LSB \quad (\text{A.76})$$

$$= 7.629 \times 10^{-7} V \quad (\text{A.77})$$

$$B_4 = \text{Offset Error} = \pm 1.0 \times 10^{-6} V \quad (\text{A.78})$$

$$B_{DAQ-card} = \sqrt{B_1^2 + B_2^2 + B_3^2 + B_4^2} \quad (\text{A.79})$$

Therefore, the total bias error from the DAQ card is,

$$B_{DAQ-card} = 3.025 \times 10^{-6}V \quad (A.80)$$

A.3.2 Uncertainty Associated With the Signal Conditioner

The signal conditioner contains the data acquisition card, the module, and the terminal block. The bias errors included from the signal conditioner are differential non linearity and offset error. Using the RSS method, these errors are found as,

$$B_1 = \text{Differential Non Linearity} = \pm 0.005\% \text{ FSR} \quad (A.81)$$

$$= \pm \frac{0.005}{100} [50 - (-50)] \times 10^{-3}V \quad (A.82)$$

$$= 5 \times 10^{-6}V \quad (A.83)$$

$$B_2 = \text{Offset Error} = \pm 1.5 \times 10^{-6}V \quad (A.84)$$

Therefore, the total bias errors from the signal conditioner is,

$$B_{SCXI} = \sqrt{B_1^2 + B_2^2} \quad (A.85)$$

$$= 5.22 \times 10^{-6}V \quad (A.86)$$

Since the terminal block and the module are placed inside the signal conditioner, the uncertainty of the signal conditioner accounts for the errors of its elements.

Total uncertainty of the DAQ components is,

$$B_{DAQ-system} = \sqrt{B_{DAQ-card}^2 + B_{SCXI}^2} \quad (A.87)$$

$$= 6.033 \times 10^{-6}V \quad (A.88)$$

A.4 Uncertainty in the Liquid Side Temperatures

To measure the inlet and the outlet temperatures of the glycol, Ultra Precise RTDs were used. Along with the measurement of the temperatures, errors such as bias, random, and DAQ components are included. These errors are explained as follows.

The bias error provided from the Omega company for this particular RTD is,

$$B_{RTD} = \pm \frac{1}{10} [0.3 + 0.005|T(^{\circ}C)|] \quad (A.89)$$

While the random errors related to the inlet and outlet temperature measurement of the liquid side are based on the data distribution. The overall uncertainty in the RTD measurement can be found as,

$$U_{RTD} = \pm \sqrt{B^2 + P^2} \quad (A.90)$$

$$U_{RTD} = \pm \sqrt{\left[\frac{1}{10} (0.3 + 0.005|T(^{\circ}C)|)\right]^2 + \left[1.96 \frac{S_{RTD,T}}{\sqrt{N}}\right]^2} \quad (A.91)$$

The resistance-temperature relation is provided as either,

$$R_T = R_0 [1 + AT + BT^2 + C (T - 100^{\circ}C)T^3] \text{ for } T < 0^{\circ}C \quad (A.92)$$

Or,

$$R_T = R_0[1 + AT + BT^2] \text{ for } T > 0^\circ\text{C} \quad (\text{A.93})$$

Where,

$$R_0 = 100\Omega \quad (\text{A.94})$$

$$A = 3.9083 \times 10^{-3}\text{C}^{-1} \quad (\text{A.95})$$

$$B = -5.775 \times 10^{-7}\text{C}^{-2} \quad (\text{A.96})$$

Since the experimental temperature was above 0°C , therefore equation (93) will be considered in the calculation of the liquid temperature uncertainty. The sensitivity of the RTD can be found from,

$$I = 100 \times 10^{-6}\text{A} \quad (\text{A.97})$$

$$V = IR_T \quad (\text{A.98})$$

$$V = I R_0[1 + AT + BT^2] \quad (\text{A.99})$$

$$\frac{\delta V}{\delta T} = R_0 I[A + 2BT] \quad (\text{A.100})$$

$$\frac{\delta V}{\delta T} = [3.908 \times 10^{-5} - 1.16038 \times 10^{-8}T] \frac{V}{^\circ\text{C}} \quad (\text{A.101})$$

Therefore, the sensitivity of the RTD can be used to convert the uncertainty of the DAQ components from V reading to $^\circ\text{C}$.

$$U_{DAQ} = \pm \frac{6.033 \times 10^{-6}\text{V}}{\left(\frac{\delta V}{\delta T}\right)} \text{ } ^\circ\text{C} \quad (\text{A.102})$$

$$= \pm \frac{6.033 \times 10^{-6}}{3.908 \times 10^{-5} - 1.16038 \times 10^{-8} |T|} \text{ } ^\circ\text{C} \quad (\text{A.103})$$

Thus, the uncertainty of the liquid temperature using the RSS method can be found using the uncertainty of the DAQ components and the uncertainty of the RTD as follows.

$$U_{T,g} = \pm \sqrt{\left[\frac{6.033 \times 10^{-6}}{3.908 \times 10^{-5} - 1.16038 \times 10^{-8} |T|} \right]^2 + \left[\frac{1}{10} (0.3 + 0.005 |T|) \right]^2 + \left[1.96 \frac{S_{RTD,T}}{\sqrt{N}} \right]^2} \quad (\text{A.104})$$

The bulk temperature of the glycol can be found as,

$$T_{g,b} = \frac{T_{g,i} + T_{g,o}}{2} \quad (\text{A.105})$$

And its uncertainty is found as,

$$U_{T_{g,b}} = \pm \sqrt{\left(\frac{\partial T_{g,b}}{\partial T_{g,i}} U_{T_{g,i}} \right)^2 + \left(\frac{\partial T_{g,b}}{\partial T_{g,o}} U_{T_{g,o}} \right)^2} \quad (\text{A.106})$$

$$\frac{\partial T_{g,b}}{\partial T_{g,i}} = \frac{1}{2} \quad (\text{A.107})$$

$$\frac{\partial T_{g,b}}{\partial T_{g,o}} = \frac{1}{2} \quad (\text{A.108})$$

A.5 Uncertainty in the Liquid Side Density

The uncertainty of the glycol density can be found as,

$$U_{\rho_g} = \frac{1}{2} |[\rho_g@T_{g,b,max}] - [\rho_g@T_{g,b,min}]| \quad (\text{A.109})$$

A.6 Uncertainty in the Liquid Side Viscosity

The uncertainty of the glycol viscosity can be estimated as,

$$U_{\mu_g} = \frac{1}{2} |[\mu_g@T_{g,b,max}] - [\mu_g@T_{g,b,min}]| \quad (\text{A.110})$$

A.7 Uncertainty in the Liquid Side Specific Heat

The uncertainty of the glycol specific heat can be found as follows,

$$U_{c_{p,g}} = \frac{1}{2} |[c_{p,g}@T_{g,b,max}] - [c_{p,g}@T_{g,b,min}]| \quad (\text{A.111})$$

A.8 Uncertainty in the Airside Temperatures

For air temperature measurement, 2 grids were used; one at the inlet and the other at the outlet. The first error is from the instruments, also those two grids, 9 thermocouples at the inlet, and 25 thermocouples at the outlet contribute to a spatial variation error. The last error is due to the 3 to 4 minutes data collecting at a sampling rate of 1 kHz and it is called temporal variation. Since the thermocouples are well calibrated, the last two errors have no significance on the uncertainty calculation. Additionally to these errors, the DAQ

components contribute to the total uncertainty of the temperature measurement. The bias error from the thermocouples is assumed to be 0.1°C.

$$B_1 = 0.1^\circ\text{C} \quad (\text{A.112})$$

There is no precision error due to the instrumentation since they only deal with the design stage uncertainty. The precision error due to the spatial variation taking into consideration the number of samples $N=180000\sim 240000$ readings is found as,

$$P_2 = \frac{S_T}{\sqrt{M}} B_1 = 0.1^\circ\text{C} \quad (\text{A.113})$$

Where,

$$S_T = \sqrt{\frac{\sum_{m=1}^M (\bar{T}_m - \langle \bar{T} \rangle)^2}{M-1}} \quad (\text{A.114})$$

$$\bar{T}_m = \frac{1}{N} \sum_{n=1}^N T_{mn} \quad (\text{A.115})$$

$$\langle \bar{T} \rangle = \frac{1}{M} \sum_{m=1}^M \bar{T}_m \quad (\text{A.116})$$

$$v_2 = M - 1 \quad (\text{A.117})$$

S_T : The standard deviation of each thermocouple at the inlet and outlet

\bar{T}_m : Mean of the samples number for a specific thermocouple

v_2 : Degree of freedom

$\langle \bar{T} \rangle$: The mean of each thermocouples reading at the inlet and outlet

The precision error from the temporal variation is,

$$P_3 = \frac{(S_p)}{\sqrt{MN}} \quad (\text{A.118})$$

Where,

$$S_p = \sqrt{\frac{\sum_{m=1}^9 \sum_{n=1}^N (\bar{T}_{mn} - \langle \bar{T} \rangle)^2}{M(N-1)}} \quad (\text{A.119})$$

$$v_3 = M(N - 1) \quad (\text{A.120})$$

S_p : The pooled standard deviation of all the thermocouple and samples

v_3 : Degree of freedom

The degree of freedom used with the precision error is found using Welch-Satterthwaite (W-S) method as,

$$v = \frac{(\sum_{i=1}^3 P_i^2)^2}{\sum_{i=1}^3 \left(\frac{P_i^4}{v_i} \right)} = \frac{(P_2^2 + P_3^2)^2}{\frac{P_2^4}{v_2} + \frac{P_3^4}{v_3}} \quad (\text{A.121})$$

$$t_{v,95} = 1.96 \quad (N > 1000) \quad (\text{A.122})$$

The total uncertainty associated with the thermocouples reading includes the bias and the precision error, and it is found using the RSS method as,

$$U_{thermocouples} = \pm \sqrt{B^2 + (t_{v,95}P)^2} \quad (\text{A.123})$$

To convert the voltage reading of the thermocouples to a °C reading, and include it with the uncertainty calculation, the sensitivity is found as,

$$\frac{\partial V}{\partial T_{thermocouple}} = 43 \times 10^{-6} \frac{V}{^{\circ}\text{C}} \quad (\text{A.124})$$

$$U_{DAQ} = \pm \frac{6.033 \times 10^{-6} V}{\frac{\partial V}{\partial T_{thermocouple}}} = \frac{6.033 \times 10^{-6} V}{43 \times 10^{-6} V/^{\circ}\text{C}} = 0.14^{\circ}\text{C} \quad (\text{A.125})$$

The uncertainty of the airside temperature is found using the RSS method accounting for the uncertainty of the DAQ components and the thermocouples uncertainty is as follows,

$$U_{T_a} = \pm \sqrt{U_{DAQ}^2 + U_{thermocouple}^2} \quad (\text{A.126})$$

The bulk temperature of the air inlet and outlet temperatures is found as,

$$T_{a,b} = \frac{T_{a,i} + T_{a,o}}{2} \quad (\text{A.127})$$

$$U_{T_{a,b}} = \pm \sqrt{\left(\frac{\partial T_{a,b}}{\partial T_{a,i}} U_{T_{a,i}}\right)^2 + \left(\frac{\partial T_{a,b}}{\partial T_{a,o}} U_{T_{a,o}}\right)^2} \quad (\text{A.128})$$

Where,

$$\frac{\partial T_{a,b}}{\partial T_{a,i}} = \frac{1}{2} \quad (\text{A.129})$$

$$\frac{\partial T_{a,b}}{\partial T_{a,o}} = \frac{1}{2} \quad (\text{A.130})$$

The fluids (air and glycol) inlet temperatures ratio T_R is found as,

$$T_R = \frac{T_{h,i}}{T_{c,i}} \quad (\text{A.131})$$

$$U_{T_R} = \pm \sqrt{\left(\frac{\partial T_R}{\partial T_{h,i}} U_{T_{h,i}}\right)^2 + \left(\frac{\partial T_R}{\partial T_{c,i}} U_{T_{c,i}}\right)^2} \quad (\text{A.132})$$

$$\frac{\partial T_R}{\partial T_{h,i}} = \frac{1}{T_{c,i}} \quad (\text{A.133})$$

$$\frac{\partial T_R}{\partial T_{c,i}} = -\frac{T_{h,i}}{T_{c,i}^2} \quad (\text{A.134})$$

A.9 Uncertainty in the Airside Density

The uncertainty of the air density can be estimated as,

$$U_{\rho_a} = \frac{1}{2} |[\rho_a @ T_{a,b,max}] - [\rho_a @ T_{a,b,min}]| \quad (\text{A.135})$$

A.10 Uncertainty in the Liquid Side Viscosity

The uncertainty of the air viscosity can be found as,

$$U_{\mu_a} = \frac{1}{2} |[\mu_a @ T_{a,b,max}] - [\mu_a @ T_{a,b,min}]| \quad (\text{A.136})$$

A.11 Uncertainty in the Airside Specific Heat

The uncertainty of the air specific heat can be found as follows,

$$U_{c_{p,a}} = \frac{1}{2} |[c_{p,a} @ T_{a,b,max}] - [c_{p,a} @ T_{a,b,min}]| \quad (\text{A.137})$$

A.12 Uncertainty in the Airside Pressures

To measure the air pressures, pressure transducers PTDs of the PX series were used. The specifications of the PTDs are provided from the Omega company manufacturers. The pressure range of the Pitot static tube is (0-1" H₂O). The bias error from this PTD includes the instrument accuracy which includes linearity, repeatability, and hysteresis. The other bias error is due to the thermal effects. Therefore the total bias error can be represented as,

$$B_{Pitot} = \pm \sqrt{B_{accuracy}^2 + B_{thermal\ effect}^2} \quad (A.138)$$

$$= \pm \sqrt{(0.01FS)^2 + (0.02\ FS/^{\circ}C)^2} \quad (A.139)$$

$$= \pm \sqrt{0.01 + 4 \times 10^{-6}T^2} \quad V \quad (A.140)$$

Since the pressure transducers used are from the same series, they have the same error sources and the only difference is the range of pressure used for each one of them. The differential pressure transducer has a pressure range of (0-5" H₂O). The instrument accuracy for the transducer accounts for the linearity, repeatability, and hysteresis. The other uncertainty source beside the accuracy is the thermal effect. The transducer bias error can be shown as,

$$B_{\Delta p, MCHX} = \pm \sqrt{B_{accuracy}^2 + B_{thermal\ effect}^2} \quad (A.141)$$

$$= \pm \sqrt{(0.01FS)^2 + (0.02\ FS/^{\circ}C)^2} \quad (A.142)$$

$$= \pm \sqrt{0.01 + 4 \times 10^{-6} T^2} \quad \text{V} \quad (\text{A.143})$$

The scatter of the data presents a random error for the differential pressure and Pitot dynamic pressure. This random error is found as,

$$P_{\Delta p, MCHX} = \pm t_{N,95\%} S_{\bar{P}} \approx \pm 1.96 \frac{S_{\Delta p, MCHX}}{\sqrt{N}} \quad (\text{for } N \geq 1000) \quad (\text{A.144})$$

$$P_{Pitot} = \pm t_{N,95\%} S_{\bar{P}} \approx \pm 1.96 \frac{S_{Pitot}}{\sqrt{N}} \quad (\text{for } N \geq 1000) \quad (\text{A.145})$$

The overall uncertainty due to the differential pressure transducer and Pitot static tube are given in the following equation,

$$U_{\Delta p, MCHX} = \pm \sqrt{B_{\Delta p, MCHX}^2 + P_{\Delta p, MCHX}^2} \quad (\text{A.146})$$

$$= \pm \sqrt{[0.01 + 4 \times 10^{-6} T^2] + \left[1.96 \frac{S_{\Delta p, MCHX}}{\sqrt{N}}\right]^2} \quad \text{V} \quad (\text{A.147})$$

$$U_{Pitot} = \pm \sqrt{B_{Pitot}^2 + P_{Pitot}^2} \quad (\text{A.148})$$

$$= \pm \sqrt{[0.01 + 4 \times 10^{-6} T^2] + \left[1.96 \frac{S_{Pitot}}{\sqrt{N}}\right]^2} \quad \text{V} \quad (\text{A.149})$$

After introducing the error sources for the differential pressure transducer and Pitot static tube, the total uncertainty associated with the pressure for both of them can be given as follows,

$$U_{diff, pressure} = \pm \sqrt{U_{\Delta p, MCHX}^2 + U_{DAQ}^2} \quad (\text{A.150})$$

$$= \pm \sqrt{[0.01 + 4 \times 10^{-6}T^2] + \left[1.96 \frac{S_{\Delta p, MCHX}}{\sqrt{N}}\right]^2 + [6.033 \times 10^{-6}]^2} \quad (\text{A.151})$$

$$= \pm \sqrt{[0.01 + 4 \times 10^{-6}T^2] + \left[1.96 \frac{S_{\Delta p, MCHX}}{\sqrt{N}}\right]^2 + 36.397 \times 10^{-12}} \quad V \quad (\text{A.152})$$

$$U_{Pitot, pressure} = \pm \sqrt{U_{Pitot}^2 + U_{DAQ}^2} \quad (\text{A.153})$$

$$= \pm \sqrt{[0.01 + 4 \times 10^{-6}T^2] + \left[1.96 \frac{S_{Pitot}}{\sqrt{N}}\right]^2 + [6.033 \times 10^{-6}]^2} \quad (\text{A.154})$$

$$= \pm \sqrt{[0.01 + 4 \times 10^{-6}T^2] + \left[1.96 \frac{S_{Pitot}}{\sqrt{N}}\right]^2 + 36.397 \times 10^{-12}} \quad (\text{A.155})$$

In order to convert the uncertainty of the pressure reading from voltage to Pascal reading, a calibration voltage-pressure curve is plotted and the sensitivity can be presented as,

$$\frac{\partial P}{\partial V_{\Delta p, MCHX}} = 124.55 \frac{Pa}{V} \quad (\text{A.156})$$

$$\frac{\partial P}{\partial V_{Pitot}} = 24.39 \frac{Pa}{V} \quad (\text{A.157})$$

By multiplying the sensitivity of the differential pressure transducer and Pitot static tube with their uncertainties, the final uncertainty of the pressure reading in terms of Pa is given below as,

$$U_{diff, pressure} = \pm 124.55 \sqrt{[0.01 + 4 \times 10^{-6}T^2] + \left[1.96 \frac{S_{\Delta p, MCHX}}{\sqrt{N}}\right]^2 + 36.397 \times 10^{-12}} \quad Pa \quad (\text{A.158})$$

$$U_{Pitot, pressure} = \pm 24.39 \sqrt{[0.01 + 4 \times 10^{-6}T^2] + \left[1.96 \frac{S_{Pitot}}{\sqrt{N}}\right]^2 + 36.397 \times 10^{-12}} \quad Pa \quad (\text{A.159})$$

The outlet to inlet pressure ratio of the airside is given in the following form,

$$r_P = \frac{P_{a,o}}{P_{a,i}} \quad (\text{A.160})$$

Where,

$$\frac{\partial r_P}{\partial P_{a,o}} = \frac{1}{P_{a,i}} \quad (\text{A.161})$$

$$\frac{\partial r_P}{\partial P_{a,i}} = -\frac{P_{a,o}}{(P_{a,i})^2} \quad (\text{A.162})$$

The uncertainty associated with this pressure ratio is presented as,

$$U_{r_P} = \pm \sqrt{\left[\frac{\partial r_P}{\partial P_{a,o}} U_{P_{a,o}} \right]^2 + \left[\frac{\partial r_P}{\partial P_{a,i}} U_{P_{a,i}} \right]^2} \quad (\text{A.163})$$

A.13 Uncertainty Related to the Liquid Side Mass Flow Rate

The amount of liquid was measured in two ways: bucket and stop watch, and by the use of the digital flow meter. The bucket and stop watch liquid mass flow rate was compared with the mass flow rate taken from the digital flow meter, and they were found to agree well with each other. This digital flow meter is provided by Proteus Company and it is made of a stainless steel of the 04004SN1-XXX series with a range of (0.4-5.3 LPM). The digital flow meter was found to contribute a bias error of an accuracy which includes

linearity and a precision error of repeatability as provided by the manufacturer data sheet.

These errors are presented as in the following,

$$B_{accuracy} = 1\% FS \quad (A.164)$$

$$B_{linearity} = 1.5\% FS \quad (A.165)$$

Therefore, the overall bias error can be found as,

$$B_{digital\ flow\ meter} = \pm \sqrt{B_{accuracy}^2 + B_{linearity}^2} \quad (A.166)$$

$$= \pm \sqrt{(0.01 FS)^2 + (0.015 FS)^2} \quad (A.167)$$

$$B_{digital\ flow\ meter} = \pm 0.018 FS \quad (A.168)$$

The precision error associated with this digital flow meter is due to the repeatability and the collection of the experimental data. The repeatability provided by the manufacturer is 0.01 FS.

$$P_{repeatability} = \pm 0.01 FS \quad (A.169)$$

$$P_{Exp,data} = \pm t_{N,95\%} S_{\bar{V}} \approx \pm 1.96 \frac{S_{\bar{V}}}{\sqrt{N}} \quad (for\ N \geq 1000) \quad (A.170)$$

$$P_{digital\ flow\ meter} = \pm \sqrt{[0.01 FS]^2 + \left[1.96 \frac{S_{\bar{V}}}{\sqrt{N}}\right]^2} \quad (A.171)$$

Therefore, the total uncertainty in the digital flow meter including the bias and the precision error can be found as follows,

$$U_{digital\ flow\ meter} = \pm\sqrt{B^2 + P^2} \quad (A.172)$$

Since $N \geq 180000$, therefore $\frac{S\bar{V}}{\sqrt{N}} \cong 0$ and the total uncertainty will be,

$$U_{digital\ flow\ meter} = \pm 0.020615\ FS \quad (A.173)$$

Adding the uncertainty of the DAQ components, the uncertainty is found as,

$$U_{digital\ flow\ meter} = \pm\sqrt{U_{digital\ flow\ meter}^2 + U_{DAQ}^2} \quad (A.174)$$

$$U_{digital\ flow\ meter} = \pm\sqrt{[0.020615\ FS]^2 + [6.033 \times 10^{-6}]^2} \quad (A.175)$$

$$U_{digital\ flow\ meter} = \pm\sqrt{4.249 \times 10^{-4}FS^2 + 36.397 \times 10^{-12}} \quad V \quad (A.176)$$

From the volume flow rate to voltage relationship, the sensitivity of the digital flow meter is found as,

$$\frac{\partial \dot{V}}{\partial V} = 1.792V - 0.3264 \left(\frac{LPM}{V} \right) \quad (A.177)$$

The uncertainty of the digital flow meter in terms of LPM reading can be found as,

$$U_{flow\ rate} = \pm(1.792V - 0.3264)\sqrt{4.249 \times 10^{-4}FS^2 + 36.397 \times 10^{-12}} \quad LPM \quad (A.178)$$

A.14 Uncertainty Related to the Liquid Mass Flow Rate

The mass flow rate of the glycol can be found as follows.

$$\dot{m}_g = \dot{V}_g \rho_g \quad (\text{A.179})$$

$$\frac{\partial \dot{m}_g}{\partial \rho_g} = \dot{V}_g \quad (\text{A.180})$$

$$\frac{\partial \dot{m}_g}{\partial \dot{V}_g} = \rho_g \quad (\text{A.181})$$

The overall uncertainty of the liquid mass flow rate is found as,

$$U_{\dot{m}_g} = \pm \sqrt{\left[\frac{\partial \dot{m}_g}{\partial \rho_g} U_{\rho_g} \right]^2 + \left[\frac{\partial \dot{m}_g}{\partial \dot{V}_g} U_{\dot{V}_g} \right]^2} \quad (\text{A.182})$$

A.15 Uncertainty of the Air Mass Flow Rate

In order to determine the air mass flow rate, the velocity of the air should be determined.

The air velocity expression is given as in the following.

$$V_a = \sqrt{\frac{2\Delta p_{dynamic}}{\rho_a}} \quad (\text{A.183})$$

$$\frac{\partial V_a}{\partial \Delta p} = \frac{1}{\sqrt{2\Delta p_{dynamic}}} \quad (\text{A.184})$$

$$\frac{\partial V_a}{\partial \rho_a} = -\frac{1}{2} \frac{\sqrt{2\Delta p_{dynamic}}}{\rho_a^{3/2}} \quad (\text{A.185})$$

$$U_{V_a} = \pm \sqrt{\left[\frac{\partial V_a}{\partial \Delta p_{dynamic}} U_{\Delta p_{dynamic}} \right]^2 + \left[\frac{\partial V_a}{\partial \rho_a} U_{\rho_a} \right]^2} \quad (\text{A.186})$$

The air mass flow rate equation is given in the following form.

$$\dot{m}_a = \rho_a V_a A_{min,a} \quad (A.187)$$

$$\frac{\partial \dot{m}_a}{\partial \rho_a} = V_a A_{min,a} \quad (A.188)$$

$$\frac{\partial \dot{m}_a}{\partial V_a} = \rho_a A_{min,a} \quad (A.189)$$

$$\frac{\partial \dot{m}_a}{\partial A_{min,a}} = \rho_a V_a \quad (A.190)$$

$$U_{\dot{m}_a} = \pm \sqrt{\left[\frac{\partial \dot{m}_a}{\partial \rho_a} U_{\rho_a} \right]^2 + \left[\frac{\partial \dot{m}_a}{\partial V_a} U_{V_a} \right]^2 + \left[\frac{\partial \dot{m}_a}{\partial A_{min,a}} U_{A_{min,a}} \right]^2} \quad (A.191)$$

A.16 Uncertainty in the Liquid Reynolds Number

Reynolds number of the glycol depends on other parameters and the expression of the number is given as,

$$Re_g = \frac{\dot{m}_g}{51\pi\mu_g D} \quad (A.192)$$

$$\frac{\partial Re_g}{\partial \dot{m}_g} = \frac{1}{51\pi\mu_g D} \quad (A.193)$$

$$\frac{\partial Re_g}{\partial \mu_g} = -\frac{\dot{m}_g}{51\pi\mu_g D} \quad (A.194)$$

$$\frac{\partial Re_g}{\partial D} = -\frac{\dot{m}_g}{51\pi\mu_g D^2} \quad (A.195)$$

The total uncertainty associated with the glycol Reynolds number is calculated as,

$$U_{Re_g} = \pm \sqrt{\left[\frac{\partial Re_g}{\partial \dot{m}_g} U_{\dot{m}_g}\right]^2 + \left[\frac{\partial Re_g}{\partial \mu_g} U_{\mu_g}\right]^2 + \left[\frac{\partial Re_g}{\partial D} U_D\right]^2} \quad (\text{A.196})$$

A.17 Uncertainty in the Air Reynolds Number

The expression of the Reynolds number is given as in the following.

$$Re_a = \frac{G_a D_{h,a}}{\mu_a} \quad (\text{A.197})$$

Where G is the air mass velocity and it is calculated as,

$$G_a = \frac{\dot{m}_a}{A_{a,min}} \quad (\text{A.198})$$

$$\frac{\partial G_a}{\partial \dot{m}_a} = \frac{1}{A_{a,min}} \quad (\text{A.199})$$

$$\frac{\partial G_a}{\partial A_{a,min}} = -\frac{\dot{m}_a}{(A_{a,min})^2} \quad (\text{A.200})$$

The uncertainty of the mass velocity can be found as follows.

$$U_{G_a} = \pm \sqrt{\left[\frac{\partial G_a}{\partial \dot{m}_a} U_{\dot{m}_a}\right]^2 + \left[\frac{\partial G_a}{\partial A_{min,a}} U_{A_{min,a}}\right]^2} \quad (\text{A.201})$$

The uncertainty of the glycol Reynolds number can be calculated as,

$$\frac{\partial Re_a}{\partial G_a} = \frac{D_{h,a}}{\mu_a} \quad (\text{A.202})$$

$$\frac{\partial Re_a}{\partial D_{h,a}} = \frac{G_a}{\mu_a} \quad (\text{A.203})$$

$$\frac{\partial Re_a}{\partial \mu_a} = -\frac{G_a D_{h,a}}{\mu_a^2} \quad (\text{A.204})$$

$$U_{Re_a} = \pm \sqrt{\left[\frac{\partial Re_a}{\partial G_a} U_{G_a} \right]^2 + \left[\frac{\partial Re_a}{\partial D_{h,a}} U_{D_{h,a}} \right]^2 + \left[\frac{\partial Re_a}{\partial \mu_a} U_{\mu_a} \right]^2} \quad (\text{A.205})$$

A.18 Uncertainty in the Glycol Heat Transfer Rate

The glycol heat transfer rate depends on the liquid mass flow rate, temperature difference between the inlet and the outlet, and the specific heat.

$$\dot{Q}_g = \dot{m}_g c_p (T_{g,i} - T_{g,o}) \quad (\text{A.206})$$

$$\frac{\partial \dot{Q}_g}{\partial \dot{m}_g} = c_p \Delta T_g \quad (\text{A.207})$$

$$\frac{\partial \dot{Q}_g}{\partial c_p} = \dot{m}_g \Delta T_g \quad (\text{A.208})$$

$$\frac{\partial \dot{Q}_g}{\partial \Delta T_g} = c_p \dot{m}_g \quad (\text{A.209})$$

$$U_{\dot{Q}_g} = \pm \sqrt{\left[\frac{\partial \dot{Q}_g}{\partial \dot{m}_g} U_{\dot{m}_g} \right]^2 + \left[\frac{\partial \dot{Q}_g}{\partial c_p} U_{c_p} \right]^2 + \left[\frac{\partial \dot{Q}_g}{\partial \Delta T_g} U_{\Delta T_g} \right]^2} \quad (\text{A.210})$$

A.19 Uncertainty in the Air Heat Transfer Rate

$$\dot{Q}_a = \dot{m}_a c_p (T_{a,o} - T_{a,i}) \quad (\text{A.211})$$

$$\frac{\partial \dot{Q}_a}{\partial \dot{m}_a} = c_p \Delta T_a \quad (\text{A.212})$$

$$\frac{\partial \dot{Q}_a}{\partial c_p} = \dot{m}_a \Delta T_a \quad (\text{A.213})$$

$$\frac{\partial \dot{Q}_a}{\partial \Delta T_a} = c_p \dot{m}_a \quad (\text{A.214})$$

$$U_{\dot{Q}_a} = \pm \sqrt{\left[\frac{\partial \dot{Q}_a}{\partial \dot{m}_a} U_{\dot{m}_a} \right]^2 + \left[\frac{\partial \dot{Q}_a}{\partial c_p} U_{c_p} \right]^2 + \left[\frac{\partial \dot{Q}_a}{\partial \Delta T_a} U_{\Delta T_a} \right]^2} \quad (\text{A.215})$$

A.20 Uncertainty in the Average Heat Transfer Rate

The heat transfer rate can be found from the following relationship.

$$\dot{Q} = \frac{\dot{Q}_g + \dot{Q}_a}{2} \quad (\text{A.216})$$

$$\frac{\partial \dot{Q}}{\partial \dot{Q}_g} = \frac{1}{2} \quad (\text{A.217})$$

$$\frac{\partial \dot{Q}}{\partial \dot{Q}_a} = \frac{1}{2} \quad (\text{A.218})$$

$$U_{\dot{Q}} = \pm \sqrt{\left[\frac{\partial \dot{Q}}{\partial \dot{Q}_g} U_{\dot{Q}_g} \right]^2 + \left[\frac{\partial \dot{Q}}{\partial \dot{Q}_a} U_{\dot{Q}_a} \right]^2} \quad (\text{A.219})$$

A.21 Uncertainty in Effectiveness

The effectiveness of a heat exchanger depends on the average heat transfer rate, liquid mass flow rate, and the inlet temperatures difference of the two fluids. Effectiveness is defined as in the following equation,

$$\varepsilon = \frac{\dot{Q}}{\dot{Q}_{max}} \quad (\text{A.220})$$

$$\varepsilon = \frac{\dot{Q}}{(\dot{m}c_p)_{min}(T_{g,i}-T_{a,i})} \quad (A.221)$$

$$\frac{\partial \varepsilon}{\partial \dot{Q}} = \frac{1}{\dot{m}_g c_p (T_{g,i} - T_{a,i})} \quad (A.222)$$

$$\frac{\partial \varepsilon}{\partial \dot{m}_g} = -\frac{\dot{Q}}{\dot{m}_g^2 c_p (T_{g,i} - T_{a,i})} \quad (A.223)$$

$$\frac{\partial \varepsilon}{\partial c_p} = -\frac{\dot{Q}}{\dot{m}_g c_p^2 (T_{g,i} - T_{a,i})} \quad (A.224)$$

$$\frac{\partial \varepsilon}{\partial T_{g,i}} = -\frac{\dot{Q}}{\dot{m}_g c_p (T_{g,i} - T_{a,i})^2} \quad (A.225)$$

$$\frac{\partial \varepsilon}{\partial T_{a,i}} = \frac{\dot{Q}}{\dot{m}_g c_p (T_{g,i} - T_{a,i})^2} \quad (A.21)$$

Therefore, the total uncertainty in effectiveness is,

$$U_\varepsilon = \pm \sqrt{\left[\left[\frac{\partial \varepsilon}{\partial \dot{Q}} U_{\dot{Q}} \right]^2 + \left[\frac{\partial \varepsilon}{\partial \dot{m}_g} U_{\dot{m}_g} \right]^2 + \left[\frac{\partial \varepsilon}{\partial c_p} U_{c_p} \right]^2 + \left[\frac{\partial \varepsilon}{\partial T_{g,i}} U_{T_{g,i}} \right]^2 + \left[\frac{\partial \varepsilon}{\partial T_{a,i}} U_{T_{a,i}} \right]^2 \right]} \quad (A.226)$$

A.22 Uncertainty in the Heat Capacity Rate Ratio

The heat capacity rate ratio depends on the mass flow rates and the specific heat of the two fluids. Its uncertainty can be found as follows,

$$C^* = \frac{\dot{m}_g c_{p_g}}{\dot{m}_a c_{p_a}} \quad (A.227)$$

$$\frac{\partial C^*}{\partial \dot{m}_g} = \frac{c_{p_g}}{\dot{m}_a c_{p_a}} \quad (A.228)$$

$$\frac{\partial C^*}{\partial c_{p_g}} = \frac{\dot{m}_g}{\dot{m}_a c_{p_a}} \quad (\text{A.229})$$

$$\frac{\partial C^*}{\partial \dot{m}_a} = -\frac{\dot{m}_g c_{p_g}}{(\dot{m}_a)^2 c_{p_a}} \quad (\text{A.230})$$

$$\frac{\partial C^*}{\partial c_{p_a}} = -\frac{\dot{m}_g c_{p_g}}{\dot{m}_a (c_{p_a})^2} \quad (\text{A.231})$$

The total uncertainty in the heat capacity rate ratio is presented in the following equation.

$$U_{C^*} = \sqrt{\left[\frac{\partial C^*}{\partial \dot{m}_g} \times U_{\dot{m}_g} \right]^2 + \left[\frac{\partial C^*}{\partial c_{p_g}} \times U_{c_{p_g}} \right]^2 + \left[\frac{\partial C^*}{\partial \dot{m}_a} \times U_{\dot{m}_a} \right]^2 + \left[\frac{\partial C^*}{\partial c_{p_a}} \times U_{c_{p_a}} \right]^2} \quad (\text{A.232})$$

A.23 Uncertainty in the Entropy Generation Number

The entropy generation number expression as provided in the design and methodology section can be obtained as,

$$N_s = \frac{\dot{S}_{gen}}{\dot{m}_g c_p} \quad (\text{A.233})$$

The total uncertainty in this entropy generation number is found as in the following.

$$\frac{\partial N_s}{\partial \dot{S}_{gen}} = \frac{1}{\dot{m}_g c_p} \quad (\text{A.234})$$

$$\frac{\partial N_s}{\partial \dot{m}_g} = -\frac{\dot{S}_{gen}}{\dot{m}_g^2 c_p} \quad (\text{A.235})$$

$$\frac{\partial N_s}{\partial c_p} = -\frac{\dot{S}_{gen}}{c_p^2 \dot{m}_g} \quad (\text{A.236})$$

$$U_{N_s} = \sqrt{\left[\frac{\partial N_s}{\partial \dot{S}_{gen}} \times U_{\dot{S}_{gen}} \right]^2 + \left[\frac{\partial N_s}{\partial \dot{m}_g} \times U_{\dot{m}_g} \right]^2 + \left[\frac{\partial N_s}{\partial c_p} \times U_{c_p} \right]^2} \quad (\text{A.237})$$

The uncertainties of the main design parameters are listed in table (4):

Table 4 Uncertainties in design parameters

Design Parameters	V _a (3m/s)	V _a (5m/s)	V _a (7m/s)
\dot{m}_g (kg/s)	0.0260± 0.00019	0.0256± 0.000187	0.0257± 0.000187
T _{g,b} [°C]	57.55 ± 0.115	56.7 ± 0.119	56.04 ± 0.117
T _{a,b} [°C]	39.79 ± 0.115	38.58 ± 0.123	37.74 ± 0.139
V _a [m/s]	3.21 ± 0.078	5.01 ± 0.115	7.03 ± 0.151
\dot{m}_a [kg/s]	0.343 ± 0.0076	0.535± 0.0114	0.752 ± 0.0153
Re _a	885.7 ± 27.9	1382.7 ± 42.8	1946.4 ± 58.9
Re _g	147.1 ± 5.23	145.8 ± 5.20	146.3 ± 5.21
ε	0.82 ± 0.0142	0.88 ± 0.0144	0.91 ± 0.0141
Q _a [W]	2768.2 ± 71.14	2941.7 ± 70.6	3085.5 ± 69.7
Q _g [W]	2840 ± 20.7	3033 ± 22.1	3173.4 ± 23
Q _{avg} [W]	2804 ± 37.3	2987 ± 38.2	3129 ± 37.5
C*	0.262 ± 0.0506	0.165 ± 0.0325	0.118 ± 0.0231
Ns	0.0037 ± 0.00375	0.00537 ± 0.00547	0.00952 ± 0.0097
Ns _{mod}	0.00513 ± 0.004	0.00636 ± 0.0041	0.01233 ± 0.0076
ΔP _{mid} [kPa]	0.066 ± 0.002072	0.147 ± 0.004455	0.255 ± 0.00732
r _p	0.9993 ± 0.007078	0.9985 ± 0.007075	0.9973±0.0007071

Design Parameters	V _a (9m/s)	V _a (11m/s)
\dot{m}_g (kg/s)	0.0256 ± 0.000187	0.0253 ± 0.000184
T _{g,b} [°C]	55.81 ± 0.122	55.62 ± 0.127
T _{a,b} [°C]	37.58 ± 0.165	37.07 ± 0.192
V _a [m/s]	8.92 ± 0.179	10.92 ± 0.208
\dot{m}_a [kg/s]	0.953 ± 0.0185	1.167 ± 0.0221
Re _a	2468.6 ± 73.3	3027.7 ± 88.7
Re _g	146.2 ± 5.20	144.9 ± 5.17
ϵ	0.93 ± 0.0137	0.94 ± 0.0132
Q _a [W]	3100.1 ± 66.3	3133.4 ± 64.5
Q _g [W]	3208 ± 23.4	3246 ± 23.7
Q _{avg} [W]	3154 ± 36.3	3189 ± 35.4
C*	0.0932 ± 0.0182	0.075 ± 0.0148
Ns	0.01447 ± 0.01474	0.02301 ± 0.02345
Ns _{mod}	0.01718 ± 0.01	0.02693 ± 0.013
ΔP_{mid} [kPa]	0.383 ± 0.01	0.534 ± 0.0135
Γ_p	0.9961 ± 0.007067	0.9947 ± 0.007061

APPENDIX B

Calibration Curves

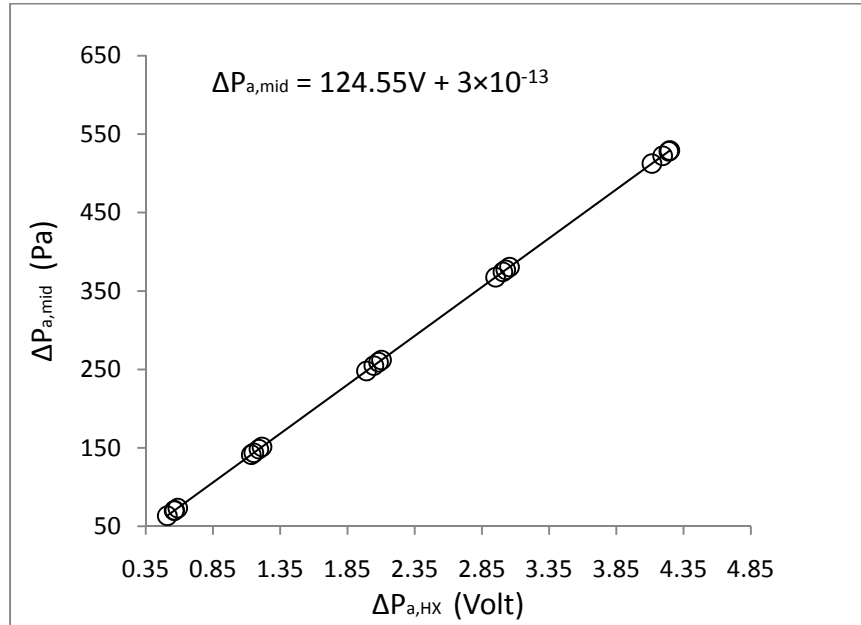


Figure 28 Calibration curve for PX277-05D5V

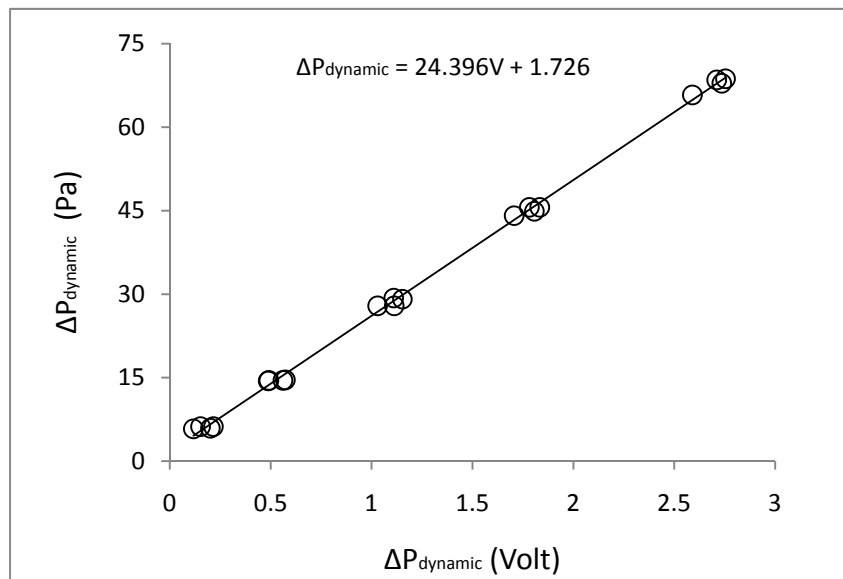


Figure 29 Calibration curve for PX277-01D5V

VITA AUCTORIS

Serena A. Al-Obaidi was born in Baghdad, Iraq in the winter of 1986. She obtained her Bachelor of Applied Science, B.A.Sc., degree in Mechanical Engineering from the University of Technology, Baghdad, Iraq in 2007. In 2008, she migrated with her family to Windsor, Canada where she settled. She continued her study at the University of Windsor, Windsor, Ontario, Canada at the department of Mechanical, Automotive, and Materials Engineering. Currently, she is a candidate for the degree of Master of Applied Science, M.A.Sc., in Mechanical Engineering. The expected completion date of that M.A.Sc. is June of 2011.